UNIVERSITY OF CALIFORNIA, SAN DIEGO

Synoptic Sensitivities of Subtropical Clouds
Separating Aerosol Effects from Meteorology

A dissertation submitted in partial satisfaction of the
requirements for the degree Doctor of Philosophy
in
Oceanography

by

Guillaume S. Mauger

Committee in charge:

Joel R. Norris, Chair
Sarah Gille
Michael Holst
Dan Lubin
Lynn Russell

2008

The dissertation of Guillaume Mauger is approved, and it is acceptable in quality and form for publication on microfilm and electronically:

_____

_____

_____

_____

_____

Chair

University of California, San Diego

2008

to my family and to Mary, for all of their support.

TABLE OF CONTENTS

LIST OF SYMBOLS

ALB	albedo
g	Assymetry parameter
θ	Potential Temperature (K)
μ	Cosine of solar zenith angle
ρ	Density (kg m^{-3})
τ	Optical depth
Q_E	Extinction efficiency
ω	Single scattering Albedo
AOD	Aerosol Optical Depth
α_{exp}	Angström Exponent
CF	Cloud Fraction
LWC	Liquid Water Content (g m^{-3})
LWP	Liquid Water Path (g m^{-2})
LTS	Lower Tropospheric Stability ($\theta_{700} - \theta_{SFC}$, K)
N_D	Cloud droplet concentration (cm^{-3})
R_E	Cloud droplet effective radius (μm)
τ_{CLD}	Cloud optical depth
h	Inversion height (m)
w_E	Entrainment rate (cm s^{-1})
w_S	Subsidence rate (cm s^{-1})
C_T	Bulk transfer coefficient
L	Latent Heat of Vaporization (J kg^{-1})
q	Specific Humidity (g kg^{-1})
s	Moist static energy ($s = c_P T + gz + Lq$, J)
F_{RAD}	Radiative Flux (W m^{-2})
P	Precipitation rate (kg m^{-2} s^{-1})

η^+	Value of the quantity η immediately above the inversion
$\bar{\eta}$	mean value of the quantity η within the boundary layer
η_0	Value of the quantity η at the surface
q_0^*	Saturation specific humidity at the surface
LTS	Lower Tropospheric Static Stability ($\theta_{700} - \theta_0$, K)
SST	Sea Surface Temperature (K)
q_{700}	Specific humidity at 700 hPa (g kg^{-1})
WVP	Water Vapor Path (mm)
TA_{SFC}	Surface Temperature Advection (K s^{-1})
F_{LH}	Surface Latent Heat Flux (W m^{-2})
DIV	Surface Divergence (s^{-1})

LIST OF FIGURES

LIST OF TABLES

ACKNOWLEDGMENTS

I have been fortunate enough to benefit from the help of a wide variety of people throughout the duration of my studies at Scripps. First and foremost, I am indebted to my advisor, Joel Norris, who has provided steady guidance and support and consistently made himself available to discuss, interpret, and direct the course of my research. I have learned a lot from my time working with Joel, and am grateful to have had the opportunity.

As a member of the Scripps community, I feel fortunate for the exposure to such a wide breadth of disciplines, and have benefited from the interdisciplinary perspective this affords. I owe thanks to many Scripps students, researchers, and professors, from whom I have gained a better understanding of my own discipline as well as the overall process of research.

In my first years as a graduate student I learned a great deal from my participation in two field campaigns thanks to the gracious support of V. Ramanathan. I owe thanks to Ram for his insightful "big picture" perspectives, introduction to field measurements, and his willingness to entrust students with responsibility for major components of the overall project.

Much of my work making field measurements and interpreting their results was spent working in parallel with Greg Roberts. Apart from proving to be a great leader and excellent coworker on field campaigns, Greg has been an unflagging source of help and support throughout my thesis. I owe particular thanks to him for his guidance in science writing and the development of my PhD project.

I have also been fortunate enough to interact with scientists beyond Scripps. I owe many thanks to Dr. Yi Ming at GFDL for his willingness to provide model output for analysis and configure model runs based on my requests. Without his help, the final chapter of this dissertation would not exist. I am also indebted to Phil Rasch and Andrew Gettleman for their help in designing model

experiments and for informative discussions on the status of climate modeling at NCAR and GFDL.

As a student at Scripps I owe special thanks to Odelle Hadley, Dave Mansbach, John Holecek, and Steve Taylor, all of whom have been great to work with. In their own way, each has taught me something – ranging from the technical aspects of research to the practical issues of day-to-day research and progress as a graduate student.

Finally, I cannot complete my acknowledgments without recognizing the influence and motivation gained from a scientific father, analytical mother, and two inspiring sisters. I was also lucky enough to have a motivational coach in Mary, whose untiring patience and sage advice are complimented by her status as the best editor I know. As in everything I do, their unconditional support is a source of both affirmation and encouragement, the importance of which cannot be overstated.

Chapter II, in part, is a reprint of the material as it appears in the following publication: Mauger, G. S., and J. R. Norris, Meteorological bias in Satellite estimates of Aerosol-Cloud Relationships, Geophysical Research Letters, Vol. 34, L16824, doi:10.1029/2007GL029952, 2007. The dissertation author was the primary investigator and author of this paper.

VITA

2001	B. S., Applied Physics, Harvey Mudd College
2002–2008	Research Assistant, Scripps Institution of Oceanography, University of California, San Diego
2008	Ph. D., Oceanography, Scripps Institution of Oceanography, University of California, San Diego.

PUBLICATIONS

Mauger, G. and J. R. Norris, 2007: Meteorological Bias in Satellite Estimates of aerosol-cloud relationships. *Geophysical Research Letters*, **34**, L16824.

Hadley, O. L., V. Ramanathan, G. R. Carmichael, Y. Tang, C. E. Corrigan, G. C. Roberts, and G. S. Mauger, 2007: Trans-Pacific transport of black carbon and fine aerosols (D $<$ 2.5 μm) into North America. *Journal of Geophysical Research*, **112(D5)**, D05309.

Roberts, G. C., G. Mauger, O. Hadley, V. Ramanathan, 2006. North American and Asian aerosols over the Eastern Pacific Ocean and their role in regulating cloud condensation nuclei, *Journal of Geophysical Research*, **111(D13)**, D13205.

PRESENTATIONS

Mauger, G., 2008: Stratocumulus Sensitivity to Aerosols and Dynamics: Evaluating Aerosol-Cloud Parameterizations, *Atmospheric Model Working Group Meeting, National Center for Atmospheric Research*, Boulder, CO.

Mauger, G., 2007: Stratocumulus Sensitivity to Aerosols and Dynamics: Evaluating Aerosol-Cloud Parameterizations, *American Geophysical Union*, San Francisco, CA.

Mauger, G., 2007: Stratocumulus Sensitivity to Aerosols and Dynamics, *American Meteorological Society*, San Antonio, TX.

Mauger, G., 2006: Stratocumulus Sensitivity to Aerosols and Dynamics, *American Geophysical Union*, San Francisco, CA.

Mauger, G., 2005: Aerosol-Cloud Interactions during the Cloud Indirect Forcing EXperiment (CIFEX), *American Meteorological Society*, San Diego, CA.

ABSTRACT OF THE DISSERTATION

Synoptic Sensitivities of Subtropical Clouds
Separating Aerosol Effects from Meteorology

by

Guillaume S. Mauger
Doctor of Philosophy in Oceanography
University of California, San Diego, 2008
Professor Joel R. Norris, Chair

The fundamental goals of this study are to 1) quantify the link between aerosols, low-level clouds, and meteorology, and 2) evaluate model representation of aerosol-cloud interactions.

Recent in-situ and remote sensing studies indicate that meteorological effects which influence cloud liquid water path dominate the aerosol signal in stratocumulus clouds. To address this issue, Chapter II undertakes a synoptic-scale investigation of aerosol-cloud interactions. Using parcel back-trajectories, we develop a method to isolate meteorological from aerosol impacts on clouds, and evaluate results over the Northeast Atlantic stratocumulus regime. Using MODIS observations and ECMWF analyses, we show that controlling for variations in lower tropospheric stability reduces the dependence of cloud fraction on AOD by at least 24%. We conclude that meteorological forcing must be accounted for in assessing aerosol impacts on cloud forcing, and that doing so requires a Lagrangian analysis of parcel histories.

Chapter III extends the analysis in Chapter II by performing an in-depth analysis of the meteorological sensitivities of Northeast Atlantic stratocumulus clouds. Additional satellite observations are obtained from CERES, SSM/I and

QuikScat. Compositing is used to quantify the sensitivity of cloud fraction to variations in meteorological state along 72 hour Lagrangian back trajectories. Clouds are found to respond to variations in stability, free tropospheric humidity, and sea surface temperature (SST) advection over long time scales while being influenced by changes in surface divergence over much shorter time scales. Cloud sensitivity to both divergence and stability is shown to be robust and not significantly affected through covariance with other forcings. An additional finding is that the sign of the relationship between cloud fraction and several quantities, including divergence, temperature advection, and surface fluxes, is reversed for long time lags. Along with the differences in stability, SST, and boundary layer humidity that are maintained throughout the trajectories, it is suggested that these point to decoupling of the cloud and sub-cloud layers as a possible cause for cloud dissipation. In contrast, the large cloud fraction composite appears to be more shallow and well-mixed at earlier times in the trajectory, thus maintaining a strong coupling with the surface.

In Chapter IV, the observational sensitivities observed in Chapters II and III are compared with model representations of aerosol-cloud interactions. Since model parameterizations of aerosol-cloud interactions can be switched on or off, climate simulations can be used to separately quantify the impacts of aerosols and meteorology on cloud cover. Both the ECMWF and GFDL models are analyzed using the trajectory method developed in previous chapters. Both are consistent with Chapter II in showing that a significant fraction of the correlation between AOD and CF results from meteorological covariations. However, the two differ significantly in the magnitude of the correction and in their representation of low-level clouds. The ECMWF model, which shows a 43% correction to the AOD-CF sensitivity, also shows a weak correlation (R^2=14.4%) when MODIS cloud cover is compared with ECMWF cloud cover predictions. Alternatively, if the dynamical sensitivities of MODIS clouds are compared to those of the ECMWF clouds, the

two compare reasonably well. In contrast, the GFDL model shows a 100% correction, indicating that within the confidence limits of our analysis, low-level cloud cover is not affected by changes in aerosol. However, the GFDL model's treatment of clouds does not compare well with the observational cloud sensitivities identified in Chapter III. Since the model results are only relevant to the observational analysis if the simulations accurately represent cloud cover, from these results it is not possible to quantitatively conclude on a corrected sensitivity of cloud cover to changes in aerosol optical depth. However, the results do qualitatively confirm the results of Chapter II. In addition, the Lagrangian technique developed in previous chapters proves useful in providing detailed diagnostic information on model performance, in particular as a means of testing cloud parameterizations.

I Introduction

The vertical, horizontal, and spectral distributions of radiation in the atmosphere are what ultimately drive the climate system. Clouds play a significant role in modulating the Earth's energy balance, through impacts on the Earth's albedo in the shortwave and the effective radiating temperature at long wavelengths. The radiation budget is also influenced by atmospheric particles, or aerosols, both through their direct impacts on radiation and their influence on cloud properties. The large magnitude of cloud radiative forcing implies that small errors in their representation can lead to large uncertainties in climate projections. In order to properly quantify the energy budget and accurately simulate changes in the Earth's climate, cloud sensitivities must be well-understood in terms of both the meteorological and aerosol conditions that impact their evolution. The task of quantifying these sensitivities, as well as the relative magnitude of aerosol and dynamical impacts on cloud properties, is an area of active research that remains unsolved. In the following chapters we introduce a new approach to addressing a specific aspect of this important problem, and apply it to the investigation of meteorological and aerosol impacts on subtropical clouds in the Northeast Atlantic.

The dominant role of clouds in determining the Earth's radiation budget has been long-established by observational and modeling studies alike. Ramanathan et al. (1989) presented results from the Earth Radiation Budget Experiment (ERBE), showing that the Earth's albedo is doubled by the presence of clouds and furthermore that the balance between the cooling (shortwave) and

warming (longwave) effects of clouds is dominated by the former. Globally, the ERBE observations show that the radiative effect of clouds is three to five times larger than that due to a doubling of carbon dioxide, emphasizing the notion that small changes in cloud properties are important for climate. This is confirmed by model simulations (*e.g.,* Slingo, 1990), which show that only modest changes in cloud properties are sufficient to offset the greenhouse forcing.

The subtropical cloud regimes found over eastern ocean basins contribute significantly to the global cooling effect of clouds. Over these regions, Ramanathan et al. (1989) found reductions of diurnally averaged solar radiative flux of up to 100 W m^{-2}. The powerful cooling effect of these clouds is due in part to their low latitudes. The structure and properties of the cloud field are at play as well. Stratocumulus clouds, which dominate these regions, are characterized by long lifetimes, overcast conditions, and high albedo relative to ocean, all of which significantly reduce the proportion of absorbed solar radiation. Due to their warm temperatures, the shortwave cooling by subtropical clouds is not significantly offset by longwave warming. An important consequence of their strong cooling effect is that the climate is particularly sensitive to small perturbations in these clouds, and it is this sensitivity that motivates the present investigation of aerosol impacts on low-level subtropical clouds.

It is now well established that aerosols have the potential to exert indirect effects on climate by perturbing both cloud albedo and cloud lifetime (Albrecht, 1989; Twomey, 1977). In what may amount to the earliest satellite observations of anthropogenic influence on the atmosphere, Conover (1966) noted the impact of ship-borne emissions on oceanic clouds. Often referred to as "ship tracks," these provide a rare opportunity in atmospheric science: a controlled experiment in which the only change is a local modification of the aerosol population. In response to the ship-borne emissions, clouds can become significantly brighter. An open question, discussed further in Chapter II, is whether this localized effect

resulting from highly concentrated emissions can be generalized to the global-scale effects of aerosols on cloud properties.

Aerosols can also impact cloud cover in a variety of other ways. Recent studies indicate that aerosols can also influence cloud type, as well as both the nature and amount of precipitation (Liepert et al., 2004; Rosenfeld, 2000; Rotstayn and Lohmann, 2002). Aerosols can also impact the stability of the atmosphere, either through a reduction in surface radiation or a heating through absorption of radiation aloft. Changes to the stability can result in a drying of the cloud layer or conversely in an increase in cloud cover, dependent on the vertical distribution of aerosol heating (Johnson et al., 2004; Ackerman et al., 2000). Clouds also exert significant influences on aerosol through, for example, cloud processing (*e.g.,* Hoppel et al., 1990) and wet removal of aerosols by precipitation.

In the present work we focus on aerosol microphysical impacts on cloud properties. These refer to the impacts on clouds through droplet nucleation as a result of changes in the chemistry and amount of aerosol, and are conventionally referred to as the indirect effects. Discussed in more detail in Chapter II, changes in the concentration of activated droplets can impact cloud albedo by increasing the scattering efficiency of the droplet population, and can also modify cloud lifetime, either through suppression of precipitation or promotion of entrainment.

Twohy et al. (2005) analyzed coincident in-situ observations of stratocumulus clouds and aerosol characteristics from an ensemble of clouds observed during the Second Dynamics and Chemistry of Marine Stratocumulus (DYCOMS-II) experiment. Although their results showed a significant association between aerosol concentration, cloud drop concentration, and cloud drop effective radius, they found no significant relationship with cloud optical thickness or albedo, indicating that variations in liquid water path dominate the albedo signal. Not surprisingly, these result suggest that the aerosol impacts alone cannot be used to diagnose cloud radiative properties: the underlying dynamics provide a strong

forcing from which the aerosol signal must be decoupled. This is consistent with the findings of Schwartz et al. (2002), who used satellite retrievals of albedo, effective radius, and liquid water path along with a chemical transport model to show that changes in cloud liquid water path dominate the albedo signal. This conclusion can be generalized to note that meteorological effects that impact *any* cloud property must be decoupled from aerosol variations in order to accurately quantify aerosol impacts.

This dissertation seeks to address the question of separating aerosol from meteorological impacts on low-level subtropical clouds through the introduction of a new analysis technique. In Chapter II we investigate aerosol-meteorological covariations and assess how these could impact the observed relationship between aerosols and clouds. A new method is developed to account for both the instantaneous and historical impacts of meteorology on cloud properties. Chapter III seeks to inform the discussion of Chapter II by analyzing the sensitivity of cloud cover to variations in meteorology. The meteorological analysis in Chapter III is further motivated by its potential to provide new diagnostic information on model cloud parameterizations. In Chapter IV, two examples are discussed in which model simulations are used to separate aerosol from meteorological impacts. This is complemented by a comparison of model cloud sensitivities to the observations of Chapter III, which provides new insight into the cloud parameterizations used in the simulations. The dissertation is concluded with a summary of the findings and a brief discussion of the potential for continued investigation.

II Meteorological bias in satellite estimates of aerosol-cloud relationships

II.1 Abstract

Several recent studies have reported a substantial correlation between satellite retrievals of aerosol optical depth (AOD) and cloud fraction, which is ascribed to an aerosol microphysical mechanism. Another possible explanation, however, is that the history of meteorological forcing controls both AOD and cloud fraction. The present study examines the latter hypothesis by comparing meteorological conditions along parcel back-trajectories for cases of large and small AOD and cloud fraction. Cloud and aerosol observations are obtained from the MODIS instrument aboard Terra, and meteorological information is obtained from ECMWF analyses. For continuity with previous investigations, the analysis focuses on the stratocumulus cloud region of the Northeast Atlantic during June through August 2002, the season of maximum cloud cover. Results show that scenes with large AOD and large cloud fraction had origins closer to Europe and experienced greater lower tropospheric static stability (LTS) during the past 2-3 days than did scenes with small AOD and small cloud fraction. Controlling for variations in LTS reduces the dependence of cloud fraction on AOD by at least 24%. We conclude

that meteorological forcing must be accounted for in assessing aerosol impacts on cloud forcing, and that doing so requires a Lagrangian analysis of parcel histories.

II.2 Introduction

It is well established that stratocumulus clouds found over eastern ocean basins exert a strong cooling effect on the Earth's climate, primarily due to their weak greenhouse effect, extensive coverage, and high albedo relative to the ocean. Anthropogenic aerosols can impact cloud properties by increasing the number of nuclei on which cloud drops form. If cloud water remains constant, an increase in the cloud drop population will result in smaller droplets and consequently, a higher albedo (Twomey, 1977). Smaller droplets are also less likely to collide and coalesce, which may inhibit precipitation formation and thus increase cloud water and cloud fraction (Albrecht, 1989) However, in some situations increased entrainment drying, a consequence of decreased precipitation, can be sufficient to offset the increase in cloud water (Ackerman et al., 2004). The effects on albedo and cloud water are known as the first and second aerosol indirect effects, respectively. Due to the high albedo of stratocumulus clouds, small changes due to aerosols have the potential to strongly perturb the Earths energy balance. It is therefore important to quantify the response of stratocumulus clouds to changes in aerosol burden.

The present investigation is focused on the relationship between cloud cover and aerosols. Numerous researchers have used remote sensing data to investigate this relationship on regional and global scales (*e.g.*, Matheson et al., 2005; Kaufman et al., 2005a; Myhre et al., 2007). These investigations are consistent in noting a significant relationship between aerosol optical depth (AOD) and cloud fraction (CF). With specific regard to the the North Atlantic, Kaufman et al. (2005a) use MODIS observations to associate a 0.1 increase in AOD with a cloud

cover increase that ranges from 0.06 to 0.12. Similarly, Matheson et al. (2005) use retrievals from the Advanced Very High Resolution Radiometer (AVHRR) to find AOD-CF sensitivities that depend strongly on geographic region, but whose average shows a 0.04 increase in cloud cover for a 0.1 increase in AOD. Finally, Myhre et al. (2007) show that the MODIS AOD-CF sensitivity is also a strong function of AOD, indicating that clean clouds are more strongly influenced by changes in aerosol. Specifically, for AOD<0.2 Myhre et al. (2007) show a cloud cover increase of 0.18 to 0.22 for a 0.1 increase in AOD. Although they do not isolate the results by cloud regime, the results of Myhre et al. (2007) show similar AOD-CF sensitivities in the Northern and Southern regimes of both the Pacific and Atlantic oceans.

All of the above results suggest a strong impact on shortwave cloud forcing resulting from changes in cloud cover due to aerosol impacts. Using the observations cited above, Kaufman et al. (2005a) estimate that the instantaneous forcing resulting from aerosol-induced changes in cloud cover ranges from -2 to -5 W m^{-2} for each 0.1 increase in AOD. Given the consistency between the observational results in the Atlantic and Pacific ocean basins, the sensitivity of cloud forcing estimated by Kaufman et al. (2005a) is likely to be representative of that observed in other ocean basins. Using a global model, Lohmann et al. (2006) find a total indirect forcing (first and second indirect effects) over the North Atlantic that is within the range cited by Kaufman et al. (2005a). Radiative forcings of this magnitude represent significant perturbations to the energy budget, and thus warrant further investigation. Specifically, since correlation does not imply causation, such results cannot simply be used to attribute cloud variations to aerosol microphysical impacts. Alternative explanations must first be excluded, including measurement biases, sampling biases, and systematic variations in meteorological state.

As a specific example, geographic variations in climatology, if unaccounted for, can contribute to erroneously large correlations between aerosols and clouds.

This can be seen, for example, in the subtropical North Atlantic, where high concentrations of pollutants emitted from Europe coincide with a stratocumulus regime. In the central Atlantic, where cloud cover is climatologically low, pollutant concentrations are significantly less compared to the eastern Atlantic. As a result, a correlation that includes both of these regions will reflect climatological variations instead of aerosol impacts. Similarly, seasonal differences must be accounted for before an aerosol effect can be estimated.

A major challenge in aerosol-cloud studies is to quantify the variations in cloud properties independent of large-scale meteorological forcing. For example, large-scale convergence could increase cloudiness as well as concentrate aerosols, thus producing an apparent correlation between aerosol and cloud with no direct physical connection. Aerosol indirect effects can generally only be accurately estimated when meteorological variations are held constant. This amounts to estimating the partial derivative of each cloud property with respect to changes in aerosol by controlling for variations in dynamic and thermodynamic state. Since, for example, stratocumulus clouds respond differently to dynamics than trade cumuli, a proper analysis of aerosol-cloud impacts necessitates differentiation by cloud type (Xu et al., 2007). Most important among these considerations, aerosols and clouds can be correlated when both are driven by a similar change in dynamics. For example, large-scale convergence would be expected to increase cloudiness as well as concentrate aerosols. In general, aerosol indirect effects can only be estimated when meteorological variations are held constant. This requires separate consideration of different cloud types, accounting for differences in climatology, and the monitoring of relevant meteorological quantities.

An important consideration is that concurrent meteorological conditions are not sufficient to fully account for cloud state. Klein et al. (1995) demonstrated that low-level cloud amount correlates better with sea surface temperature (SST) and 750 hPa temperature 24 to 30 hours upwind than with the local SST and

750 hPa temperature. These results imply that stratocumulus clouds have memory, or that the history of meteorological forcing is an important determinant of cloud state. This can be interpreted in terms of the time-scale for boundary layer adjustment, as governed by surface fluxes, entrainment and subsidence rates, and temperature and humidity profiles of the free troposphere. Accounting for previous meteorological impacts necessitates a Lagrangian perspective on cloud evolution. Parcel trajectories permit a retrieval of the history of cloud forcings as well as a simple diagnosis of meteorological differences between cloud states.

The present study introduces new techniques to assess cloud sensitivities to aerosols and to examine the impact of meteorology on the observed relationship between AOD and cloud fraction. Parcel back-trajectories are used to identify the previous locations and movement of air within and above the boundary layer at the time of the cloud and aerosol measurements. The combination of reanalysis parameters and back-trajectory information is then used to determine the previous large-scale meteorological conditions experienced by the boundary layer. Comparison of cloudiness for trajectories with differing AOD but similar meteorology enables a more accurate estimation of the sensitivities of cloud properties with respect to aerosols.

II.3 Methods

The analysis is focused on the subtropical Northeast Atlantic (25-34N, 35-20W, shown in Figure II.1) during June through August 2002, chosen to correspond with the location and season of maximum cloud coverage by stratocumulus. The domain is chosen to be farther north than the domain of Kaufman et al. (2005a) in order to avoid the heavy dust region west of Africa, and farther west than the domain of Matheson et al. (2005) in order to focus on remote marine clouds. The conclusions of this study are not sensitive to the exact location of the region

Table II.1: MODIS data products used.

Dataset	MOD08_D3 C005, 1°x1° regular grid
Variables	Effective_Optical_Depth_Average_Ocean_QA_Mean
	Angstrom_Exponent_1_Ocean_QA_Mean
	Cloud_Fraction_Day_Mean
	Cloud_Effective_Radius_Liquid_QA_Mean
	Cloud_Top_Temperature_Day_Mean

considered. Reasons for the specific choice of study region are discussed in detail below.

Satellite observations of cloud and aerosol were obtained from the Moderate Resolution Imaging Spectroradiometer (MODIS) aboard Terra as daily gridded averages (MOD08_D3, Collection 005) at a resolution of 1°x1°. MODIS measures atmospheric radiances in 36 spectral bands, ranging from 0.415 to 14.235 μm (King et al., 2003). Along with its high spatial resolution (250m-1km) and broad swath (2300 km), the high spectral resolution of MODIS permits daily retrievals of a wide variety of atmospheric properties. Table II.1 lists the MODIS data products used in this study.

One shortcoming of MODIS AOD is that retrievals cannot be made in the presence of clouds. Consequently, cloud observations and aerosol observations come from different locations within a 1°x1° grid box. Nevertheless, since Anderson et al. (2003) show that aerosol variations have length scales between 40 and 400km, we believe that MODIS AOD from clear areas is largely representative of aerosol conditions in neighboring cloudy areas. Another limitation of MODIS AOD is that it does not provide information on the vertical distribution of aerosol. However, an examination of preliminary Cloud-Aerosol Lidar and Infrared Pathfinder Satellite Observation (CALIPSO) data for June through August of 2006 indicates that aerosol plumes are most common below 2 km in altitude (not shown). Thus, the aerosol particles revealed by MODIS are likely to be relevant to stratocumulus

clouds.

Meteorological parameters are obtained from the European Centre for Medium-Range Weather Forecasting (ECMWF) operational analyses. The data is available from the National Center for Atmospheric Research (NCAR) data archive, regridded from T106 spectral resolution with 21 vertical levels. ECMWF is chosen to provide meteorological fields based on its superior performance in simulating boundary layer development and evolution (Stevens et al., 2007). In contrast with the reanalysis, the ECMWF operational analysis includes the most recent model improvements and newly available observations. The analysis variables used in this study are chosen to minimize model influence and maximize relevance to the question at hand.

Parcel trajectories are computed using The Hybrid Single Particle Lagrangian Integrated Trajectory (HYSPLIT) model. A product of the National Oceanic and Atmospheric Administrations (NOAA) Air Resources Laboratory (ARL), HYSPLIT computes three-dimensional parcel trajectories using a simple advection scheme and gridded meteorological fields as input. Both to maintain internal consistency and make use of the best data available, we use ECMWF analysis winds, temperature, heights and surface pressure as input to HYSPLIT calculations. HYSPLIT trajectories are initialized at 500m and 2000m in order to track the motions of air parcels both above and within the boundary layer. Trajectories are calculated out to 72 hours prior to the time of observation, chosen to extend beyond the autocorrelation scale of cloud observations in the region while maintaining reasonable predictive skill in trajectory position.

Stohl et al. (1998) provides an excellent review of trajectory calculations and an assessment of potential sources of error, of which a number of important points should be noted. Trajectory errors primarily stem from issues associated with spatial and temporal resolution, interpolation errors, and errors in the wind field. The difficulty of assessing such errors is compounded by the fact that com-

putational errors must be separated from meteorological variations, since both will contribute to a separation of trajectories. In making such assessments, meteorological variations are likely to lead to overestimates of trajectory error. Given this caveat, studies attempting to quantify position uncertainty in trajectories generally center on a position uncertainty of 20% of the distance travelled. The mean displacement for the 72 hour back-trajectories is 1000 km. This implies a position uncertainty of approximately 200 km at the trajectory endpoints. Apart from the synoptic focus of this study, we consider the trajectory position uncertainty to be another reason that low-resolution satellite fields are an appropriate choice for the analysis. It is also worth noting that errors associated with trajectory position are unlikely to be systematically biased and will thus be reduced by averaging numerous trajectories.

Harris et al. (2005) showed that the specific computational scheme used to estimate trajectories contributes negligibly to the error, and that the dominant sources of error stem from uncertainties in the wind field and the vertical transport method. Prior work has established that 3-dimensional trajectories are the most accurate (Stohl and Seibert, 1998). Stohl and Seibert (1998) show that trajectory calculations perform well in undisturbed conditions, and that the majority of error arises in the presence of fronts, where winds and transport are poorly resolved. Focusing on stratocumulus clouds thus conveniently avoids the dominant sources of error.

An important caveat to the use of trajectories is that air parcels do not travel adiabatically along wind streamlines, but instead mix with their environment. This is particularly true in the planetary boundary layer, where parcel trajectories more closely represent an estimated path of a plume centroid than a unique parcel path. However, the proposed analysis is focused on the impact of large-scale meteorological forcings on clouds and not on the mesoscale interactions between dynamics and clouds, nor is this study predicated on the conservation

of tracer mass. As a result, use of low-resolution, large-scale meteorological and satellite fields provides an appropriate measure of the forcing while also conveniently accounting for parcel dispersion. In addition, tests have been performed by running multiple adjacent trajectories for each observation. These have shown that there is very little impact on results, indicating that in the regimes observed the length scale of meteorological variations is large enough that mixing can be neglected.

Scene selection was designed to maximize the number of aerosol and low-level cloud observations while excluding high-level clouds, dust, and overly polluted scenes. Mid- and high-level cloud observations were screened out by rejecting all cases with a grid box mean cloud-top pressure less than 640 hPa, or where ice particles were detected in any of the nine adjacent grid boxes. Since dust has the potential to contaminate measurements due to ambiguities in distinguishing dust from clouds (Gao et al., 2002) and to complicate aerosol-cloud interactions through infrared absorption, our study region was chosen to avoid regions of heavy dust influence. The primary extent of Saharan dust influence was identified from Aerosol Index maps obtained from the Total Ozone Mapping Spectrometer (TOMS) and the Advanced Very High Resolution Radiometer (A. Zhu, personal communication, 2006). Solar absorption by dust and pollution plumes (semi-direct effect) can also impact cloud dynamics. In order to minimize this effect, we limited the analysis to observations of AOD less than 0.3. AOD retrievals from the Aerosol Robotic Network (AERONET) site on the Azores islands (38.5°N, 28.6°W, site maintained by Dr. Brent Holben) show that greater than 98% of AOD retrievals are less than 0.3. MODIS retrievals over the present study region also confirm that limiting the AOD observations to less than 0.3 does not significantly impact the sampling. Further motivation for this choice stems from the potential for comparison with the results of Kaufman et al. (2005a) and Myhre et al. (2007), who report that cloud cover is most sensitive to aerosol when AOD is less than

0.2. Finally, regarding MODIS retrievals of AOD, it is possible that ambiguities in distinguishing clouds from clear sky in the presence of aerosols may lead to an artificial positive correlation between retrieved AOD and retrieved cloud fraction (Charlson et al., 2007; Matheson et al., 2005). Although this issue is mitigated by the sample selection outlined above as well as the rigid cloud screening of MODIS measurements of AOD (Kaufman et al., 2005b), it is possible that some bias remains.

As discussed in the introduction, it is important to avoid sampling biases associated with geographic and seasonal variations in aerosols and cloudiness that could artificially increase the apparent correlation between the two. In order to eliminate this possibility, the analysis region was divided into 3°x3° grid boxes. The same number of cases were selected from each grid box for each month, thus ensuring unbiased sampling throughout the domain.

II.4 Results

Table II.2 shows linear correlations between AOD and several cloud properties over the region considered in this study. Correlations were computed from daily anomalies obtained by subtracting the mean for each 1°x1° grid box for each month, in order to remove geographic and seasonal biases. AOD and cloud fraction are substantially correlated, consistent with the results of Kaufman et al. (2005a). However, only a very weak relationship exists between AOD and cloud droplet effective radius, an indication that variations in dynamical factors are impacting cloud response. Similarly, there is no aerosol microphysical mechanism by which AOD could strongly influence lower tropospheric static stability (LTS, defined as $\theta_{700} - \theta_{SFC}$), a parameter that is symptomatic of variations in the large-scale meteorological state. The strong correlation with LTS is of particular interest because it is closely connected to variations in low-level cloud fraction (Klein and Hart-

Table II.2: Correlation of aerosol optical depth (AOD) with cloud fraction (CF), droplet effective radius (R_E), liquid water path (LWP), lower tropospheric static stability (LTS), and cloud-top pressure (CTP), showing 95% confidence limits in parentheses.

Variable	Correlation w/ AOD (95% conf. lim.)
CF	0.40 (.36, .44)
R_E	-0.13 (-.18, -.09)
LWP	-0.005 (-.05, .04)
LTS	0.26 (.22, .30)
CTP	-0.29 (-.33, -.25)

mann, 1993). While by no means precluding an aerosol microphysical effect on cloudiness, these results suggest that the observed correlations are due in part to other factors.

In order to explore the possibility that meteorological variations are contributing to the aerosol-cloud correlations in Table II.2, we analyzed the subset of cases that contribute most to the observed AOD-cloud fraction relationship. Specifically, we selected the daily 1°x1° observations that fall within the upper terciles of both AOD and cloud fraction, again selecting data uniformly from each 3°x3° grid box and month. For convenience, these are called LCLA cases: Large Cloud fraction, Large Aerosol optical depth. Similarly, we selected the observations that corresponded to the opposite extreme, SCSA: Small Cloud fraction, Small Aerosol optical depth. Although our results do not depend on selecting only the more extreme values in cloud fraction and AOD, doing so increases the signal to noise ratio, thus simplifying the diagnosis of dominant parameters. Given the selected observations, back-trajectories were then calculated for the date and location of each contributing daily 1°x1° observation. Figure II.1 shows the altitude and position of the mean trajectories, averaged over all LCLA and all SCSA cases. The mean trajectories are plotted relative to the center of the study region, each representing the average of approximately 45 trajectories. The boundary of the

study region is also plotted, and visible in the southeast corner are the Canary Islands and a small portion of the continent of Africa. Two important conclusions can be drawn from Figure II.1. First, LCLA cases tend to have origins closer to Europe and thus closer to pollution sources. Second, consideration of parcel histories provides new information for differentiating between observations.

In Figure II.1 and all subsequent plots, error bars indicate the 95% confidence interval determined using a bootstrap method. The bootstrap method works by sampling with replacement from the pool of trajectories in a particular composite. Autocorrelation between observations is accounted for by including all trajectories that are autocorrelated with the one selected. Using a simple compositing scheme the spatial and temporal autocorrelation of cloud fraction are estimated at approximately 230 km and less than one day, respectively. A mean is computed from the randomly selected sample and the iteration is repeated 1000 times. This permits an estimation of the probability distribution of outcomes, from which we obtain our 95% confidence limits.

Comparison of atmospheric properties at locations along the LCLA and SCSA trajectories permits an analysis of the meteorological differences between the two. Figure II.2 shows the mean values of AOD, cloud fraction, droplet effective radius (R_E), and LTS averaged over the LCLA and SCSA trajectories for the three days prior to the time of observation. By construction we see that large cloud fraction is associated with large AOD and small cloud fraction is associated with small AOD. Moreover, R_E is generally smaller for larger AOD, as would be expected if aerosol particles act as cloud condensation nuclei. There is also a large difference in LTS between the LCLA and SCSA cases that becomes more significant as we look back into the history of each parcel. The greater distinction in LTS for prior days indicates that an examination of atmospheric conditions only at the time of the cloud and aerosol observations is not sufficient to fully characterize the meteorological forcing experienced by the clouds and aerosols. In fact, the

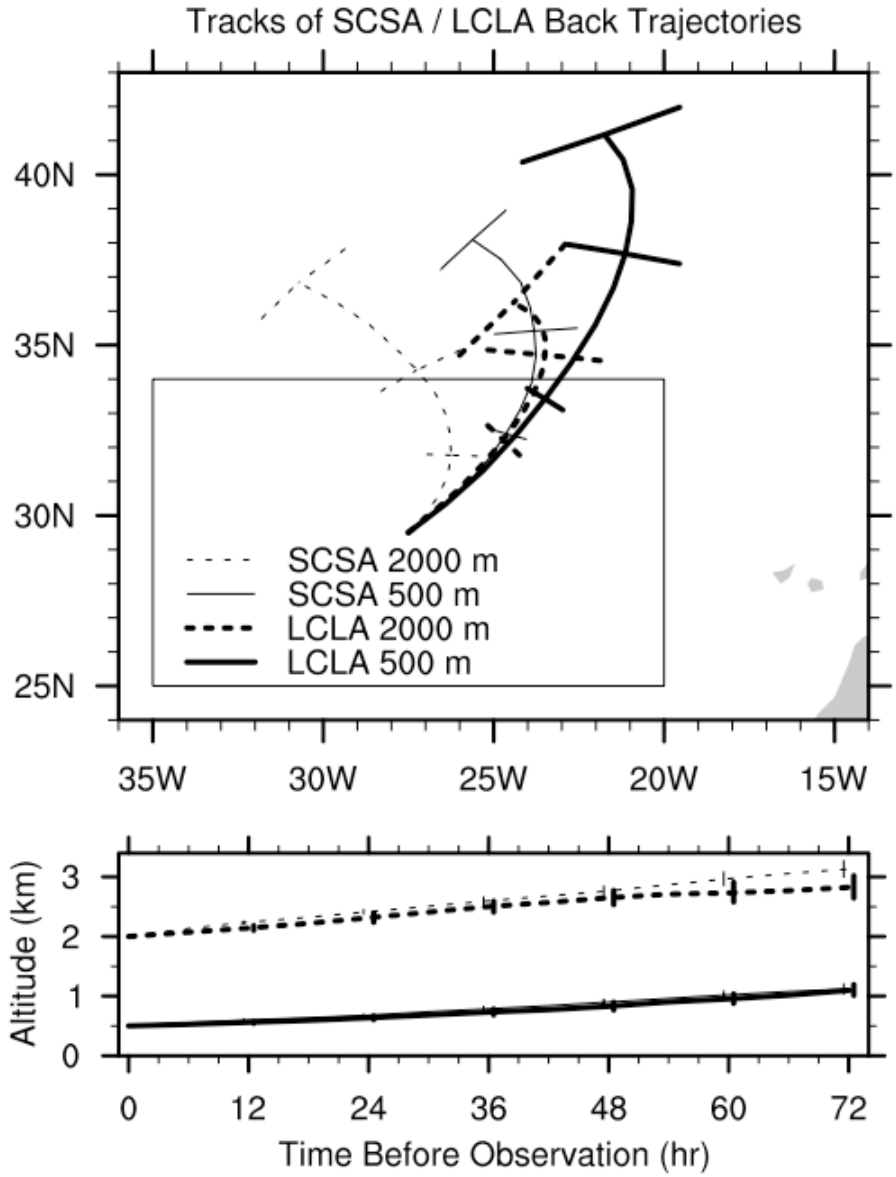

Figure II.1: Geographic position and altitude of the mean large cloud fraction, large AOD (LCLA, thick lines) and small cloud fraction, small AOD (SCSA, thin lines) trajectories. The solid lines represent trajectories that are initiated within the boundary layer, at 500m, and the dashed lines represent trajectories that begin at 2000m. Error bars indicate 95% confidence intervals for parcel positions. The plot also shows an outline of the study region as well as the Canary Islands and the Northwest tip of the African continent.

correlation between cloud fraction and LTS averaged over the previous 48 hours is 0.26 whereas the correlation between cloud fraction and LTS at the observation time is only 0.07.

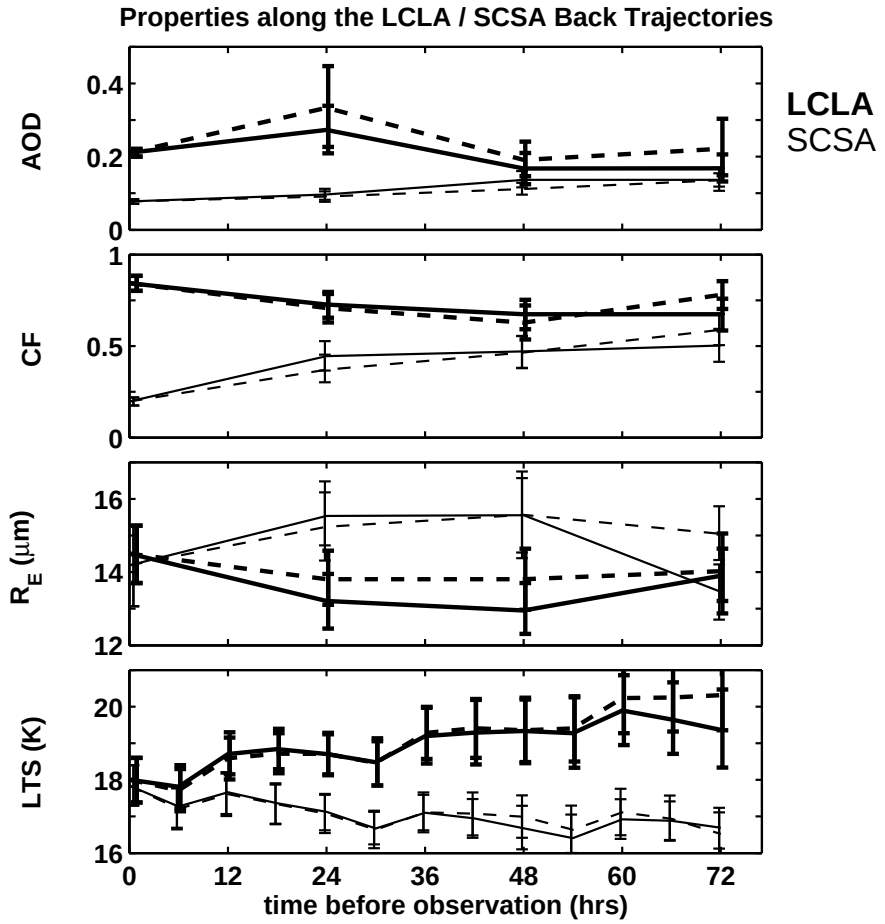

Figure II.2: Average AOD, cloud fraction, R_E, and LTS along the LCLA (thick lines) and SCSA (thin lines) back trajectories displayed in Figure II.1. Error bars indicate 95% confidence intervals.

The evidence in Figure II.2 implies that covariation of LTS and AOD is artificially increasing the correlation between cloud fraction and AOD. However, it is possible that entire difference in LTS is simply attributable to the differences in cloud fraction as constrained by the LCLA/SCSA sampling. A first test of this result must therefore verify that extrema in AOD are both associated with

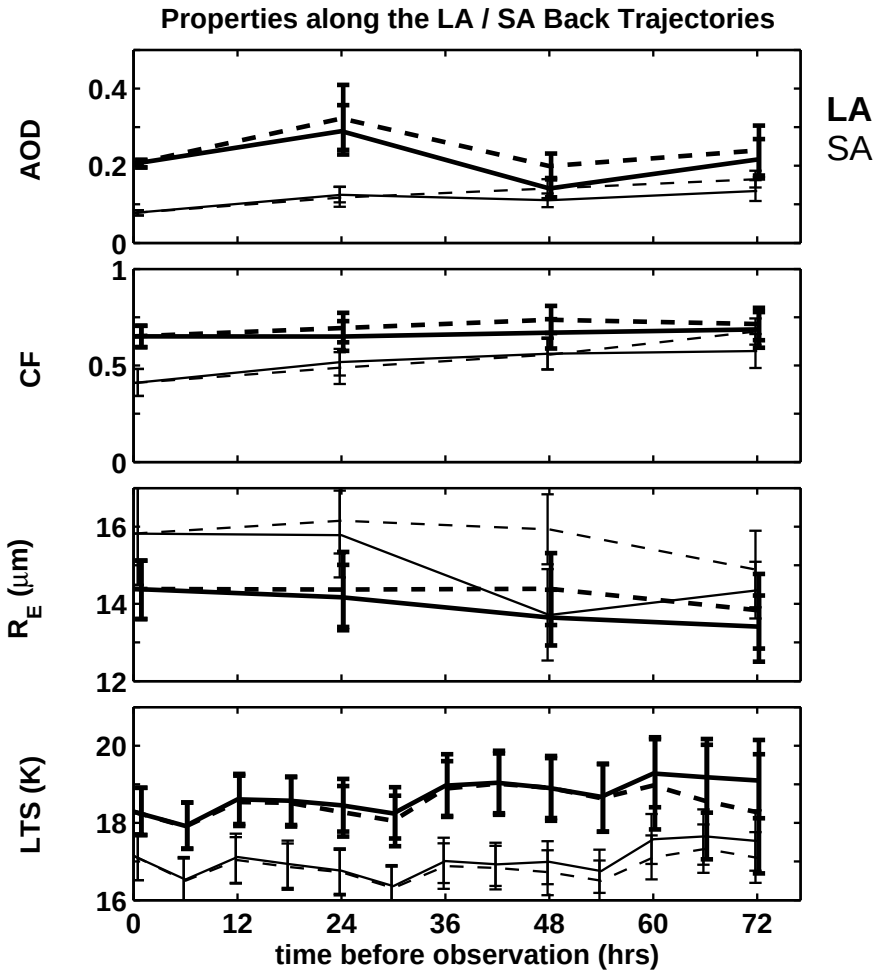

Figure II.3: As in Figure II.2, except for large AOD (LA, thick lines) and small AOD (SA, thin lines) back trajectories.

differences in cloud fraction and LTS. Figure II.3 shows the mean AOD, CF R_E, and LTS for cases that have been selected from the upper (LA) and lower (SA) terciles in aerosol optical depth. These show a decreased difference in cloud fraction, as expected given a lack of constraint on cloud cover in the compositing. Despite this, significant differences in cloud fraction remain, and the differences in LTS are significant and remain so throughout the history of the trajectories. This confirms the result for the LCLA/SCSA trajectories that a systematic covariation is present between observations of LTS and AOD.

To quantify this covariation, we resampled from the data, taking high and low aerosol observations while keeping LTS constant. This allows us to make an LTS-independent estimate of aerosol impacts on cloud properties. For each daily 1°x1° observation, the average along-trajectory LTS was computed over the 48 hours prior to the observation time. Large and small AOD cases were selected from the subset of samples for which the 48-hour mean LTS was closest to its median value. Figure II.4 displays the mean trajectories for cases of MSLA (median stability, large AOD) and MSSA (median stability, small AOD). As before, each average represents the mean of approximately 45 individual trajectories.

An examination of mean LTS along the MSLA and MSSA trajectories demonstrates that the sample selection has successfully constrained LTS to be nearly identical across cases of large and small AOD. Although the difference in AOD between MSLA and MSSA is nearly as large as that in Figure II.2, the differences in cloud fraction and R_E are significantly smaller. Since this change in outcome is solely the result of a constraint on LTS, we conclude that a substantial fraction of the observed aerosol-cloud correlation is caused by systematic variations in lower tropospheric stability rather than aerosol microphysical effects. Similar results are obtained if estimated inversion strength (EIS) (Wood and Bretherton, 2006) is used instead of LTS.

Since the preceding results considering median stability are based on a small fraction of the data, we recompute an estimate of the sensitivity of cloud fraction to AOD, this time using a majority of the data. The cloud sensitivity without correction for LTS was obtained by using the original daily 1°x1° values and compositing the data into terciles of aerosol optical depth (LA/SA). The sensitivity is estimated by dividing the composite difference in cloud fraction by the composite difference in AOD. In this case, a 0.1 increase in AOD is associated with a 0.18 increase in cloud fraction over the summertime subtropical Northeast Atlantic. The confounding influence of LTS within AOD variability was then

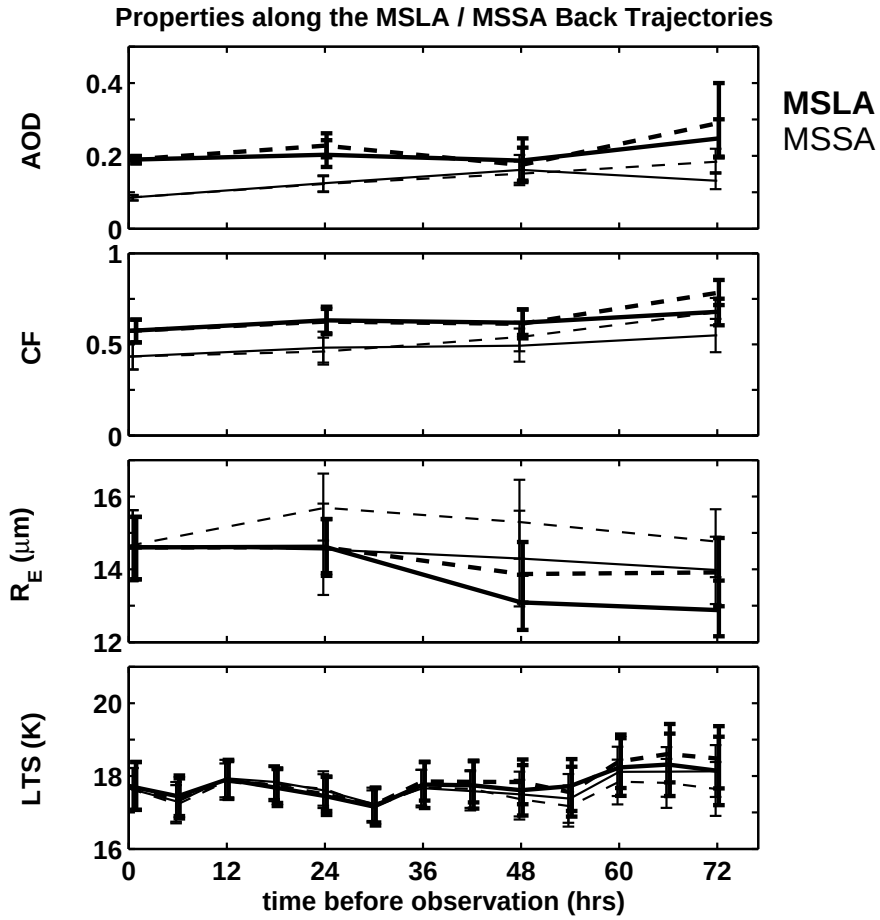

Figure II.4: As in Figure II.2, except for median LTS, large AOD (MSLA, thick lines) and median LTS, small AOD (MSSA, thin lines) back trajectories.

removed by taking the composite sensitivity for AOD observations that lie within the middle tercile of LTS. As for the MSLA/MSSA cases, the LTS was averaged over the 48 hours prior to the observation time in order to control for the history of meteorological conditions. The resulting coefficient represents the sensitivity of cloud fraction to changes in AOD for median values of LTS. Now, a 0.1 increase in AOD is associated with only a 0.14 increase in cloud fraction, a value that is 24% smaller than the coefficient when LTS is not taken into account.

The true sensitivity is likely to be even weaker than 0.14 cloud fraction per 0.1 AOD for three reasons. The first is that LTS is probably not the only me-

teorological parameter correlated with both cloud fraction and AOD. Were these additional meteorological effects to be removed, we expect that AOD would explain even less independent variance in cloud fraction. The second reason is that the ECMWF analysis is an imperfect measure of the true atmospheric state. While we have no reason to believe that errors in the analysis are systematically related to variations in AOD, random errors will reduce the apparent correlation between meteorological parameters and AOD. This will lead to an underestimate of the variance removed from AOD by compositing on parameters like LTS and consequently lead to an overestimate of the variance in cloud fraction explained by the AOD residual. Finally, due to ambiguities in defining cloud boundaries, hygroscopic growth of aerosols in areas of elevated humidity near clouds is likely to cause a significant correlation between cloud fraction and aerosols that does not reflect microphysical changes in cloud properties (e.g., Charlson et al., 2007).

II.5 Conclusions

This study presents a new technique for distinguishing the impacts of past meteorological forcing from the influence of aerosol on the development of boundary layer clouds. Computed parcel back-trajectories are used to evaluate the origin and atmospheric conditions previously experienced by observed low-level clouds. The method was applied to the stratocumulus region of the subtropical northeast Atlantic, where recently published studies have presented evidence for a substantial correlation between satellite-retrieved aerosol and cloud fraction. We found aerosol-cloud relationships similar to those reported by prior studies but additionally discovered that both aerosol amount and cloud fraction covaried with the static stability of the lower troposphere during the previous several days along the parcel back trajectories. Controlling for variations in static stability reduced the estimated sensitivity of cloud fraction to aerosol by at least 24%, which repre-

sents a significant correction to the indirect forcing estimates of previous studies. Our results do not preclude the existence of a measurable aerosol impact on cloud properties, but they do indicate that sensitivity estimates based solely on satellite observations of aerosol burden and cloudiness grossly overestimate the magnitude of the indirect effect. It is essential to take into account the meteorological history experienced by clouds and aerosols.

II.6 Acknowledgements

Chapter II, in part, is a reprint of the material as it appears in the following publication: Mauger, G. S., and J. R. Norris, Meteorological bias in Satellite estimates of Aerosol-Cloud Relationships, Geophysical Research Letters, Vol. 34, L16824, doi:10.1029/2007GL029952, 2007. The dissertation author was the primary investigator and author of this paper.

III Lagrangian analysis of subtropical cloud sensitivities

III.1 Abstract

This study presents findings from the application of a new Lagrangian method used to evaluate subtropical cloud sensitivities in the northeast Atlantic. Satellite retrievals from MODIS, CERES, QuikScat, and SSM/I provide measurements of cloud properties as well as atmospheric state. These are complemented by meteorological fields from the ECMWF operational analysis model. Parcel back trajectories are used to account for the influence of previous meteorological conditions on cloud properties. Observations are composited by cloud fraction and mean trajectories are used to evaluate differences between each composite.

Systematic differences in meteorological conditions are found to extend through the full 72 hour trajectories, confirming the need to account for cloud history in assessing impacts on cloud properties. The findings associate increased stability, cooler SSTs, a more humid free troposphere, stronger cold advection, and a decrease in divergence with an increase in cloud fraction. Significantly, in the early part of the trajectories this association is reversed for several of the above quantities. In particular, surface divergence, cold advection, and surface fluxes are seen to be larger for the small cloud fraction cases at 72 hours prior to the time of observation. Since this is associated with a drier yet deeper boundary layer as

well as consistently warmer SSTs, it is suggested that this is symptomatic of a decoupling of the boundary layer.

III.2 Introduction

The subtropical cloud regimes found over eastern ocean basins are responsible for a significant cooling effect on the Earth's climate. As a result, small perturbations to these clouds have the potential to significantly impact the Earth's energy balance. An improved understanding of boundary layer cloud sensitivities is necessary to estimate the magnitude of aerosol-cloud effects, improve current model parameterizations, and properly assess the consequences of climate change.

The motivations for investigating the relationship between cloud forcing and meteorology are manifold. In Chapter II we investigated the impact of aerosols on cloud properties. In doing so, we found evidence that variations in the dynamical conditions in which clouds form significantly impact the observed relationship between aerosols and clouds. This is consistent with other studies, both in-situ and remotely sensed (e.g.: Twohy et al., 2005; Schwartz et al., 2002). However, this does not mean that cloud properties are necessarily independent of aerosols. Instead, we can only conclude that the aerosol signal is difficult to distinguish from the "noise" that exists due to meteorological variations. Consequently, in order to uncover the sensitivity of cloud radiative forcing to aerosols it is necessary to quantify and constrain the impact of meteorology. This requires an investigation of the dominant dynamical sensitivities of subtropical clouds.

Another reason to quantify cloud dynamical sensitivities is to provide improved constraints on model parameterizations of boundary-layer clouds. Numerous studies highlight parameterizations of boundary-layer clouds as the chief source of uncertainty in climate projections (*e.g.:* Bony and Dufresne, 2005; Soden and Held, 2006; Meehl et al., 2007). Bony and Dufresne (2005) emphasize that

accurate model representation of clouds is not sufficient: the *sensitivity* of cloud properties to environmental conditions must also be correctly simulated. They add that the sensitivity of cloud radiative forcing alone is an insufficient constraint since it can result from compensating errors. Cloud parameterizations are typically assessed through comparison of monthly mean climatologies or trends in large-scale averaged fields. In a coupled system that operates on multiple spatial and temporal scales, this approach is well justified. The present study provides a complement to this approach by instead focusing on synoptic-scale sensitivities. The Lagrangian approach is designed to separately quantify the impacts of each forcing parameter on cloud fraction. As discussed in the following chapter, these synoptic-scale sensitivities can provide detailed diagnostic information for use in model evaluation. In this chapter we develop the observational basis for this comparison.

In the following discussion, the terms "meteorology" and "dynamics" are used interchangeably to refer to both the large-scale circulation of the atmosphere and its thermodynamic structure. Prior work indicates that the dynamical forcing of stratocumulus clouds occurs at scales larger than the mesoscale (Rozendaal and Rossow, 2003; Lewis et al., 2004), meaning it is feasible to assess dynamical impacts using large-scale datasets. Norris and Iacobellis (2005) combined surface observations with meteorological reanalysis data to show that the dominant parameters associated with cloud properties are vertical velocity, advection, and SST. An earlier study by Klein et al. (1995) combined several decades of surface observations from the Northeast Pacific with radiosonde data and large-scale observations. They showed that low-cloud amount correlates better with SST and upper air temperature 24 to 30 hours upwind than with the local SST and upper air temperature. These results imply that stratocumulus clouds have memory, or that the history of forcings is an important determinant of cloud state. This can be interpreted in terms of the time scale for boundary-layer adjustment, as governed by surface fluxes, entrainment and subsidence rates, and temperature and

humidity profiles of the free troposphere. Accounting for previous meteorological impacts necessitates a Lagrangian perspective on cloud evolution. Parcel trajectories permit a retrieval of the history of cloud forcings, as well as a simple diagnosis of meteorological differences between cloud states. The present work uses back trajectory information in order to quantify the influence of dynamics on cloud fraction.

Ultimately, the goal of this study is to isolate the causal relationships that relate atmospheric state to cloud forcing. Prior work has established the importance of understanding cloud meteorological sensitivities, both from the perspective of climate simulations and for obtaining unbiased estimates of the indirect forcing. The present work employs the trajectory analysis method described in Chapter II to quantify subtropical cloud sensitivities over the Northeast Atlantic.

III.3 Conceptual Picture

The intent of this study is to consider the relationship between large-scale meteorological state and cloud radiative forcing. Our intent is to provide cloud sensitivities at scales that are relevant to the global energy balance, while also providing quantities that offer straightforward translation as model diagnostics. Since the full spectrum of boundary-layer cloud types can inhabit the same region, differentiating between these would limit the applicability of these results. Fortunately, the transition from stratocumulus to trade cumulus is continuous rather than discrete, and simple bulk-model boundary layer concepts provide a useful conceptual framework for evaluating variations within and between these cloud regimes.

Subtropical clouds are typically found in subsiding regimes over regions of cold sea surface temperature. These conditions are responsible for the stable environmental lapse rates common to stratocumulus regions. Mixing, driven by

cloud-top radiative cooling, maintains a neutrally stable boundary layer profile while simultaneously creating a sharp capping inversion, effectively decoupling the layer motions from the free troposphere. Layer budgets of heat and moisture are governed by a balance between surface fluxes of heat and moisture and the combination of entrainment fluxes and radiative cooling at cloud top. The mass budget is represented by the change in layer depth; the result of a balance between the subsidence rate and entrainment.

The well-mixed assumption breaks down when the cloud layer becomes decoupled from the surface layer. This can be seen as a consequence of the contrasting moisture between ascending and descending parcels in the cloud layer, which result in a stable layer just below cloud base (Schubert et al., 1979; Bretherton and Wyant, 1997). As the moisture flux to the cloud layer increases, convective energy fluxes in the cloud layer increase and the sub-cloud inversion becomes more pronounced. When the negative buoyancy generated at cloud top can no longer maintain the negative buoyancy fluxes below cloud, the boundary layer becomes decoupled, often giving way to surface-driven cumuliform clouds. In this transition region, cumulus clouds can act to provide the moisture flux necessary to maintain the stratiform cloud deck at the boundary layer top (*e.g.:* Albrecht et al., 1995). Eventually, however, the moisture flux is insufficient to counteract entrainment drying of the stratiform deck and the boundary layer gives way to a trade cumulus regime. This provides a simplified model for the evolution of a cloud deck through deepening over a warming SST gradient. Other manifestations of boundary-layer cloud variations can result from different changes in forcing, including variations in the subsidence rate, variations in free-tropospheric moisture, and the onset of drizzle.

A simple model for the formation and maintenance of boundary layers was first developed by Lilly (1968). Budget equations are represented below for mass (III.1), energy (III.2), and moisture (III.3) (variable definitions are listed in

the list of symbols included at the beginning of the dissertation). They form the bulk, or vertically integrated, formulation of the stratocumulus-topped boundary layer. It is important to note that these equations simply constrain the vertical integral, and not the shape of the boundary layer profile, and are therefore not exclusive to well-mixed boundary layers. The formulation is particularly useful for assessing the impacts of large-scale meteorological forcings on cloud state. From equations III.1 through III.3, we can identify a number of meteorological variables that are likely to influence cloud state.

$$\frac{Dh}{dt} = w_E + w_S \tag{III.1}$$

$$\frac{Ds}{dt} = w_E \cdot (s_+ - \bar{s})/h - C_T V(\bar{s} - s_0) - F_{RAD} + L \cdot P \tag{III.2}$$

$$\frac{Dq}{dt} = w_E \cdot (q_+ - \bar{q})/h - C_T V(\bar{q} - q_0) - P \tag{III.3}$$

III.4 Methods

Consistent with the previous chapter, the analysis is focused on the Northeast Atlantic. Shown in Figure III.1, the study region is larger than that of Chapter II, extending from 24N to 40N and 35W to 10W. These bounds are chosen to include all regions influenced by subtropical clouds while avoiding the heavy dust region west of Africa and the predominance of extratropical cyclones to the North. In order to maximize the statistical significance of the results, observations are obtained for June through August 2000-2006.

Although other stratocumulus regions are known to have more uniform cloud cover and more persistent cloud decks, we choose to focus our study on the Northeast Atlantic for two reasons. The first is historical: the current study builds on the work of Chapter II by investigating the dependence of low-level cloud fraction on meteorology. Second, our goal is not to exclusively study the dynamics of stratocumulus but to study the sensitivities of low-level cloud forcing

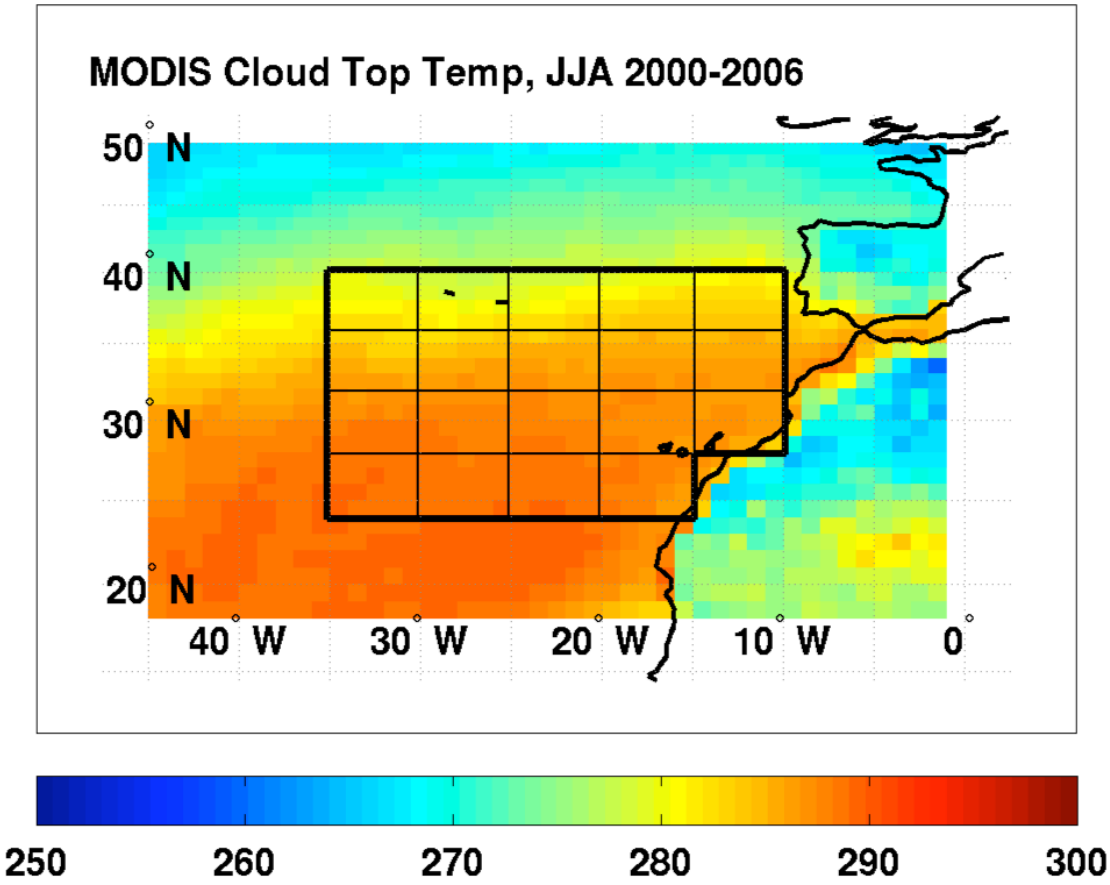

Figure III.1: The study region used in the present work, outlined in thick black lines (24-40N, 35-10W). The region is chosen to be farther North than the dominant area of Saharan dust influence and farther South than the storm track. The thin black lines denote the grid boxes used to ensure even sampling throughout the domain. A climatology of cloud-top temperature (CTT) for the dates used in this study (JJA 2000-2006) is plotted in the background.

over subtropical oceans. We judge that it would be less representative of the real-world climate sensitivity to focus uniquely on stratocumulus clouds.

The trajectory technique is described in detail in Chapter II; here we provide a brief summary. Parcel back-trajectories are computed from European Centre for Medium range Weather Forecasting (ECMWF) operational analyses using the Hybrid Single-Particle Lagrangian Integrated Trajectory Model (HYS-

PLIT). Trajectory calculations are started at two altitudes, one within and one above the boundary layer (500 and 2000m), and extend 72 hours prior to the time of observation. Satellite observations and meteorological analyses, described in more detail below, are interpolated onto trajectory positions to obtain estimates of past meteorological conditions.

An advantage of using the ECMWF operational analysis is that it includes the latest model developments as well as the most recently available observations. It should be noted, however, that as opposed to the reanalysis, the operational model has been modified over the time period under consideration. Although it is possible that these changes are reflected in some of the model fields considered, there are a number of reasons why we do not expect these to significantly impact the results. First, an investigation of the changes made in assimilated variables did not reveal any changes that directly impact the results (ECMWF, 2007). Second, changes in the simulations primarily took the form of increased resolution, without significant alterations to the model formulation. Also, analysis variables were generally selected so as to minimize model influence. Finally, since the present work is concerned with the relative changes in cloud and meteorological quantities on synoptic scales and the sampling is constrained to be uniform across the time period under consideration, any long-term systematic trends will be largely removed.

Low-level cloud fraction is chosen as the dependent variable in this study. Cloud fraction has the advantage of being more straightforward to define observationally relative to other cloud properties such as water path and albedo. Cloud cover is also commonly used in sensitivity studies, and exerts the greatest influence on shortwave cloud forcing. In addition, an investigation of cloud fraction sensitivities relates directly to the central issue introduced in Chapter II.

Samples are selected randomly from the upper, middle, and lower terciles of cloud fraction, given varying constraints on the overall sample, as described in the Results section below. For consistency with the model grids used in Chapter IV,

Table III.1: Estimates of the autocorrelation scales for MODIS liquid water cloud fraction. These were used to obtain an estimate of the degrees of freedom in a typical data sample used in the present study.

Dimension	Autocorrelation scale
Meridional	300 km
Zonal	260 km
Temporal	0.55 day (∼13 hrs)

the study region is split into 19 grid boxes, each one 4° latitude by 5° longitude. These dimensions are consistent with our estimate of the autocorrelation scale, discussed below. As described in Chapter II, the data are sampled uniformly from each grid box for each month in order to maintain even sampling throughout the domain. Composite differences are used to estimate sensitivities. Uncertainties in all composites are estimated using the bootstrap method described in Chapter II, with the modification described below.

The dependent variable in this study, cloud fraction, is used to obtain estimates of the autocorrelation scale for meridional, zonal, and temporal variations separately. We obtain the autocorrelation scale by estimating the e-folding scale for lagged autocorrelations. These new estimates of autocorrelation scales are displayed in Table III.1. The decorrelation length is estimated at twice the autocorrelation scale. An estimate of the degrees of freedom is obtained using another bootstrap method. Starting with a set of cloud observations, we randomly select one observation of cloud fraction. Any observations that are within 500 km or 1 day are identified and excluded from further sampling. The process is repeated until all of the data are exhausted, and the fraction of the original data that remain give an estimate of the sample degrees of freedom. The above routine is iterated to verify the consistency of the results. Our estimate of the degrees of freedom is remarkably robust, always reflecting a sample reduction very close to a factor of 5. This new estimate of the sample degrees of freedom is implemented in the bootstrap error calculation described in Chapter II by reducing the number of

points included in each randomly selected composite. An important note should be made regarding the distinction between the Eulerian autocorrelation described above and the autocorrelation along a Lagrangian trajectory. As expected, the analysis presented below indicates that the latter time-scale is much longer than 13 hours.

III.5 Satellite Data

Satellite observations are obtained from four different instruments, described below, and are used to assess meteorological state as well as validate analysis fields. An advantage of the trajectory technique is that satellite observations need not be coincident in order to provide useful information: observations are simply interpolated to the times and positions for which data are available. A list of the variables obtained from each dataset is shown in Table III.2.

Cloud microphysical and macrophysical properties are obtained from MODIS as daily gridded averages (MOD08_D3, Collection 005) at a resolution of 1°x1°. The MOD08 processing computes statistics (mean, standard deviation, histograms, etc.) by subsampling at the resolution of the relevant Level-2 product. In the case of clouds, the MOD06 product has a resolution of 5 km, meaning that approximately 480 pixels go into the MOD08 computation of statistics for the average 1°x1° box, instead of the approximately 12000 pixels retrieved at 1 km within each grid box (King et al., 2003). Naturally, not all pixels will be used for a given computation since, for example, cloud retrievals will only be performed for cloudy pixels. Still, this should constitute a more than adequate sample size to provide a robust average of each cloud property at the 1 resolution. Oreopoulos et al. (2000) evaluated the impact of subsampling on cloud effective radius and optical thickness and found that the associated bias is small and randomly distributed. This is further supported by the discussion above regarding autocorrelation scales. Another

Table III.2: Satellite data products used in the present study.

Instrument, Dataset, Resolution	Data Products Used
MODIS, MOD08_D3 C005,	Cloud_Top_Pressure_Day_Mean
1°x1° regular grid	Cloud_Top_Temperature_Day_Mean
	Cloud_Optical_Thickness_Liquid_QA_Mean
	Cloud_Effective_Radius_Liquid_QA_Mean
	Cloud_Water_Path_Liquid_QA_Mean
	Cloud_Phase_Infrared_Day_Histogram_Counts
	Cloud_Fraction_Liquid
	Cloud_Fraction_Ice
	Cloud_Fraction_Combined
	Cirrus_Fraction_SWIR
CERES, CER_SSF Ed2B,	SSF-34 : Radiance and Mode flags
12.5 km swath	SSF-25: Surface type index
	SSF-26: Surface type percent coverage
	SSF-27: CERES SW ADM type for inversion
	SSF-38: CERES SW TOA flux - upwards
	SSF-39: CERES LW TOA flux - upwards
SSM/I, RSS Ocean Products v6,	L: Cloud Liquid Water
25 x 25 km regular grid*	V: Column Water Vapor
QuikScat, QS_2B, 25 km swath*	wind_dir
	wind_speed
	wind_speed_selection, DIRTH**
	wind_dir_selection, DIRTH**
	wvc_quality_flag

*As described in the text, data from ascending and descending passes are treated separately.

** DIRTH = Direction Interval Retrieval with Threshold Nudging, described in this section

significant detail about the MOD08 regridding is discussed below, regarding the differentiation between daytime and nighttime observations.

For low-level clouds, MODIS cloud-top property retrievals are made using the 11 μm brightness temperature. Retrievals are performed for all pixels identified by the cloud mask as either probably cloudy or cloudy. The MODIS cloud mask is clear-sky conservative, using a variety of threshold tests that classify a pixel on a scale between 1 (high confidence clear) and 0 (low confidence clear). Significantly, this means that the mask will err on the side of mislabeling a pixel as cloudy in order to minimize the risk of the converse. In practice, the vast majority of pixels

over ocean are classified with high confidence as either clear or cloudy. Only a very small proportion, generally near cloud edges, are classified as uncertain (Platnick et al., 2003). However, this does not rule out misidentification of a clear pixel or partially cloudy pixel as overcast, which could be a source of error in cloud-top temperature (CTT) and pressure (CTP) retrievals.

Several authors have indicated the potential for retrieval biases in pixels that are only partially covered by cloud (Wielicki and Parker, 1992; Matheson et al., 2006). Matheson et al. (2006) compare threshold cloud retrievals with cloud properties derived from a new method which accounts for the sub-pixel cloud fraction. Using Advanced Very High Resolution Radiometer (AVHRR) data at 4-km resolution, their analysis suggests this bias is small relative to other factors that influence cloud forcing. Nevertheless, since MODIS retrievals assume an overcast 1 km pixel, the presence of partially filled pixels will result in a bias. Similarly, MODIS cloud-top temperature (CTT) and pressure (CTP) retrievals do not differentiate between low and high cloud pixels, leading to a negative bias when high clouds are present. Figure III.2 shows composite anomalies of CTT relative to liquid cloud fraction and cirrus cloud fraction. Although all of the trends are within the range of the variability in the observations, they indicate that ice clouds result in a linear decrease in CTT while the partial pixel contamination is most pronounced for cloud cover less than about 30%.

MODIS cloud fraction, effective radius, and water path retrievals all require a modified cloud detection scheme relative to the clear-sky conservative mask described above. Cloud phase is determined through the use of near and far infrared channels that exploit both the different optical constants of water and ice as well as the different temperatures at which each phase occurs. Cloud scenes are identified as liquid, ice, mixed phase, or uncertain. Here we focus our discussion on the potential for high clouds overlying low clouds to be detected and/or to influence the results. Recent studies indicate that the Cloud_Fraction_Ice product

is not sensitive to ice clouds with optical depths less than approximately 1 (*e.g.,* Meyer, 2008). The retrievals of ice cloud fraction are often dramatically smaller than the MODIS "Cirrus fraction" derived from the 1.38 μm reflectance. Due to strong water vapor absorption, the 1.38 μm band is generally minimally influenced by the surface and lower atmosphere, and thus can provide a sensitive test for upper-level clouds.

In this study we use a simplified filtering for high clouds in order to obtain reliable estimates of cloud-top properties. We first constrain Cloud_Fraction_Ice to be less than 1%. Tests indicate that this removes a significant fraction of ice cloud observations. However, as shown in Figure III.2, a systematic trend in CTT remains with regard to the 1.38 μm test for Cirrus fraction. It should be noted that in dry atmospheres such as those predominating over stratocumulus regions the 1.38 μm band may be sensitive to low-level clouds. Although the algorithm for Cirrus cloud fraction accounts for this through comparison with 0.67 μm reflectance, it is possible that the Cirrus fraction product is systematically biased by changing low cloud properties. The authors found evidence for this in a global composite of Cirrus_Fraction_SWIR which showed local maxima in ice cloud cover over stratocumulus regions. Since such regions are characterized by subsidence and the retrieval showed greater cirrus coverage in these than in adjacent mid-latitude or tropical regions, this is likely indicative of a bias resulting from the high albedo of low clouds. Nevertheless, we opt to use a more conservative test for high cloud by constraining Cirrus fraction to less than 25%. This value is chosen based on Figure III.2 as a compromise between sample size and high cloud contamination.

In contrast with the cloud-top temperature and pressure retrievals, MODIS retrievals of effective radius and water path are separated by cloud phase. Similar plots are displayed in Figure III.2 for effective radius, indicating a weak sensitivity to ice cloud cover for cirrus coverage beyond 60-80%. Composited against

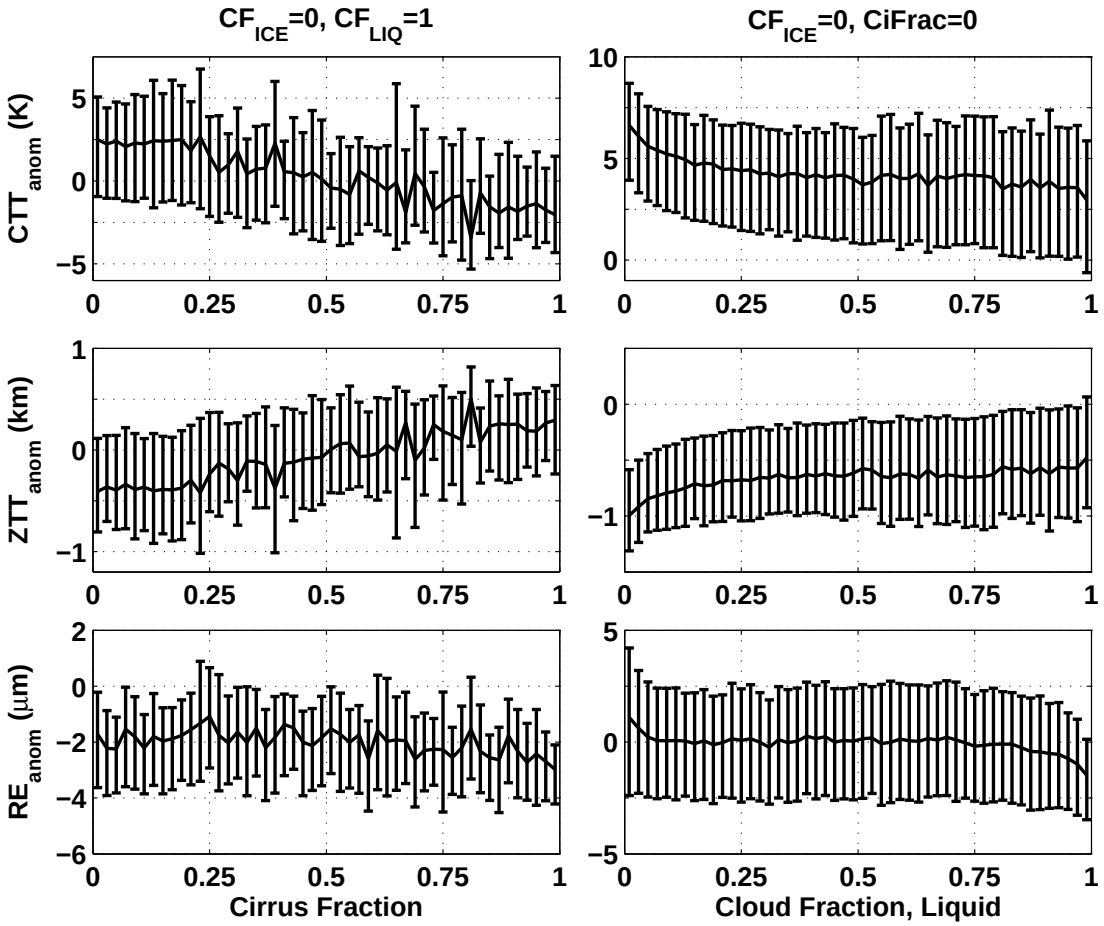

Figure III.2: MODIS cloud-top temperature (CTT), MODIS-ECMWF cloud-top height (Z_{TOP}) and MODIS effective radius (R_E) anomalies, composited with respect to MODIS retrievals of cirrus fraction (CiFrac) and liquid water cloud fraction (CF_{LIQ}). Cloud top height is computed using the difference between sea surface temperature (SST) and CTT along with an assumed lapse rate of 6.5 K km^{-1} ($Z_{TOP} = (SST - CTT)/6.5$). Note that the y-axes all have different scales. Error bars display the 25^{th} and 75^{th} precentiles. Anomalies are computed with respect to geographic and monthly means, consistent with the sampling methodology used throughout this study. In all plots, ice clouds are filtered from the analysis using the MODIS Cloud_Fraction_Ice product. In the first column it is evident that ice cloud detection does not remove all high clouds, since a trend in CTT is still apparent with respect to cirrus fraction, despite low-level cloud fraction being held fixed at 100%. In the second column, a more stringent test is applied in order to consider partial pixel biases only.

liquid water cloud fraction, variations in effective radius are less straightforward to interpret, though partial pixel biases appear to only impact retrievals for cloud cover less than 10%. It should be noted that the above sensitivity tests were performed for the Northeast Atlantic only. It is likely that these biases are manifested differently in other regions.

Although high clouds are an issue that must be addressed in order to ensure high quality cloud-top property retrievals, exclusion of such scenes from the analysis could bias the results (for example, by constraining the upper-level divergence). It is therefore important to include high cloud scenes in the analysis, since it is possible that these vary systematically with low-level cloud fraction, and thus could constitute a relevant diagnostic. An important consideration when observing low clouds in the presence of high clouds is the possibility of overlapped low clouds. We use a random overlap assumption to account for low clouds that are masked by thick high clouds. Tests employing both minimum and maximum overlap assumptions indicate a negligible sensitivity to the overlap assumption used. The results section below discusses the approach used to address the competing concerns of inclusive sampling and quality-assured cloud-top property retrievals.

All of the following satellite datasets are regridded from their native resolutions to match the MOD08 1°x1° grid. As discussed in Chapter 2, this ensures consistency with the synoptic-scale focus of the study and also accounts for the spatial averaging due to mixing along parcel trajectories. Overpass times are assigned to the 3-hourly bin that is most representative of overpass times for the study region and the satellite platform under consideration. For sun-synchronous polar orbiters this is an adequate representation of the bulk of overpass times. It should be noted, however, that small systematic variation in overpass times could produce a bias resulting from diurnal variations. Given the large sample size used in this study and the large variance in day-to-day observations relative to typical diurnal variations in cloud fraction (Rozendaal and Rossow, 2003; Bretherton

et al., 1995b), it is unlikely that this contributes significantly to the error in our method.

Data from the Clouds and the Earths Radiant Energy System (CERES) instrument aboard Terra are obtained from the Atmospheric Science Data Center at the NASA Langley Research Center. The CERES instrument measures atmospheric radiances from three broadband channels: shortwave (0.3-5μm), window (8-12μm), and total (0.3-200μm) (Geier et al., 2003). The Terra satellite is equipped with two CERES instruments which can be run in different scan modes, thus permitting the creation of empirical Angular Distribution Models (ADMs). These ADMs are used to estimate hemispheric fluxes from CERES observed radiances based on viewing geometry, solar position, and the MODIS-derived scene type . This study uses the swath-level Single Scanner Footprint (SSF) product to obtain observations of scene albedo and top-of-atmosphere radiative flux. Both quantities are retrieved for all-sky conditions. Since the three-dimensional properties of clouds can significantly impact fluxes at large solar zenith angles, zenith angles greater than 70° are screened from the data. The regridding also only includes over-ocean observations and excludes regions of sun-glint. Finally, CERES pixels are rejected if the retrieval used is obtained by using the CERES Artificial Neural Network technique to obtain the scene ADM (Loukachine and Loeb, 2003). This is a detail specific to CERES processing that is important for energy balance studies, which rely on global, uninterrupted coverage. For such studies, CERES produces estimated radiances when MODIS retrievals cannot be used to identify scene type. In order to maintain consistency between retrievals, we do not include retrievals that employ this neural network technique.

All-sky liquid water path is obtained from the Special Sensor Microwave Imager (SSM/I). There are multiple SSM/I instruments currently in orbit as part of the Defense Meteorological Satellites Program (DMSP) managed by the US Air Force. The SSM/I retrieval uses a model for the brightness temperature at

four microwave wavelengths to solve for the column vapor amount, cloud water, surface wind speed, and rain rate (Wentz, 1997; Wentz and Spencer, 1998). For this study we use data obtained from SSM/I instruments onboard the f13, f14, and f15 satellites. The retrieval products are obtained from Remote Sensing Systems, Inc. using the version 6 (V6) retrieval algorithm. Daily retrievals are obtained at 0.25° resolution and averaged to a 1°x1° grid.

Microwave measurements provide an independent liquid water path (LWP) estimate to contrast with MODIS, which uses visible and near-infrared radiances to estimate LWP. A comparison of measurements from the two sensors is shown in Figure III.3. LWP from each SSM/I instrument and the average of the 3 are composited with respect to all-sky liquid water path from MODIS. Ice cloud scenes are excluded from the composites using the filtering described above. Inclusion of such scenes only has the effect of increasing the variance, and does not introduce a systematic bias in the result. The agreement is generally well within the estimated accuracy of 25 g m^{-2} for SSM/I retrievals (Wentz, 1997). However, a systematic bias is apparent in Figure III.3, with SSM/I predicting larger LWP for thin clouds and smaller LWP for thick clouds relative to MODIS. MODIS LWP is computed using the product of effective radius (R_E) and cloud optical depth (τ_{CLD}) retrievals. While a partially filled pixel will result in an overestimate in R_E (warmer brightness temperature), the same situation results in an underestimate in τ_{CLD} (decreased reflectance). As a result, MODIS retrievals of LWP in partly cloudy pixels result from a partial cancellation of errors and it is unclear whether or not a partial pixel bias can explain the observed disagreement with SSM/I. An important detail of the comparison in Figure III.3 is that the disagreement is greatest for f13 and least for f15. This is consistent with the fact that the overpass time for f15 is much closer to that of Terra (∼1 hour previous) than is the case for f13 (∼4 hours previous). This suggests that the primary source of differences between SSM/I and MODIS water paths results from sampling the cloud field at

different points in the diurnal cycle. Although this comparison is important as a validation of the two independent retrievals of water path, it should be noted that the difference in overpass times is not an issue in the analysis presented here. Since the present work makes use of back trajectories to ascertain prior influence on cloud properties, we can simply assign retrieved cloud properties to the time and location at which the observations are made. Since the satellite overpass times are fairly regular we are able to compare day-to-day observations for the same time of day, thus eliminating any concern for diurnal variations.

Surface divergence is computed from QuikScat wind retrievals (Level 2B swath). The SeaWinds instrument on QuikScat uses polarized microwave radar to retrieve surface wind speed and direction. Wind retrievals are performed using radar backscatter measurements received from a set of 2-4 azimuth angles. Since these are generally not orthogonal, wind direction solutions can be non-unique. Stiles (1999) describes the direction interval retrieval with threshold nudging (DIRTH) technique, designed to resolve this issue. In this study we use the Level 2B DIRTH products from QuikScat.

Numerous studies have tested the veracity of QuikScat measurements, most often by comparison with moored meteorological buoys (*e.g.,* Ebuchi et al., 2002; Draper and Long, 2002). These are consistent in showing that QuikScat retrievals are well within the mission requirement of 2 m s^{-1} accuracy in wind speed and in keeping with the mission requirement of 20° for wind direction. Another result from the validation studies is that the greatest error in scatterometer wind retrievals occurs in areas of light wind or rain. Rain has the potential to corrupt QuikScat measurements through atmospheric attenuation and roughening of the ocean surface. Although rain is not likely to be appreciable over stratocumulus regions, rain-flagged retrievals are excluded from the regridding. The analysis of Milliff et al. (2004) indicates that removal of rain-flagged data does not bias the wind observations for the region under consideration in this study. Apart from

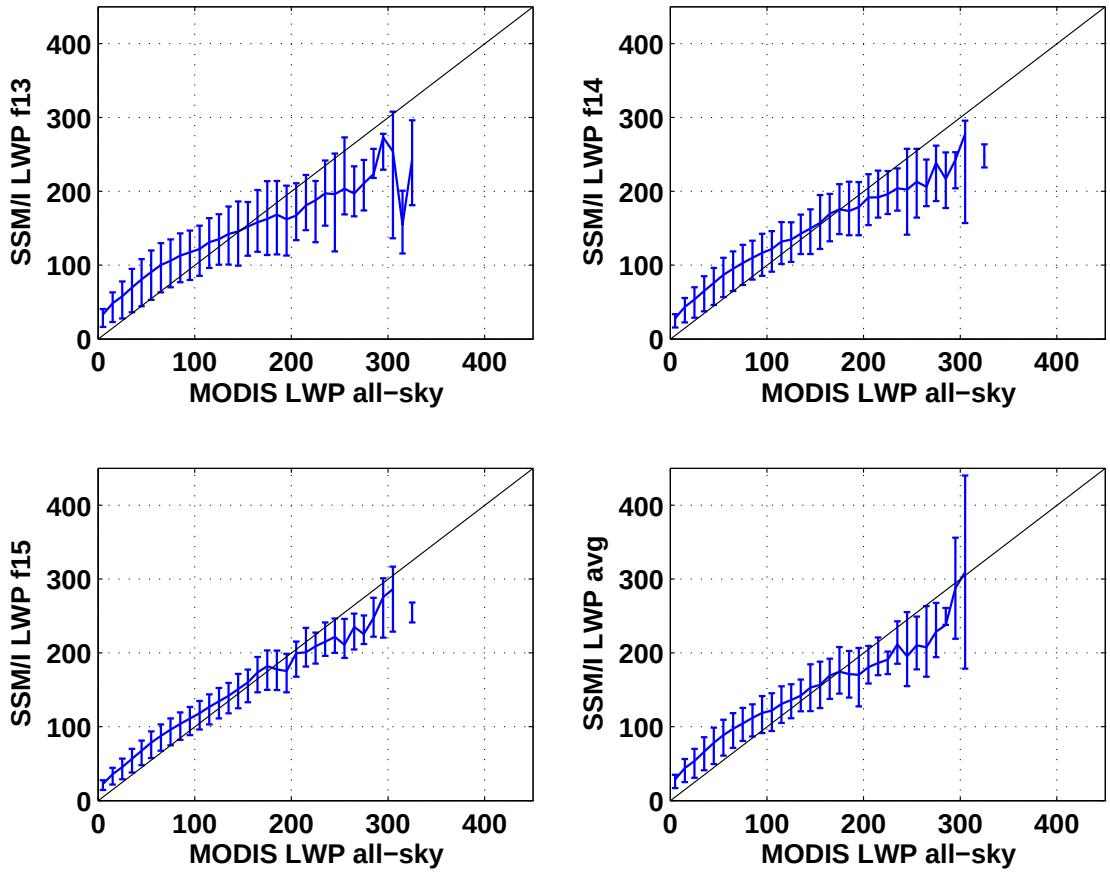

Figure III.3: SSM/I all-sky liquid water path (LWP) composited with respect to MODIS all-sky liquid water path (obtained by taking the product of MODIS water path and cloud fraction retrievals). Error bars display the 25^{th} and 75^{th} precentiles. The four plots correspond to LWP retrievals obtained from the DMSP f13, f14, and f15 satellites equipped with SSM/I as well as a fourth plot displaying results from the average of the 3 retrievals. The f15 satellite has an overpass time that best matches that of Terra, and the systematic biases with respect to MODIS appear to increase as the overpass times become less similar.

filtering the data for rain and other standard quality assurance criteria, a subtlety of the regridding for QuikScat is the fact that the level 2B grid is not orthogonal. As a result, it is necessary to average the zonal and meridional wind components separately onto a regular grid before computing the divergence.

QuikScat surface winds are assimilated into ECMWF. Recent studies indicate that the quality of the assimilation is high for divergence (McNoldy et al., 2004; Stevens et al., 2007). Indeed, there is evidence that assimilation of surface winds has significantly improved ocean surface wind predictions from ECMWF (Chelton and Freilich, 2005). However, given the potential for model influence on ageostrophic motions as well as through the surface parameterization there is reason for concern that the surface winds given by the analysis differ significantly from the observations. Although we present results below that indicate the model does remain faithful to the observations, it is for this reason that we have included the raw surface wind retrievals in the study.

An important detail of the regridding for all polar-orbiting satellite retrievals is the differentiation between ascending and descending passes, which are usually separated by approximately 12 hours. The majority of CERES and MODIS observations require a shortwave or near-infrared signal, and are thus not problematic in this respect. In contrast, QuikScat, SSM/I, and a number of MODIS observations can be made both day and night and thus must be compiled separately according to overpass time. This is a particularly important detail given that this study is focused on a synoptic-scale analysis of cloud sensitivities.

III.6 Results

The goal of the present study is to investigate the variations in dynamic and thermodynamic state associated with changes in low-level cloud fraction. Following the method developed in Chapter II, we split the data into terciles of cloud

fraction. Terciles are chosen for simplicity, though tests indicate that subdividing the data differently, such as into quartiles, does not significantly alter the results. The data are sampled evenly from each grid box and each month. Trajectories are computed for all selected cloud observations, and satellite and analysis data are interpolated onto trajectory positions. Composites are computed for all trajectories falling in each tercile. Each trajectory displayed below represents the mean of approximately 10,000 trajectories. Adjusting for autocorrelation between observations, this represents an effective sample size of 2,000. Confidence limits are estimated using the bootstrap method described in Chapter II with the modifications discussed above. Since cloud sensitivities may not vary linearly or even monotonically with cloud fraction, the middle tercile is included in the present analysis. Following the sample selection, the composite trajectories are hereafter referred to as LC (Large low-level Cloud fraction), MC (Medium low-level Cloud fraction), and SC (Small low-level Cloud fraction).

It bears recognition that compositing over many trajectories may average over multiple different modes of variability in cloud fraction. This is a concern with any work that extends beyond case studies. Our sampling strategy is designed to be inclusive in order to limit sample bias, and sampling by terciles is chosen as a compromise between minimizing intra-composite variance while maximizing sample size. In addition, the present work is focused on the mean meteorological conditions associated with mean synoptic-scale variations in cloud fraction. As such, the goal is to identify the dominant cloud sensitivities that are relevant to the broadest possible set of observations, potentially at the sacrifice of characterizing the full richness of cloud fraction variability.

III.6.A Cloud Properties

Figure III.4 shows the composite trajectories of low-level cloud fraction and CERES top-of-atmosphere net shortwave flux. For clarity, only the 500m

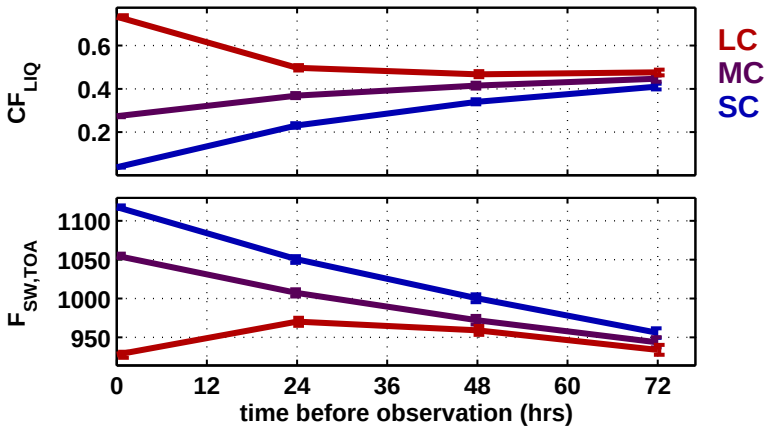

Figure III.4: Composite back trajectories for the large (LC), middle (MC), and small (SC) terciles of MODIS low-level cloud fraction. The plots show the overlap-corrected MODIS low-level cloud fraction (CF_{LIQ}) and CERES top-of-atmosphere net shortwave flux (F_{SW}, W m^{-2}). Error bars denote the 95% confidence limits obtained using the bootstrap method described in the text.

trajectories are displayed in the back-trajectory plots. In general, these are representative of the variations along the 2000m trajectories as well, however vertical shear is present in the back trajectories and differences are presented below. The first plot shows the low-level cloud fraction, confirming that the sub-sampling correctly constrains the data into terciles of cloud fraction. The differences become greatest in the final 24 hours of the trajectories, largely due to a rapid increase in cloud cover for the LC composite. Notably, the differences remain significant throughout the history of each composite, consistently showing an increase in cloud cover from the SC to LC composites.

As discussed in the methods section, low-level cloud fraction is defined using the MODIS retrieval of liquid water cloud fraction and correcting the retrieval for overlap by high cloud. A random overlap assumption is used, although a comparison with maximum and minimum overlap assumptions indicates a negligible sensitivity to the method employed. The mean cloud fraction is surprisingly low for the LC cases. Figure III.5 shows a histogram of cloud fraction including data

from all three terciles. As expected for a cloud field with a spatial autocorrelation-scale greater than the scale at which it is gridded, the distribution is U-shaped. A more interesting detail is the skewness of the distribution, which shows 2-3 times as many clear-sky as overcast days. This is consistent with observations made during the Atlantic Stratocumulus Transition Experiment (ASTEX) campaign, which took place in the same region (Bretherton et al., 1995b). The dashed lines show the average delineation between the 3 terciles. As a result of the skewness, a large number of the SC observations are clear-sky cases. However, as shown in Figure III.4, the mean of these small cloud fraction observations represent the endpoint of a continuous decline in cloud fraction over the course of a 72 hour trajectory. The goal of this work is to identify the causes for such a decline in cloud fraction, along with those that could explain the complementary rise in cloud fraction for the LC case.

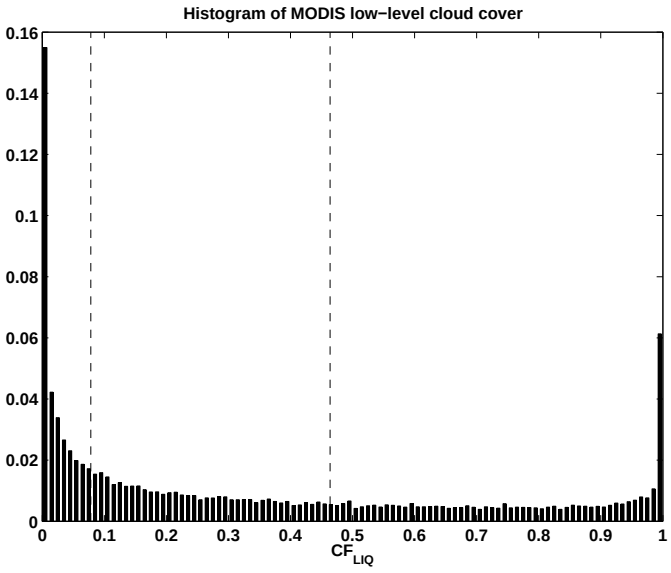

Figure III.5: Histogram of MODIS low-level cloud fraction. The y-axis denotes the fraction of all points that fall into each bin, and the dashed lines delineate terciles (SC, MC, and LC) in cloud fraction.

Associated with the changes in low-level cloud fraction, Figure III.4 shows

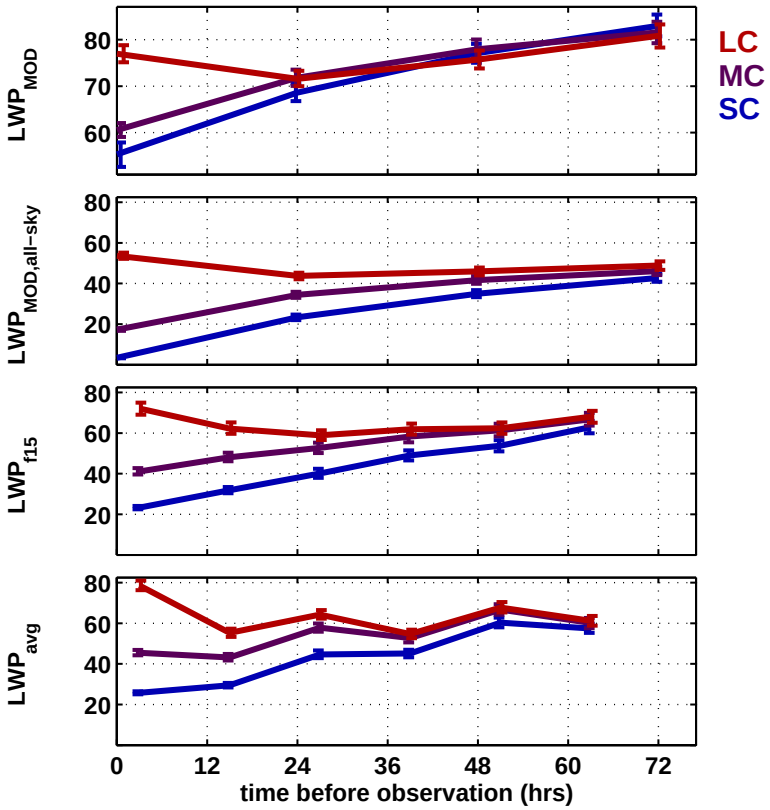

Figure III.6: As in Figure III.4 except showing different measures of cloud water path. All variables are displayed in units of g m^{-2}. Displayed from top to bottom are: MODIS in-cloud LWP, MODIS all-sky LWP, SSM/I LWP from the f15 sensor, and an average of LWP retrievals from all three SSM/I sensors. All show agreement in the relative trend in LWP over the course of the trajectories. However, SSM/I is shown to systematically retrieve larger water paths than MODIS for the LWP range considered.

the composite trajectories for top-of-atmosphere (TOA) net shortwave flux from CERES (FSW). Shortwave fluxes retrieved from CERES confirm the strong cooling effect of low-level clouds. The flux values retrieved from CERES are representative of Terra overpass times, which occur between shortly after noon local time and are thus much larger than the associated diurnally averaged fluxes. It should be noted that these observations are not filtered for high clouds, which could contribute to the observed differences between SC, MC, and LC cases.

Since the interpretation of all-sky liquid water paths can be somewhat ambiguous, Figure III.6 shows a comparison between back trajectories of MODIS in-cloud and all-sky LWP alongside all-sky LWP from the average of the three SSM/I sensors as well as SSM/I LWP from the f15 sensor only. The disagreement between retrievals is consistent with the discussion above, showing that SSM/I retrievals are consistently larger than those of MODIS for the range of water paths considered. Also notable is that the scale of the discrepancy increases as cloud cover decreases, suggesting that a partial pixel bias in the MODIS retrievals is responsible for the difference. As noted in the section above, MODIS LWP is computed from the product of R_E and τ_{CLD}. The results presented here and in Figure III.3 suggest that for water paths less than approximately 100 g m^{-2} the bias in MODIS LWP is dominated by the low bias in cloud optical depth retrievals. Overall, the retrievals presented in Figure III.6 are consistent in associating increasing water paths with growing cloud decks and the converse for dissipating clouds, as is expected. Importantly, we also see that the sign of the difference is maintained in the conversion between all-sky and in-cloud water paths.

III.6.B Thermodynamic conditions

Numerous studies, including the results cited in Chapter II, have noted the strong relationship between the stability of the lower atmosphere and stratiform cloud amount (*e.g.*, Klein et al., 1995). Lower tropospheric stability is defined here as the difference in potential temperature between 700 hPa and the surface ($\theta_{700} - \theta_0$). As discussed in the methods section above, the trajectory analysis here is motivated by the observation that cloud cover correlates best with upwind variations in SST and upper air temperature (Klein et al., 1995). Figure III.7 shows that, consistent with Chapter II, this result is confirmed by the present study. Large cloud fraction cases are associated with a significantly more stable atmosphere, a condition that persists throughout the course of the 72 hour trajectory.

The greater stability is due both to a warmer free troposphere and cooler sea surface temperature (SST), also consistent with prior assessments of conditions that promote stratiform cloud formation. The increase in stability suggests a diminished entrainment in the larger cloud cases. This is reinforced by the increase in above-cloud humidity, which lessens the impact of entrainment drying. Together, these observations imply that cloud cover and water path increase in response to a decrease in the flux of water across the inversion in response to suppressed entrainment and a decreased contrast with free tropospheric humidity. The fact that a marked difference in LTS is maintained throughout the history of the trajectories suggests that the stability acts to precondition the boundary layer for cloud growth.

It is assumed that a greater LTS reflects a stronger inversion at cloud top. Indeed, it is true that cooler SSTs as well as warmer upper air temperatures will promote a more stable environment. However, an important consideration is the vertical distribution of this temperature change. The same LTS could be representative of the typical stratocumulus 6-8K cloud-top inversion jump in temperature (Albrecht et al., 1995) or alternatively of a deep stable cloud layer capped by a weak inversion, as is representative of dissipating stratocumulus and trade cumulus boundary layers. The strong correlation and significant differences in LTS between LC, MC, and SC cases is a good affirmation that LTS is in fact a good proxy for inversion strength, since a strong inversion will promote effective cloud-top cooling and a moistening of the boundary layer. However, it is worth noting that this is an assumption, the implications of which will be discussed further below.

Surface fluxes also reflect the anticipated differences between dissipating and developing clouds. Figure III.8 shows the composite trajectories for along-trajectory sea surface temperature advection (TA_{SFC}), 10 m surface wind speed (W_{10m}), and sensible (F_{SH}) and latent heat fluxes (F_{LH}), all obtained from ECMWF analyses. A primary advantage of the Lagrangian perspective is the

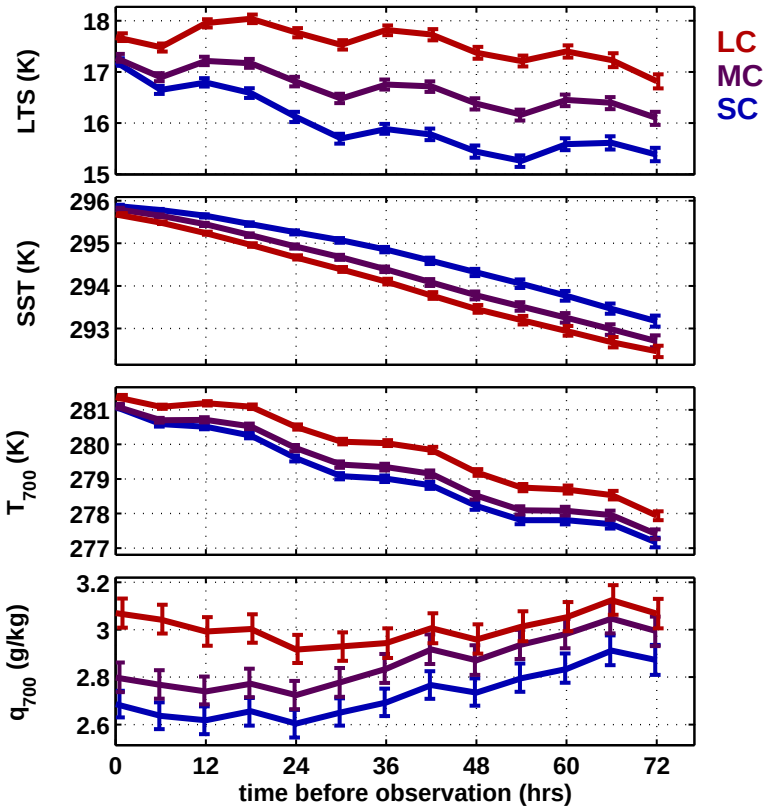

Figure III.7: As in Figure III.4 except showing lower tropospheric stability (LTS, defined as $\theta_{700} - \theta_0$, K), sea surface temperature (K), and 700 hPa temperature (T_{700}, K) and moisture (q_{700}, g kg^{-1}), all obtained from ECMWF analyses.

elimination of advective terms. The advection defined here is simply the along-trajectory rate of sea surface temperature change. This is equivalent to the conventional definition of temperature advection ($-v \bullet \bigtriangledown T$) applied to the trajectory path. Again, this result is consistent with prior work (*e.g.,* Norris and Iacobellis, 2005) associating negative temperature advection with increased incidence of low-level clouds. It is also consistent with the increased stability, since advection of warm air over a colder surface will contribute to a more lower atmosphere. The differences in TA_{SFC} are greatest near the time of observation (0 hours on plot), however trajectory separation is apparent up to 48 hours back. Surface winds, provided by ECMWF, are also stronger for the larger cloud cases. Increased cold

advection and stronger surface winds will both promote increased surface fluxes, and the SC cases show significantly weaker surface exchanges of heat and moisture when compared to the other two cases. The significant distinction between the SC and MC surface fluxes is contrasted by the weak distinction between the MC and LC cases. This is partially reflected in the TA_{SFC} trajectories, and is an indication that cloud sensitivities do not vary linearly with cloud fraction. There is also some indication that these differences are of opposite sign early on in the trajectory. Specifically, in the earliest 24 hours of the trajectories the large cloud cases are associated with *decreased* surface fluxes and *weaker* cold advection. The differences in latent heat flux are particularly large. Given the importance of sub-cloud moisture fluxes in initiating decoupling in boundary layer clouds, this surprising result has important implications and will be discussed in more detail below. Finally, it should be noted that these plots are displayed in order of increasing model influence: Surface winds and temperatures are directly observed, and although it is true that the model physics and surface parameterizations will influence these quantities, the impact is likely to be less than for surface fluxes. Consequently, more confidence should be placed in the composite differences in temperature advection and surface wind speed than with the surface fluxes.

III.6.C Large-scale Dynamics

The discussion thus far has largely focused on variables that define the thermodynamic boundary conditions influencing cloud development. Figure III.9 displays results regarding the large-scale dynamic influences on cloud fraction. Both QuikScat retrievals and ECMWF surface divergence are shown to increase with decreasing cloud fraction. This is somewhat surprising in that stratiform clouds are known to exist in regions that are climatologically defined by strong subsidence. The present results indicate that these clouds actually exist in a delicate balance between excessively divergent and insufficiently divergent regimes.

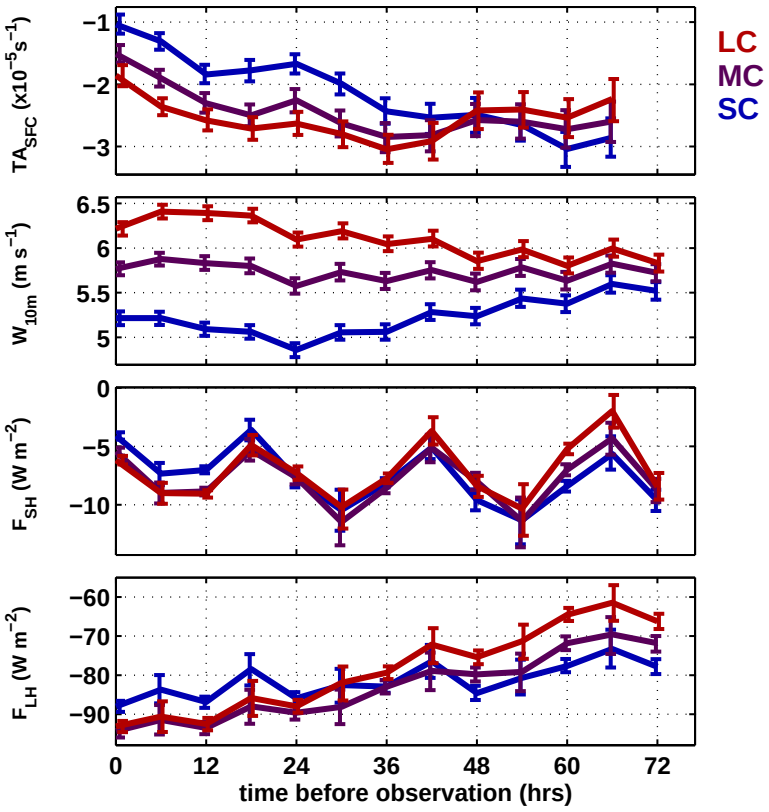

Figure III.8: As in Figure III.4 except showing along-trajectory SST advection (TA_{SFC} K s^{-1}), 10m wind speed (m s^{-1}), surface sensible heat flux (F_{SH} W m^{-2}) and surface latent heat flux (F_{LH} W m^{-2}), all obtained from ECMWF analyses.

Pressure vertical velocity at 700 hPa (ω_{700}) from ECMWF is consistent with this result, indicating a subsiding regime overall, but a decrease in cloud fraction with increases in subsidence rate. In contrast with many of the thermodynamic quantities above, the divergence and vertical velocity appear to impact cloud cover over shorter time-scales, and are primarily correlated over the 12 hours prior to the time of observation. Notably, these fields too show a reversal in the relationship with cloud cover in the early part of the trajectory, showing that beyond 48 hours the large cloud cases are slightly more shallow, subject to greater divergence, and increased subsidence.

The final set of trajectories in Figure III.9 shows the variations in cloud-

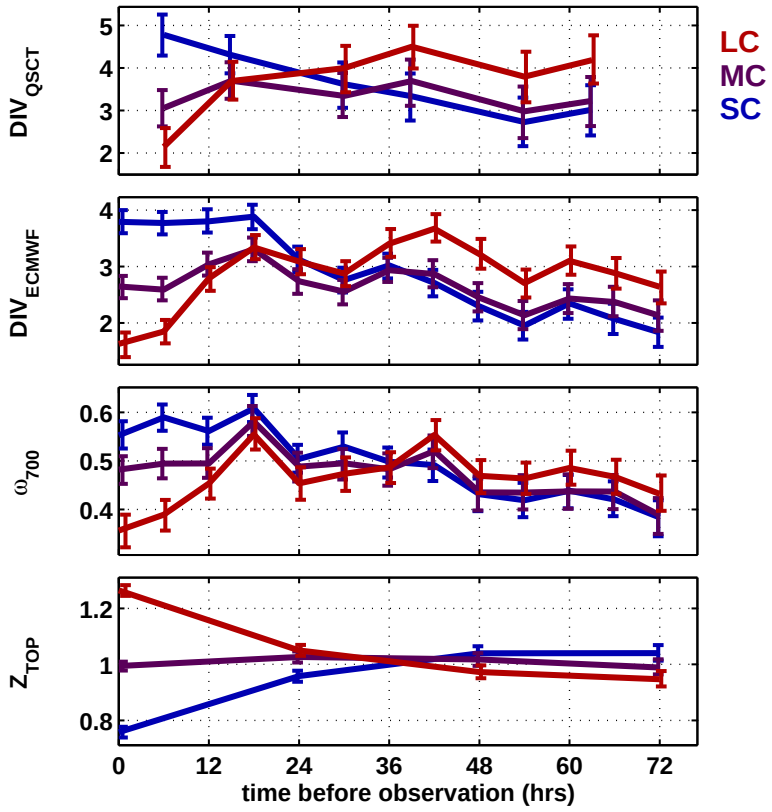

Figure III.9: As in Figure III.4 except showing QuikScat and ECMWF surface divergence (DIV_{QSCT}, DIV_{ECMWF}, x10^{-6} s^{-1}), ECMWF 700 hPa pressure vertical velocity (ω_{700}, x10^{-3} Pa s^{-1}), and MODIS cloud-top height (Z_{TOP}, defined as $(SST - CTT)/6.5$, km)

top height (Z_{TOP}) for the different terciles of cloud cover. The results are consistent with the composites of divergence and vertical velocity, associating a deepening of the cloud layer with cases of decreased surface divergence. Cloud height is estimated by using the difference between MODIS cloud-top temperature retrievals and sea surface temperature from ECMWF and applying a mean lapse rate of 6.5 K per kilometer. This is chosen over the MODIS retrievals of cloud-top height, which compare cloud-top temperature retrievals to the temperature profile obtained from the National Centers for Environmental Prediction (NCEP) Global Data Assimilation System (GDAS). Due to the strong inversion capping subtropical clouds,

this method is known to systematically overestimate cloud-top height. Although the assumption of a constant lapse rate may also induce errors, it has been shown to perform better in subtropical cloud regimes (*e.g.,* Zuidema et al., 2008) and constitutes a more easily interpretable diagnostic than the MODIS retrieval.

As discussed in the section above on satellite data, CTT retrievals are impacted both by partly cloudy pixels as well as the presence of ice clouds. No straightforward correction can be made for partially filled pixels, apart from noting that in Figure III.2, the bias appears to primarily affect retrievals for cloud cover less than 30%. However, a significant bias can be removed by excluding cases with high clouds (Figure III.2). As a result, the cloud-top height retrievals shown in Figure III.9 are screened for high clouds using the ice cloud filtering described in the methods section above. This has the potential to bias the sample in favor of a drier free troposphere and stronger upper-level convergence, the consequences of which are discussed in detail below.

An important question is whether surface divergence constitutes a valid proxy for subsidence rate at cloud top and if so how, specifically, is it related. The rate of subsidence at cloud top is a critical determinant of boundary-layer height, as shown in Equation III.1. Subsidence rate is simply the vertical integral of divergence, so that given a knowledge of the shape of the divergence profile, surface divergence can be used to estimate subsidence rate. Figure III.10 shows the composite profiles of divergence obtained from the ECMWF analyses. The profiles are consistent with the results displayed in III.9, showing increased low-level divergence for smaller cloud cover. Conveniently, the mean profiles also show an approximately linear decrease to zero at 700 hPa, permitting a straightforward estimation of the subsidence rate. A distinction is also seen at upper levels, with small cloud cases exhibiting a much stronger upper-level convergence than large cloud cases. This has implications for high cloud occurrence, indicating that an increase in low-level cloud cover may be associated with an increase in high clouds.

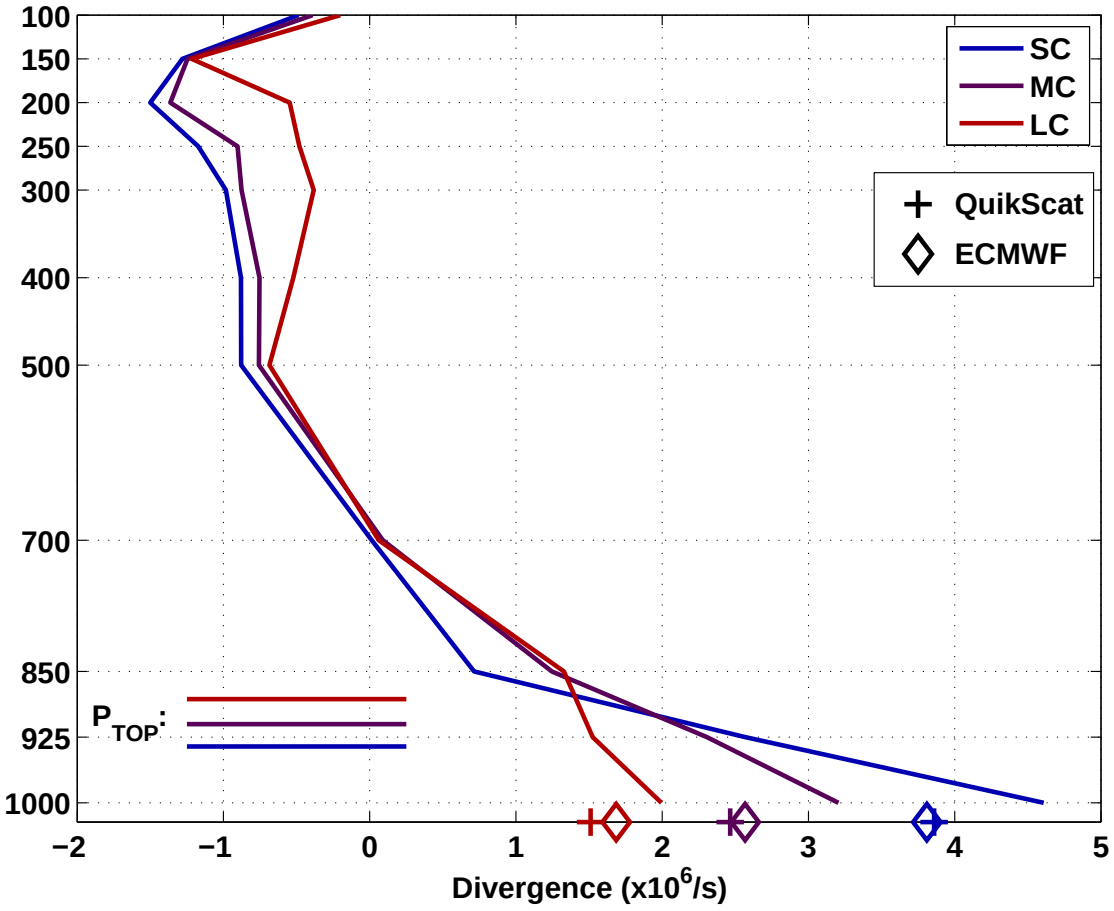

Figure III.10: Composites of the ECMWF divergence profile at the time of cloud observation (0 hours). Surface retrievals from QuikScat are compared with those of ECMWF, and cloud-top pressure (CTP) estimates are displayed in the lower right corner of the plot.

Indeed, figure III.11 confirms this suspicion, showing that MODIS retrievals of both ice cloud fraction and cirrus fraction increase systematically with low-level cloud cover. Again, although a part of this association is likely to be real, it should be noted that the author found evidence that the MODIS retrieval of cirrus fraction is influenced by the presence of low-level clouds.

Verification of ECMWF surface divergence is another important outcome of the above results. Divergence computed from ECMWF 10 m surface winds

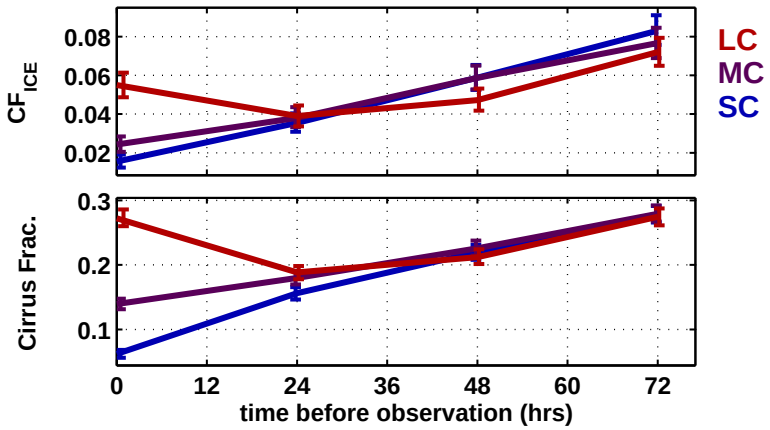

Figure III.11: As in Figure III.4 except showing MODIS retrievals of ice cloud fraction (CF_{ICE}) and cirrus fraction (CiFrac).

is plotted along with that computed directly from QuikScat retrievals for the mean surface pressure of the study region. QuikScat divergence shows slightly greater separation between composites and generally smaller divergence values than ECMWF. However, the two are largely in agreement, indicating that the ECMWF model exerts only a minor influence on the assimilated retrievals of surface winds.

III.6.D Lag Correlations and non-linearity in cloud response

The above results suggest an interesting pattern in the time dependence of different forcings in their association with cloud fraction. To begin with, the separation in cloud fraction between composites is significant throughout the entire 72 hour trajectory. Table III.3 shows the correlations between instantaneous observations of cloud fraction and a selection of the variables most strongly associated with variations in cloud fraction at different lags. Correlations are computed from samples selected uniformly from each grid box and each month, using anomalies computed relative to the monthly mean in each grid box. For each variable, the lag at which a maximum correlation is observed is highlighted in bold. Since a strong

correlation does not always indicate a strong physical relationship, we also show composite differences between the same variables and lags for comparison (Table III.4). As with the lagged correlations, the lag at which a maximum difference is observed is highlighted in bold.

Both the correlations and the differences are fairly consistent in identifying the lags at which each variable is most strongly associated with cloud fraction. It should be noted that the maximum correlation or difference is not always significantly different than adjacent lags. This is consistent with the interpretation that these lags are indicative not of a specific moment at which an influence is exerted, but of the time scales over which the boundary layer responds to each forcing. A pattern is recognizable in several categories of forcing. LTS and SST, which both contribute to the stability of the layer, are best correlated approximately 36 hours upwind of cloud observations, consistent with the results of Klein et al. (1995). In contrast, advection across the gradient in SST and the surface fluxes of heat and moisture are best correlated at a lag of 6 hours. Specific humidity at 700 hPa has a more varied response, associated with lags ranging from 0 to 12 hours. This is not surprising given its dual impacts on both the moisture budget through entrainment drying and the energy budget through the effectiveness of cloud-top radiative cooling. Finally, variations in the divergence and subsidence rates are primarily associated with near-instantaneous changes in cloud properties. Overall, these results suggest a contrast between the thermodynamic and large-scale dynamic influences on cloud fraction, in which the time scales for boundary-layer response to thermodynamic forcings is long compared to that of dynamic influences.

Bretherton et al. (1995a) present estimates of boundary-layer response time scales for a cloud deck in transition between stratocumulus and cumulus regimes. Using simple bulk scalings and observations from ASTEX the authors define three different time scales: the sub-cloud mixing time scale, the cumulus-stratocumulus layer circulation time scale, and the dilution time scale, which re-

Table III.3: Lagged correlations between low-level cloud fraction (CF_{LIQ}) at the time of observation (0 hours) for the variables and time lags listed below. Blank cells indicate that retrievals are not available at the given lag.

Variable Name	ALT	t = 0 hours	t = 6 hours	t = 24 hours	t = 36 hours	t = 48 hours
LWP_{f15}*	500m	**0.539 (0.511, 0.567)**	——	0.162 (0.124, 0.199)	0.084 (0.047, 0.122)	0.054 (0.017, 0.091)
LWP_{f15}*	2000m	**0.547 (0.519, 0.574)**	——	0.187 (0.149, 0.225)	0.088 (0.050, 0.126)	0.045 (0.007, 0.084)
LTS	500m	0.122 (0.094, 0.150)	0.187 (0.159, 0.214)	0.295 (0.269, 0.321)	**0.326 (0.300, 0.351)**	0.279 (0.253, 0.305)
LTS	2000m	0.122 (0.094, 0.150)	0.185 (0.158, 0.213)	0.207 (0.18, 0.234)	**0.253 (0.226, 0.279)**	0.144 (0.116, 0.171)
SST	500m	-0.114 (-0.142, -0.086)	-0.155 (-0.183, -0.127)	**-0.189 (-0.217, -0.162)**	-0.184 (-0.211, -0.156)	-0.151 (-0.179, -0.123)
SST	2000m	-0.114 (-0.142, -0.086)	**-0.148 (-0.176, -0.120)**	-0.141 (-0.169, -0.113)	-0.109 (-0.138, -0.081)	-0.062 (-0.091, -0.033)
F_{SH}	500m	**-0.086 (-0.114, -0.058)**	-0.073 (-0.147, 0.002)	0.015 (-0.014, 0.043)	0.035 (0.006, 0.063)	0.018 (-0.010, 0.046)
F_{SH}	2000m	**-0.086 (-0.114, -0.059)**	-0.080 (-0.154, -0.005)	-0.038 (-0.066, -0.010)	**0.069 (0.041, 0.098)**	-0.067 (-0.095, -0.039)
F_{LH}	500m	-0.027 (-0.055, 0.001)	**-0.073 (-0.148, 0.002)**	-0.001 (-0.030, 0.027)	0.050 (0.022, 0.078)	**0.090 (0.062, 0.118)**
F_{LH}	2000m	-0.027 (-0.055, 0.001)	**-0.048 (-0.122, 0.028)**	0.034 (0.006, 0.063)	0.069 (0.041, 0.097)	0.074 (0.046, 0.102)
TA_{SFC}	500m	-0.078 (-0.106, -0.050)	**-0.128 (-0.156, -0.100)**	-0.086 (-0.115, -0.058)	-0.026 (-0.054, 0.003)	0.010 (-0.019, 0.039)
TA_{SFC}	2000m	-0.074 (-0.102, -0.046)	**-0.101 (-0.129, -0.072)**	-0.038 (-0.067, -0.009)	0.020 (-0.009, 0.049)	0.030 (0.0001, 0.059)
q_{700}	500m	**0.123 (0.095, 0.151)**	0.124 (0.096, 0.152)	0.090 (0.062, 0.118)	0.068 (0.040, 0.097)	0.063 (0.034, 0.091)
q_{700}	2000m	**0.123 (0.095, 0.151)**	0.119 (0.091, 0.147)	0.115 (0.087, 0.142)	0.101 (0.073, 0.129)	0.089 (0.061, 0.117)
WVP_{f15}	500m	**0.109 (0.069, 0.148)**	——	0.044 (0.006, 0.082)	0.042 (0.004, 0.079)	0.053 (0.015, 0.090)
WVP_{f15}	2000m	**0.1 (0.061, 0.139)**	——	0.056 (0.017, 0.094)	0.054 (0.015, 0.092)	0.053 (0.015, 0.091)
DIV_Q†	500m	**-0.108 (-0.156, -0.060)**	——	0.031 (-0.018, 0.079)	——	0.063 (0.016, 0.110)
DIV_Q†	2000m	**-0.181 (-0.228, -0.134)**	——	-0.045 (-0.094, 0.003)	——	-0.011 (-0.060, 0.038)
DIV_E	500m	**-0.162 (-0.189, -0.134)**	-0.138 (-0.165, -0.110)	0.011 (-0.018, 0.039)	0.043 (0.015, 0.071)	0.077 (0.049, 0.105)
DIV_E	2000m	**-0.162 (-0.189, -0.134)**	-0.170 (-0.197, -0.142)	-0.069 (-0.097, -0.040)	-0.038 (-0.066, -0.009)	-0.024 (-0.052, 0.005)
ω_{700}	500m	**-0.117 (-0.144, -0.089)**	-0.096 (-0.124, -0.068)	-0.027 (-0.056, 0.001)	-0.009 (-0.037, 0.019)	0.004 (-0.025, 0.032)
ω_{700}	2000m	**-0.117 (-0.144, -0.089)**	-0.116 (-0.144, -0.088)	-0.071 (-0.099, -0.042)	-0.039 (-0.067, -0.010)	-0.025 (-0.053, 0.003)
Z_{TOP}	500m	**0.476 (0.450, 0.501)**	——	0.074 (0.039, 0.109)	——	-0.058 (-0.095, -0.021)
Z_{TOP}	2000m	**0.476 (0.450, 0.501)**	——	0.096 (0.061, 0.131)	——	-0.059 (-0.097, -0.020)
w_S	500m	**0.049 (0.016, 0.082)**	——	-0.042 (-0.077, -0.007)	——	**-0.061 (-0.097, -0.026)**
w_S	2000m	**0.049 (0.016, 0.082)**	——	0.028 (-0.007, 0.064)	——	-0.0229 (-0.060, 0.015)
w_E	500m	**0.265 (0.228, 0.301)**	——	0.148 (0.106, 0.189)	——	0.077 (0.030, 0.124)
w_E	2000m	**0.278 (0.241, 0.314)**	——	0.118 (0.075, 0.162)	——	0.053 (0.004, 0.102)

*Overpass times for the DMSP f15 satellite do not match Terra overpass times exactly, so that the LWP_{f15} correlations are effectively lagged by an additional 1-2 hours.

†Overpass times for the QuikScat satellite do not match Terra overpass times, so the DIV_Q correlations are lagged by approximately 6 additional hours relative to the lag denoted in each column.

Table III.4: Differences between the LC and SC composites for the variables and time lags listed below.

Variable Name	ALT	t = 0 hours	t = 6 hours	t = 24 hours	t = 36 hours	t = 48 hours
LWP_{f15}* (g m^{-2})	500m	**49.1 (46, 52)**	——	19.8 (17, 23)	12.3 (8.6, 16)	7.71 (4.0, 12)
LWP_{f15}* (g m^{-2})	2000m	**50.9 (48, 54)**	——	25.7 (22, 30)	13.2 (8.9, 17)	9.86 (4.7, 15)
LTS (K)	500m	0.477 (0.37, 0.58)	0.825 (0.72, 0.93)	1.66 (1.5, 1.7)	1.95 (1.8, 2.1)	**1.96 (1.8, 2.1)**
LTS (K)	2000m	0.477 (0.37, 0.58)	0.825 (0.72, 0.94)	1.47 (1.3, 1.7)	**1.79 (1.6, 2.0)**	1.49 (1.3, 1.7)
SST (K)	500m	-0.204 (-0.25, -0.16)	-0.306 (-0.35, -0.26)	-0.597 (-0.67, -0.53)	-0.765 (-0.86, -0.67)	**-0.859 (-0.98, -0.74)**
SST (K)	2000m	-0.204 (-0.25, -0.16)	-0.294 (-0.34, -0.25)	-0.502 (-0.58, -0.42)	**-0.623 (-0.74, -0.52)**	-0.560 (-0.72, -0.41)
F_{SH} (W m^{-2})	500m	**-2.08 (-2.6, -1.6)**	-1.66 (-3.0, -0.40)	0.52 (-0.41, 1.4)	0.395 (-0.15, 0.98)	1.20 (-0.078, 2.5)
F_{SH} (W m^{-2})	2000m	**-2.08 (-2.6, -1.6)**	-1.73 (-3.2, -0.41)	-2.04 (-3.6, -0.45)	0.871 (0.26, 1.5)	-3.18 (-5.4, -1.0)
F_{LH} (W m^{-2})	500m	-5.1 (-7.1, -3.1)	**-6.90 (-12, -1.5)**	-2.10 (-4.4, 0.21)	3.57 (1.3, 5.9)	9.23 (6.7, 12)
F_{LH} (W m^{-2})	2000m	**-5.1 (-7.1, -3.1)**	-4.89 (-10, 0.49)	0.59 (-1.6, 3.0)	5.71 (3.5, 8.1)	7.60 (4.9, 10)
TA_{SFC} (x10^{-5} K s^{-1})	500m	-0.820 (-1.1, -0.59)	**-1.05 (-1.2, -0.86)**	-0.958 (-1.2, -0.72)	-0.610 (-0.91, -0.30)	0.070 (-0.35, 0.47)
TA_{SFC} (x10^{-5} K s^{-1})	2000m	-0.806 (-1.0, -0.58)	**-0.91 (-1.1, -0.71)**	-0.737 (-1.1, -0.44)	0.292 (-0.18, 0.77)	0.551 (0.048, 1.0)
q_{700} (g kg^{-1})	500m	0.36 (0.28, 0.44)	**0.382 (0.30, 0.46)**	0.294 (0.21, 0.38)	0.242 (0.16, 0.33)	0.227 (0.14, 0.32)
q_{700} (g kg^{-1})	2000m	0.36 (0.28, 0.44)	0.371 (0.29, 0.45)	**0.376 (0.29, 0.47)**	0.360 (0.27, 0.46)	0.342 (0.25, 0.44)
WVP_{f15} (mm)	500m	**1.15 (0.72, 1.6)**	——	0.577 (0.13, 1.0)	0.375 (-0.11, 0.86)	0.64 (0.14, 1.1)
WVP_{f15} (mm)	2000m	**1.22 (0.78, 1.7)**	——	0.946 (0.45, 1.44)	0.812 (0.22, 1.4)	0.90 (0.32, 1.5)
DIV_Q† (x10^{-6} s^{-1})	500m	**-2.63 (-3.3, -2.0)**	——	0.379 (-0.41, 1.1)	——	1.07 (0.24, 1.9)
DIV_Q† (x10^{-6} s^{-1})	2000m	**-3.39 (-4.1, -2.7)**	——	-1.14 (-2.0, -3.3)	——	-0.073 (-0.97, 0.82)
DIV_E (x10^{-6} s^{-1})	500m	**-2.16 (-2.5, -1.9)**	-1.92 (-2.2, -1.6)	-0.034 (-0.35, 0.28)	0.381 (0.05, 0.72)	0.926 (0.57, 1.3)
DIV_E (x10^{-6} s^{-1})	2000m	-2.16 (-2.5, -1.9)	**-2.31 (-2.6, -2.0)**	-1.20 (-1.6, -0.86)	-0.780 (-1.2, -0.44)	-0.352 (-0.73, 0.044)
ω_{700} (x10^{-4} Pa s^{-1})	500m	-1.96 (-2.4, -1.5)	**-2.00 (-2.4, -1.6)**	-0.505 (-0.95, -0.067)	-0.118 (-0.57, 0.31)	0.379 (-0.12, 0.84)
ω_{700} (x10^{-4} Pa s^{-1})	2000m	-1.96 (-2.4, -1.5)	**-2.18 (-2.6, -1.8)**	-1.26 (-1.7, -0.83)	-0.698 (-1.2, -0.20)	-0.404 (-0.93, 0.10)
Z_{TOP} (km)	500m	**0.507 (0.48, 0.53)**	——	0.091 (0.063, 0.12)	——	-0.067 (-0.099, -0.033)
Z_{TOP} (km)	2000m	**0.507 (0.48, 0.53)**	——	0.110 (0.081, 0.14)	——	-0.041 (-0.074, -0.004)
w_S (cm s^{-1})	500m	**0.045 (0.02, 0.076)**	——	-0.035 (-0.065, -0.007)	——	-0.067 (-0.10, -0.033)
w_S (cm s^{-1})	2000m	**0.045 (0.02, 0.076)**	——	0.039 (0.006, 0.071)	——	-0.017 (-0.052, 0.018)
w_E (cm s^{-1})	500m	**0.503 (0.44, 0.56)**	——	0.270 (0.20, 0.33)	——	0.120 (0.049, 0.19)
w_E (cm s^{-1})	2000m	**0.497 (0.44, 0.55)**	——	0.211 (0.14, 0.27)	——	0.142 (0.072, 0.21)

*Overpass times for the DMSP f15 satellite do not match Terra overpass times exactly, so that the LWP_{f15} correlations are effectively lagged by an additional 1-2 hours.

†Overpass times for the QuikScat satellite do not match Terra overpass times, so the DIV_Q correlations are lagged by approximately 6 additional hours relative to the lag denoted in each column.

sults from entrainment of free tropospheric air in the presence of subsidence. They estimate that these time scales are of order 1000 s, 0.5 day, and 4 days, respectively. The boundary-layer mixing time scales of Bretherton et al. (1995a) are consistent with the findings of this study. The dilution time scale also roughly agrees with our observation that LTS, which influences the inversion strength and thus entrainment, is best correlated at longer lags. However, the response to large-scale divergence appears to be in disagreement with the Bretherton et al. (1995a) estimate of the response to subsidence.

A few points should be made about the apparent disagreement between the response time scales observed in the present study and the estimates of Bretherton et al. (1995a). First, it should be noted that the scalings put forth by Bretherton et al. (1995a) as well as for most simple models of boundary-layer clouds assume a steady subsidence rate and a gradual approach to equilibrium. A surprising outcome of the present study is that subtropical clouds appear to be significantly influenced by large, synoptic-scale variations in subsidence rate. Also, the time scale quoted from Bretherton et al. (1995a) is for steady-state boundary-layer height, implying that subsidence is balanced by entrainment. More generally, an increase in divergence will not necessarily be balanced by entrainment, and any imbalance between the two will result in a change in the inversion height. In the present case, the increase in the divergence does not appear to be balanced by a commensurate increase in the entrainment rate, causing the inversion height to lower. The cloud response to a lowering of the inversion will occur over much shorter time scales than those predicted for steady-state boundary layer height. This is discussed below as a potential explanation for the observed changes in the SC composite.

Finally, an additional specification can be made regarding the non-linearity of cloud response between the SC, MC, and LC cases. Figure III.12 shows the composites of selected variables plotted against cloud fraction. These variables are

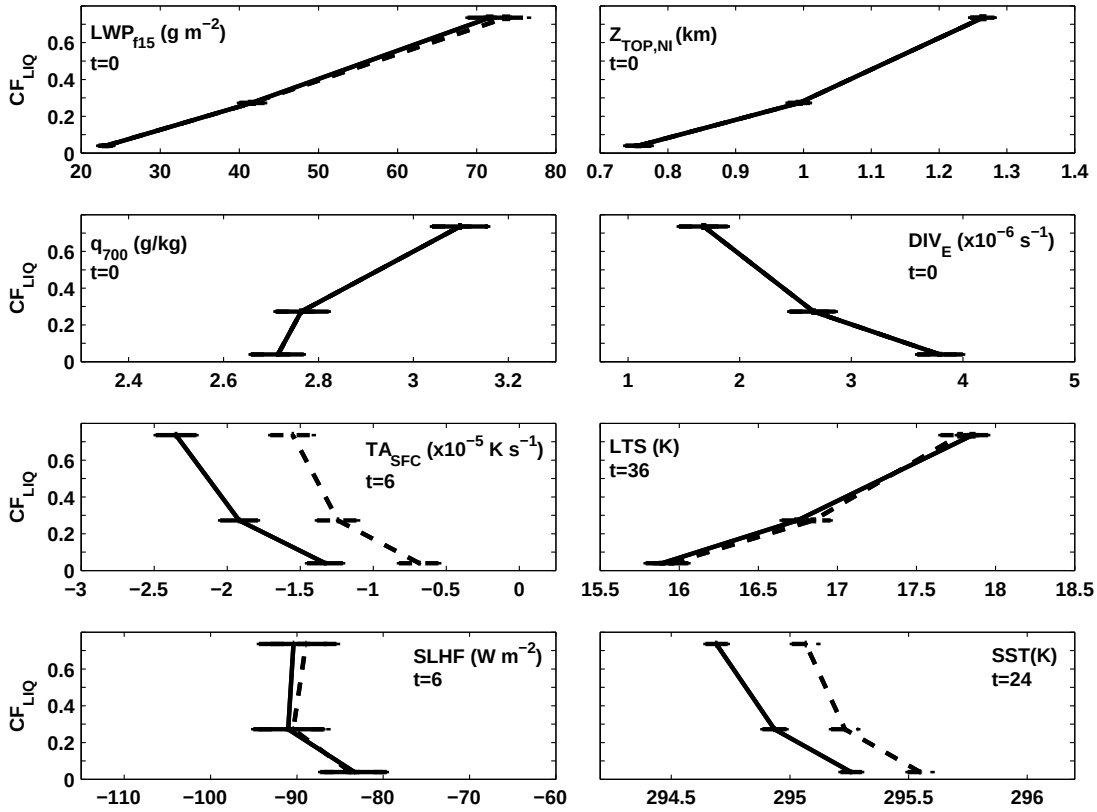

Figure III.12: Composites of selected variables for the lags identified in Tables III.3 and III.4. 95% confidence limits are shown for both the x- and y-axes in each plot. Solid lines denote the composites for the 500m trajectories, while dashed lines are for the 2000m trajectories.

selected for exhibiting a clear relationship to cloud fraction. Instead of taking the instantaneous composites of each variable, they are composited for the time lags identified in Tables III.3 and III.4. This provides a graphical representation of the non-linearity in cloud response. We can first observe that the dashed lines, denoting the 2000m trajectories, are in some cases separated from the 500m trajectories, reflecting the different origin of the above-inversion air. The relationships shown are predominantly linear, with the notable exception of the surface latent heat flux, which is significantly smaller in the SC case but remains similar between the

MC and LC cases. Interestingly, at longer lags the sign of the relationship between evaporative flux and cloud cover reverses. Again, this is consistent with the results cited above, showing a reversal at long lags in which the LC case is associated with *decreased* surface fluxes, *increased* subsidence, and lower cloud tops. This is also consistent with the mixed layer theory prediction that larger moisture fluxes will eventually lead to decoupling. At short lags such as 6 hours, however, the latent heat flux is more likely a reflection of efficient vertical moisture transport to the cloud layer through mixing.

III.6.E Subsampling to exclude high clouds

All variables derived from MODIS cloud-top height estimates are filtered for high cloud influence in order to avoid the associated cold bias in cloud temperature retrievals. Subsampling the data to remove high clouds may bias the sample in a number of ways, in particular towards a drier free troposphere and greater low-level divergence. We thus devote some discussion to a comparison of the "all-sky" to the "no ice" cases. Our goal is to evaluate the potential for Z_{TOP} taken only from scenes without high clouds to be representative of the larger set of observations that include all instances of low cloud. Results are presented below in which observations that have been filtered for high clouds are composited into terciles of large, middle and small low-level cloud fraction (LCNI, MCNI, SCNI, the "NI" denotes "no ice").

Figure III.13 displays back trajectories of cloud properties for the three composites. Liquid water cloud fraction is seen to have very similar variations to that of the LC/MC/SC trajectories. Discussed in detail in the satellite data section above, the present study screens high clouds by limiting MODIS retrievals of ice cloud fraction and cirrus cloud fraction to remain below 1% and 25% respectively, for the entire parcel trajectory. Cirrus fraction, shown in the second plot, indicates that the filtering successfully reduces the quantity to well within this range,

although a small systematic relationship still remains. Again, it should be noted that the authors found evidence of a small, systematic bias in MODIS-derived cirrus fraction, most likely resulting from the high albedo of low-level clouds. Furthermore, if these were impacting cloud-top temperature retrievals, the cold bias would impact the SC cases the most, since the cirrus cloud coverage is comparable to the mean low-level cloud cover for the SC composite. The evidence for effective high cloud filtering is further supported by the fact that going back in the trajectory the cloud-top height estimates approach a constant value that is a physically plausible value of the boundary layer height. Since the majority of trajectories travel anticyclonically from the North and West of the Atlantic, we would expect to see increased high cloud cover at earlier points in the trajectory. This is reflected in the unfiltered composites of ice cloud (Figure III.11), but is not seen in the Z_{TOP} trajectories of Figure III.9, which are filtered for high clouds. Based on these arguments, we believe that the impact of high clouds are largely removed by the present screening.

Another quantity that appears to be impacted is the shortwave flux estimate of CERES, as seen in Figure III.4. In contrast with the all-sky composites, Figure III.13 shows a decrease in reflected shortwave flux and a lesser trend towards high albedo earlier in the trajectory. Regarding the analysis of low-cloud sensitivities, the presence of high clouds is only an issue if the goal is to isolate the impact of various forcings on low-level cloud albedo rather than simply focus on the shortwave forcing associated with particular cloud conditions. The philosophy in the latter approach and that espoused in this paper is that the all-sky flux reflects the real atmospheric conditions under which the observed clouds exist. However, some of the change in shortwave flux is likely to be related to differences in the sampling, as indicated by the composites of SSM/I liquid water path. These show slightly lower LWPs than the all-sky composites, and also a decreased difference between composites.

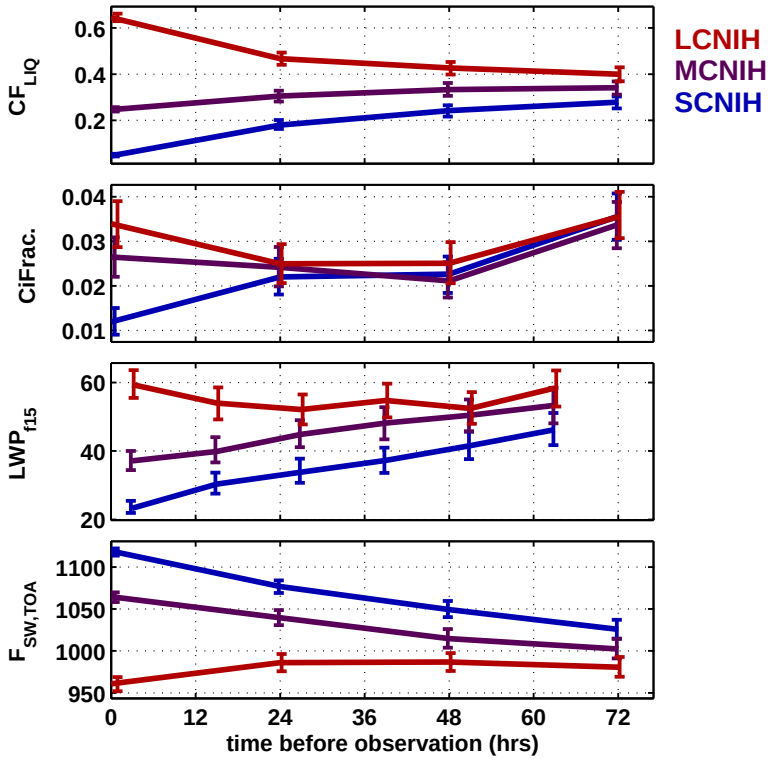

Figure III.13: Composite back trajectories for low-cloud observations that have been screened for high cloud influence (LCNIH, MCNIH, SCNIH). The plots show the overlap-corrected MODIS low-level cloud fraction (CF_{LIQ}), MODIS cirrus fraction, SSM/I LWP from the sensor aboard the f15 satellite (g m^{-2}), and CERES top-of-atmosphere net shortwave flux (F_{SW}, W m^{-2})

In order to provide a direct comparison, the lagged composites are displayed along with those for the all-sky composites in Figure III.14. In general, these show decreased variations relative to the all-sky composites. In terms of cloud properties, there is less cloud cover overall and a slight reduction in the variations in liquid water path. As expected given a constraint on high clouds, the free tropospheric moisture is decreased and the surface divergence is increased. Both show diminished variations with respect to the changes in cloud cover. The most striking change is the significant reduction in the magnitude of the latent heat flux, some of which may result from the associated decrease in temperature advection for the SC and MC cases. These changes are accompanied by a substantial increase

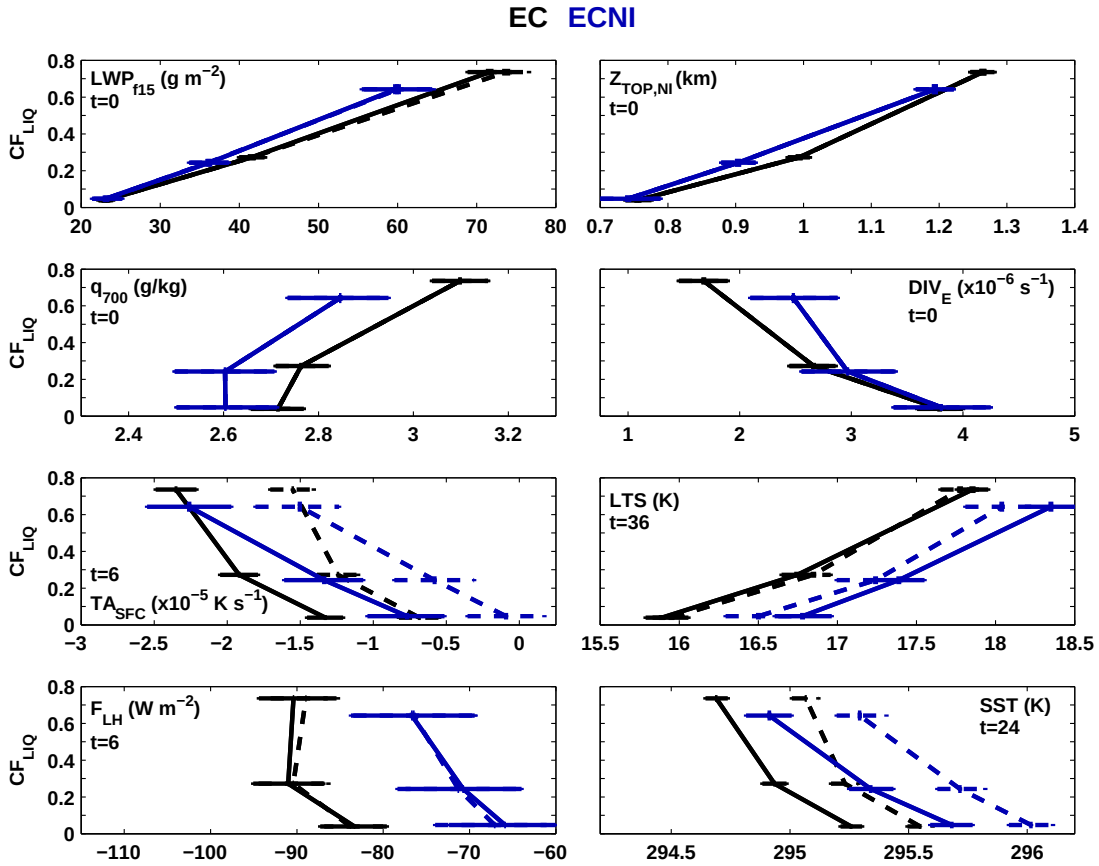

Figure III.14: As in Figure III.12 with the addition of the "no ice" composites for comparison (ECNI, blue lines).

in stability overall and a sharper association with temperature advection, which the SSTs at 24 hours also reflect. It should be noted that as with all sampling described in this study, the data are sampled uniformly for each grid box and each month. In contrast, there is no constraint on the origin of trajectories, and the evidence presented here indicates that the NI cases originate over warmer SSTs. Overall, the relative changes present in the all-sky cases are all present to some degree in those that are filtered for high clouds, and for the purposes of a qualitative assessment the cloud-top height sensitivities are likely to be a reasonable approximation. However, based on the above evidence we cannot conclude that the "all-sky" and "no ice" samples are interchangeable.

III.6.F Controlling for covariation among meteorological quantities

A primary focus of Chapter II is the idea that cloud sensitivity to each forcing parameter must be assessed independently of other influences on cloud properties. The analysis presented thus far has consisted of an assessment of the quantities that co-vary with low-level cloud cover, but has not addressed the question of either coupling or covariation between different meteorological forcings. Specifically, divergence and stability appear to be the two quantities that associate most strongly with changes in cloud cover. It is possible that the observed relationship between a given meteorological forcing and cloud cover is primarily determined through covariation with LTS. This is likewise a possibility for surface divergence, as is the possibility that the impact of LTS acts to precondition the boundary layer, thus influencing its response to divergence. In order to examine the sensitivities of low clouds in the absence of each of these, we follow the method outlined in chapter II and subsample the data for cases that are closest to the median in either LTS or divergence. Since both appear to impact the boundary layer over long time scales, the median values are selected from the 2-day average in LTS and the 1-day average in divergence.

The median divergence cases (MDEC) are shown for comparison with the EC (all conditions) cases in Figure III.15. Confirmation that the subsampling has provided the desired constraint is seen in the lack of a significant variation in divergence between the cloud cover composites. In general these show similar relatopnships to those for the all-sky composites, most important of which is the consistency in the LTS dependence. It is not surprising that the relationship between stability and cloud cover is unaffected by divergence, since observational results consistently indicate that it impacts clouds over time scales much longer than the observed variations in divergence. Temperature advection, latent heat flux, and SST show increased variations with respect to cloud fraction for the

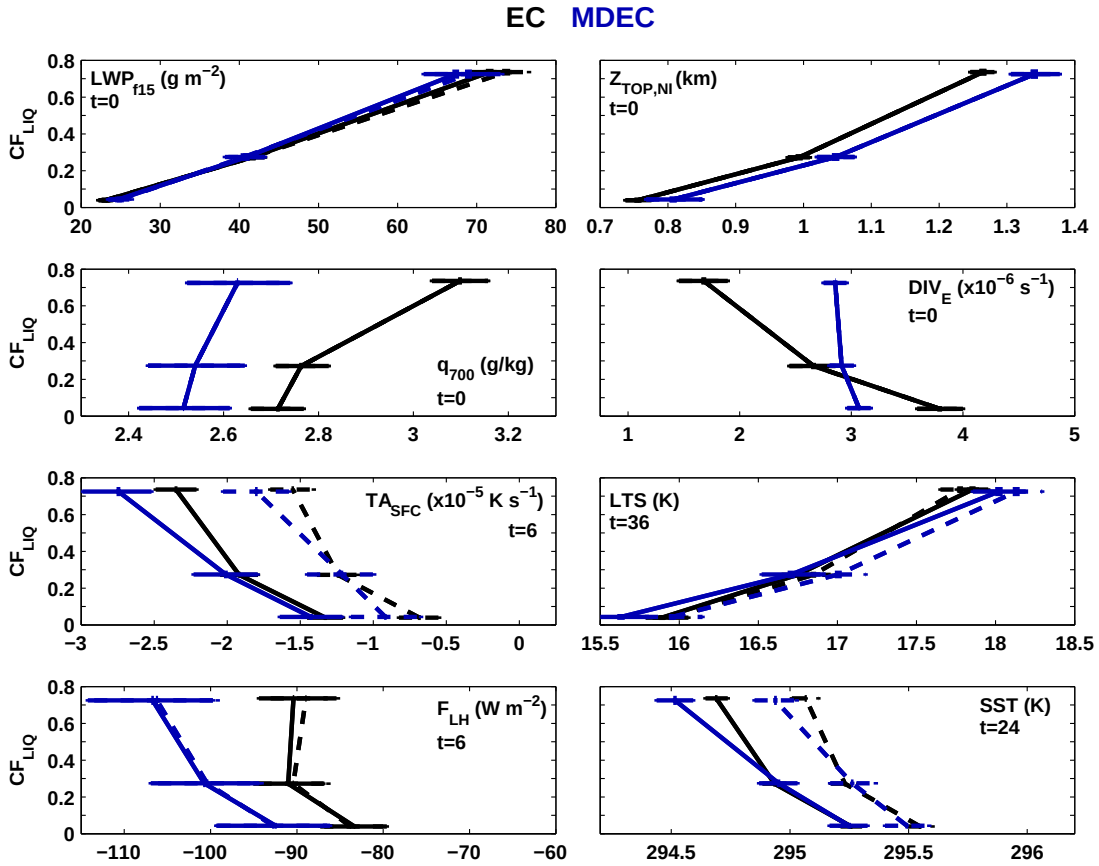

Figure III.15: As in Figure III.12 with the addition of the "median divergence" composites for comparison (MDEC, blue lines).

MDEC cases. This is accompanied by an overall drying of the free troposphere and a strengthening of surface latent heat fluxes. This evidence suggests that in the absence of changes in divergence, compensating changes in the surface heat and moisture budgets contribute to the observed changes in cloud cover. In contrast, the median stability cases (MSEC, Figure III.16) show opposing changes in TA_{SFC}, F_{LH}, and SST along with an increased cloud sensitivity to divergence. This suggests that quantities associated with the surface heat and moisture fluxes are inversely correlated with changes in divergence. Significantly, neither of the above figures reveals any evidence that the observed correlation between cloud cover and stability is simply the result of a covariation with divergence. The same

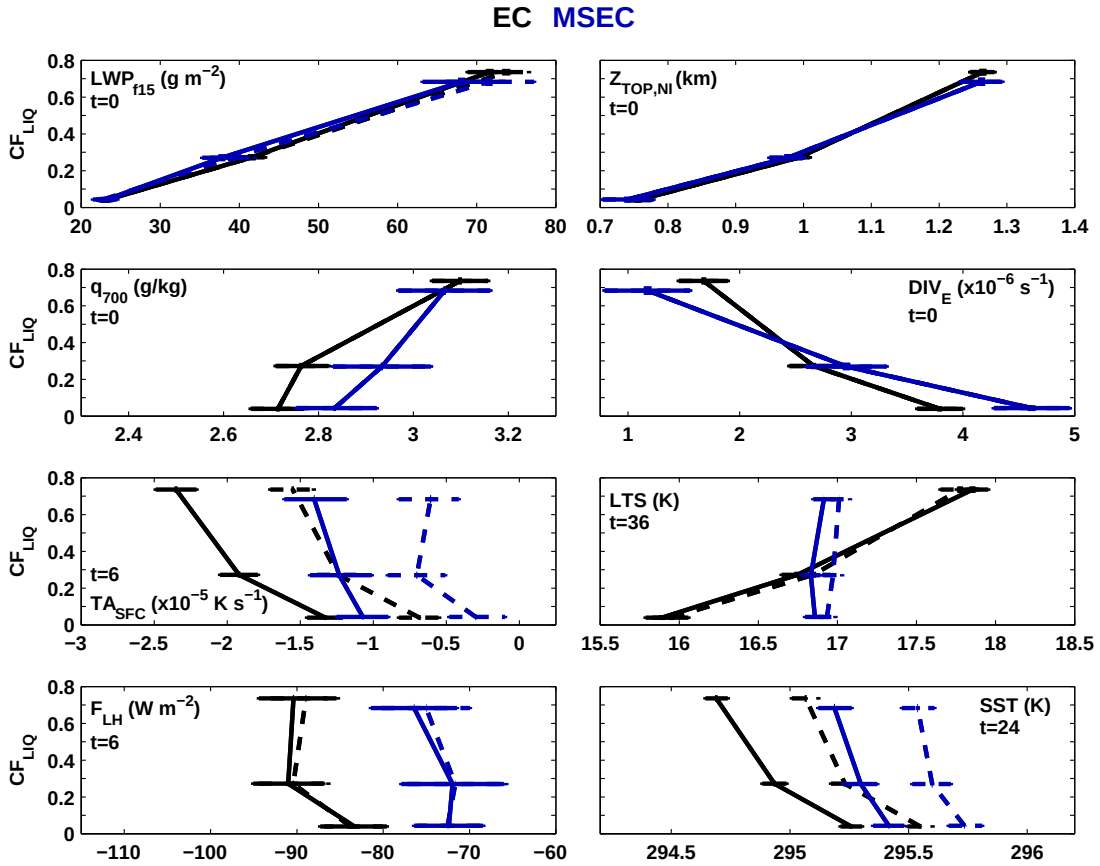

Figure III.16: As in Figure III.12 with the addition of the "median stability" composites for comparison (MSEC, blue lines).

can be said of divergence, since even an appreciable increase in the sensitivity is observed in the median stability cases. As a consequence, we can conclude that the sensitivities observed in the LC/MC/SC cases (*e.g.,* Figure III.12) are likely to be representative of the true sensitivities of cloud cover variations to divergence and lower tropospheric stability.

III.6.G Subsidence and Entrainment Rates

A number of mechanisms could be contributing to the correlation between cloud cover and surface divergence. The associated change in cloud-top height

suggests that a change in the balance between entrainment and subsidence allows developing clouds to grow and thicken. Alternatively, a thickening of the clouds under weakening subsidence could simply result from adiabatic cooling associated with a lifting of cloud top. Mixed-layer models predict a roughly inverse proportionality between divergence and cloud-top height (*e.g.,* Schubert et al., 1979), indicating that boundary-layer clouds seek to maintain a fairly constant subsidence rate at cloud-top. Given the estimates of cloud-top height and a knowledge of the divergence profile, we can use Equation III.1 to estimate the variations in entrainment rate for each trajectory. Since MODIS observations of cloud-top height can only be filtered for high clouds when shortwave and near infrared radiances needed for Cirrus_Fraction_SWIR are available, we can only obtain cloud-top height estimates once for every 24 hours. As a result, we estimate the 24 hour average in entrainment rate by differencing subsequent estimates in cloud-top height. Cloud-top subsidence rate is computed by assuming a divergence profile that decreases linearly to zero at 700 hPa and integrating up through Z_{TOP}. Sensitivity to the assumed divergence profile was tested by computing maximum and minimum subsidence rates, based on the assumption of a constant boundary layer divergence profile and a linear decrease to zero, respectively. Absolute differences between these estimates are apparent and are of order 25% ($\pm$ $\sim$0.05 cm s^{-1}). However, the relative changes in subsidence and entrainment rates are generally insensitive to the assumption used.

Figure III.17 shows composite back trajectories for the above estimates of subsidence and entrainment rates (w_S and w_E, respectively). Since these estimates rely on cloud-top height estimates, the observations used here are screened for high cloud influence. It is clear from these trajectories that partial pixel biases in cloud-top height are significantly impacting the results, in particular given that the SC composite shows a negative entrainment rate at 0 hours. The SC composite at 0 hours is primarily constituted by retrievals for cloud fractions less than the 30%

identified in Figure III.2 as being significantly impacted by partly cloudy pixels. This is true of a large fraction of the MC retrievals as well. The magnitude of the correction for these biases can be estimated based on the mean bias shown in Figure III.2. Calculations indicate that correcting for this bias will most likely reduce the difference significantly, but will probably maintain the sign of the association with cloud cover. It should be noted that such corrections should be treated with caution, since the association seen in III.2 reflects partial pixel biases as well as any true physical relationship that exists between CTT and CF_{LIQ}. The above correction should thus have the result of removing both the systematic bias as well as any real association between cloud-top temperature and low-level cloud cover. It is thus not surprising that applying such a correction would drastically reduce the distinction between the composites. Nevertheless, although we argue that the sign of the relationship will probably remain unchanged, it is undeniable that some bias exists, and that this bias significantly impacts the observed relationship between estimated entrainment rates and the composites of low-level cloud cover. These results should thus be treated with caution, and their significance weighed accordingly.

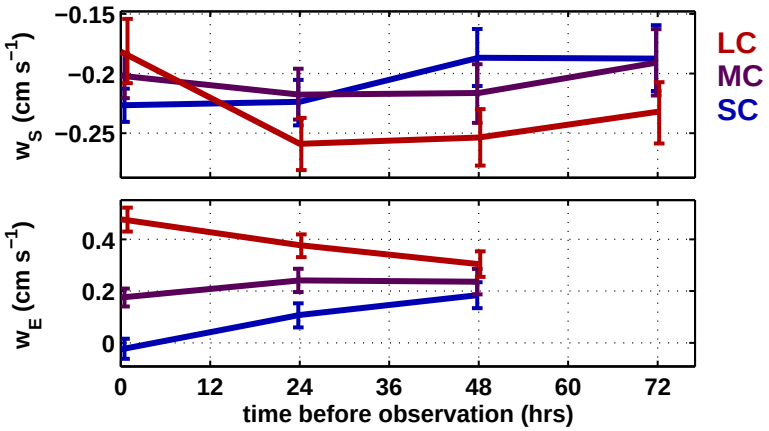

Figure III.17: LC/MC/SC composite back trajectories for cloud-top subsidence rate (w_S, cm s^{-1}) and estimated entrainement rate (w_E, cm s^{-1}).

Given the above caveats, here we discuss some of the implications of the observed differences in entrainment rate. The composites of subsidence rate are consistent with the mixed-layer predictions cited above (Schubert et al., 1979), indicating that cloud height adjusts to maintain a roughly constant subsidence rate in response to changes in divergence. The LC composite of entrainment velocity is likely to be fairly reliable based on Figure III.2, which indicates that partial pixel biases in cloud-top temperature (CTT) are primarily important for cloud fractions less than $\sim$0.3. In Figure III.17, the LC composite shows values that are within the range quoted by Bretherton et al. (1995a), who found values of 0.7$\pm$0.3 cm s^{-1} and 0.6$\pm$0.3 cm s^{-1} for observations of a solid stratocumulus deck and a decoupled dissipating boundary-layer, respectively. The entrainment rate (w_E) shows an increase in entrainment as cloud cover increases. This is somewhat unintuitive since increased entrainment should also be associated with increased warming and drying of the boundary layer. However, additional consequences of increased entrainment are a deepening of the layer and thus greater cooling and saturation of parcels mixing from the surface, a strengthening of the inversion and a more sharply defined region of radiative cooling at cloud top, thus driving stronger mixing within the layer. Greater turbulent kinetic energy (TKE) generation at cloud top will have the effect of increasing the entrainment rate until it is balanced by the subsidence rate. Based on this reasoning, the increased entrainment for the LC case is consistent with the picture outlined in previous plots of a developing stratiform cloud layer. What this result illustrates is that entrainment rate alone is insufficient to define the path of cloud evolution. This is consistent with the findings of Bretherton et al., (1995b), which associate vastly different cloud regimes with nearly identical entrainment rates. Other factors, such as the increase in tropospheric humidity (Figure III.7), the increase in cold advection over systematically warmer SSTs (Figure III.7), and the structure and type of boundary layer clouds all contribute to the conditions that favor cloud development.

III.7 Discussion

As stated in the introduction, the goal of this study is to identify the dominant physical relationships that relate atmospheric state to cloud forcing. We have presented a wide range of results and discussed both the relevance and the veracity of each. Here we summarize the findings and discuss the implications in the context of the conceptual framework outlined in the beginning of the chapter. An advantage of the Lagrangian approach is that we can do so in the context of the historical evolution of the parcel and associated forcings.

It is instructive to contrast the conditions at the time of observation (0 hours) with those at the end of the 72 hour back trajectories. The LC case exhibits significantly greater cloud cover as well as liquid water path throughout the 72 hour history. This is accompanied by a warmer free troposphere and cooler SSTs, which result in a greater stability of the lower atmosphere (LTS). Free tropospheric humidity and column water vapor are also consistently larger throughout the history of the LC composite. These are contrasted by several quantities whose relationship to cloud fraction changes sign over the course of the trajectory. Most notable among these are the surface divergence and associated cloud-top subsidence rate, which are weaker for the LC case at 0 hours but significantly stronger than the other two cases at -72 hours. Cloud top height is consistent with these changes in divergence and is fairly constant at the origin of the trajectory, indicating that the increased subsidence is matched by a stronger entrainment rate. These results are summarized in Table III.5. Discussed in terms of physical associations, at -72 hours the LC composite indicates a shallower boundary layer that experiences stronger subsidence and colder SSTs and entrains at a greater rate than the MC and SC cases. Increased moisture above the inversion makes it possible to sustain greater entrainment rates while maintaining a moist boundary layer.

The results at -72 hours highlight several unanswered questions. To begin with, if stronger entrainment is to be maintained in the face of a sharper inversion,

Table III.5: Descriptive summary of findings for selected dynamical variables. In the table, the term "constant" does not refer to the magnitude of the relationship, but its sign.

Variable	0 hour trend with CF	historical evolution
CF_{LIQ}	increasing	constant throughout parcel history
LWP	increasing	constant throughout parcel history
LTS	increasing (cooler SSTs, warmer T_{700})	constant throughout parcel history
q_{700}	increasing	constant throughout parcel history
WVP_{f15}	increasing	constant throughout parcel history
DIV_{SFC}	weakening divergence	trend reversed for t>30 hrs
ω_{700}	weakening subsidence	trend reversed for t>36 hrs
Z_{TOP}	increasing	trend reversed for t>36 hrs
TA_{SFC}	increasing cold advection	trend reversed for t>48 hrs
F_{LH}	increasing evaporative flux	trend reversed for t>30 hrs
w_S	increasing	trend reversed for t>12 hrs
w_E	increasing	constant throughout parcel history

then the boundary layer must generate a greater amount of turbulence, presumably through radiative cooling at cloud top. However, there is no discernable difference in liquid water path, and the increase in tropospheric humidity would in fact impede greater cloud-top cooling. This apparent contradiction may result from the different character of clouds in the LC versus SC composites. If the SC clouds consist of cumulus or cumulus under detraining stratiform clouds, it would be possible to have the same liquid water path for a uniform stratocumulus deck as for a cloud deck that alternates between thick and thin clouds. Similarly, a warm bias in cloud-top temperature for the SC composite, resulting from increased surface contamination for thinner clouds, would result in artificially low estimates in cloud-top height and, consequently, an underestimate of the entrainment rate. As discussed in Section III.6.G above, the latter bias is likely to be important.

Alternatively, one could conclude that the small but significant difference in LWP at -72 hours is sufficient to explain the difference in TKE generation suggested by the evidence cited above. At -72 hours, the SC composite shows warmer

SSTs, which contrast with a decrease in column water vapor. Since variations in the column vapor path are dominated by variations in the boundary layer, this suggests that the boundary layer is less humid. This is consistent with the fact that the warmer SSTs will most likely raise the lifting condensation level, yet the cloud-top height is actually slightly lower than that for the LC case. This suggests that the SC clouds are thinner than those for LC, and is consistent with the conclusion that the observed difference in LWP at -72 hours is real.

The latter scenario implies that the difference in cloud cover at 0 hours is a consequence of differences in the coupling between the surface and cloud top. One final piece of evidence is that the SC composite shows a stronger latent heat flux at -72 hours. Although this carries with it the uncertainty in the ECMWF parameterization of the surface layer, it is matched by a small and weakly significant increase in the surface temperature advection. As mentioned in section III.3, this is consistent with the predictions of several authors (*e.g.,* Schubert et al., 1979; Bretherton and Wyant, 1997), who attribute increased moisture fluxes to an increased stability of the sub-cloud layer and an eventual decoupling of the sub-cloud and cloud layers. Throughout the course of the 72 hours, the SC composite is consistent with the two-stage model suggested by Wyant et al. (1997). The authors describe a first stage in which decoupling is driven by increased surface fluxes followed by a second stage in which continually increasing SSTs contribute to a transition to progressively more vigorous cumulus convection which increasingly mixes across the inversion, causing the stratocumulus deck at the boundary layer top to dissipate. This is consistent with the fact that the SC trajectory experiences SSTs that are substantially greater than those for the LC composite.

Figure III.18 shows a schematic summarizing the implications of the above discussion. At -72 hours, the LC and SC composites show similar cloud cover. The evidence discussed above indicates that at this time the SC cases reflect a decoupling of the cloud and sub-cloud layers. An important detail that is

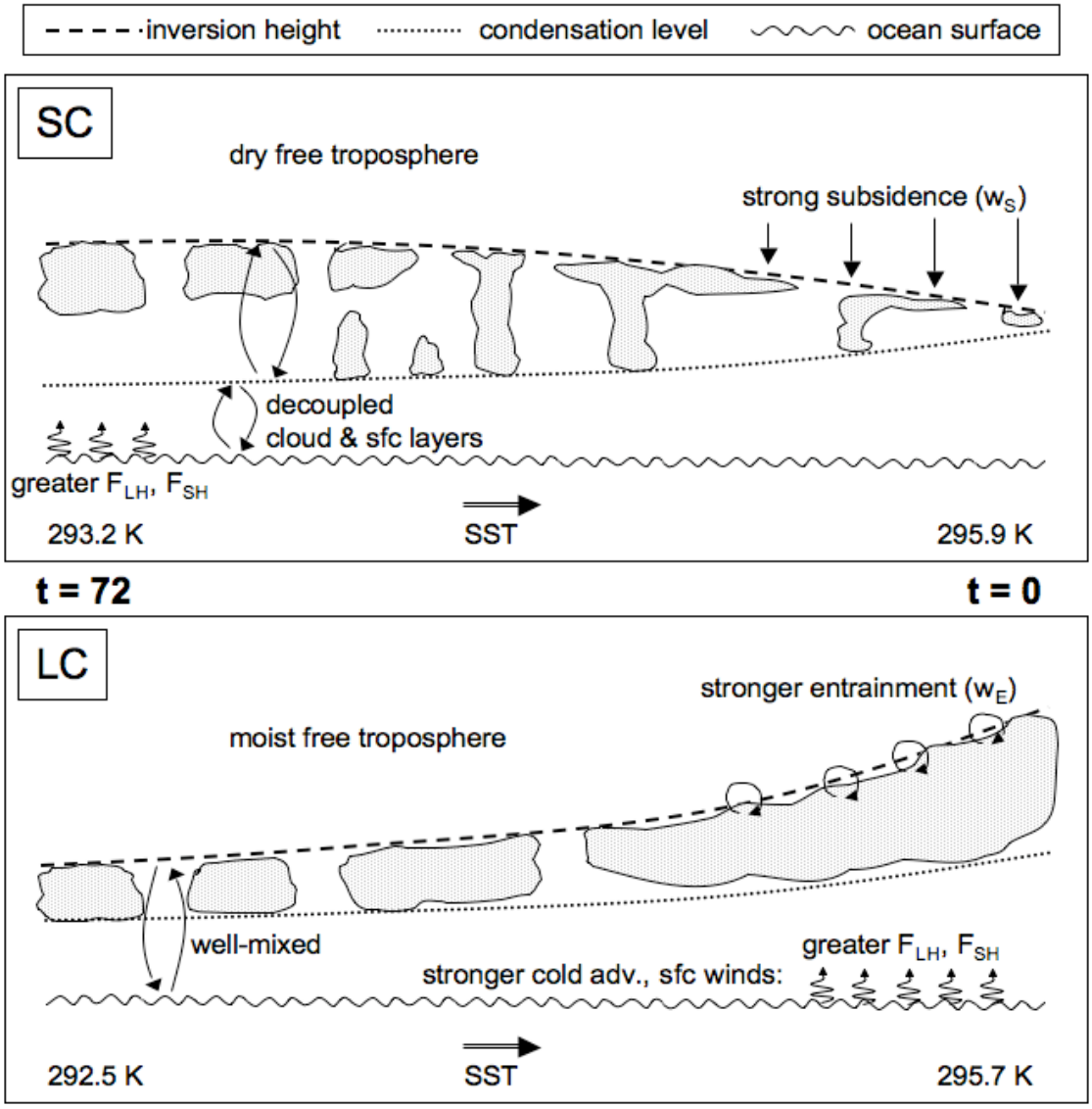

Figure III.18: Schematic interpretation of the observed differences between SC and LC cases, including several of the mechanisms that are suggested to result in the observed differences in the evolution of cloud cover along each composite trajectory. An important detail that is not included in the schematic is the stability, which is substantially greater throughout the LC trajectory.

not shown is the stability, which is not only weaker for the SC case, but the temperature difference in a decoupled boundary layer will not only reflect the inversion but also the stable sub-cloud layer. This supports the hypothesis of a weaker capping inversion and possibly greater entrainment. As the SC clouds evolve they are influenced by a weaker gradient in SST, which results in decreased moisture fluxes and a higher condensation level. Combined with the drier free troposphere for the SC cases, the boundary layer continues to dry and decouple. Finally, the pronounced increase in divergence towards the end of the trajectories acts to suppress the inversion in the face of weak entrainment, and results in a dissipation of the cloud layer.

In contrast with the SC cases, the evidence presented above indicates that the LC cases are well-mixed throughout the 72 hour trajectories. A well-mixed boundary layer implies that the 2K increase in LTS relative to the SC composite results in a substantially stronger inversion strength. The LC clouds advect over a stronger SST gradient and have stronger surface winds, prompting an increase in heat and moisture fluxes from the surface. This is complemented by an increase in free tropospheric humidity throughout the trajectory, which acts to moderate the drying due to entrainment as the cloud layer grows. As with the SC case, as the clouds advect over warmer SSTs the condensation level rises. However, in contrast with the SC case, the inversion height rises at a greater rate than the condensation level, giving way to significantly thicker clouds.

III.8 Conclusions

We have presented evidence concerning the meteorological sensitivities of Northeast Atlantic clouds at synoptic scales. The method used builds upon the Lagrangian trajectory method developed in Chapter II, with the addition of new satellite observations of broadband fluxes, cloud water, and surface winds. A

benefit of the Lagrangian analysis is that it permits the incorporation of a wide variety of non-coincident observations, as is the case for satellite platforms with different orbit characteristics. We analyze cloud cover by compositing trajectories into terciles of low-level cloud fraction, and evaluate the associated changes in meteorological and cloud properties along 3-day back trajectories. Atmospheric stability (LTS), surface divergence, free tropospheric humidity (q_{700}), sea surface temperature (SST), and SST advection are all found to contribute significantly to changes in cloud cover. These quantities are all readily observable and serve as effective proxies for the physical processes that govern boundary layer evolution. Significantly, the Lagrangian analysis identifies the time lag at which each of the above quantities exerts the greatest influence on the evolution of boundary layer clouds. A distinction is identified between dynamical variables and several thermodynamic conditions, including LTS, SST, and q_{700}, which appear to influence cloud properties over longer time scales. Although many mixed-layer simulations assume steady or slowly-varying divergence, an important finding of the present work is that large synoptic-scale variations in divergence are commonplace. These dramatic changes in divergence are found to exert a dominant influence on cloud properties.

Based on the evidence presented, we suggest that the contrasting evolution of the large and small cloud cover cases is a consequence of a decoupled boundary layer, the differing stability and SST advection, and finally, by the stark contrast in subsidence and entrainment at the end of the trajectory. Unfortunately, with the tools currently available we cannot verify that the SC cases are indeed decoupled, nor can we have high confidence in the estimate of entrainment rate. However, the veracity of our hypothesis is reinforced by the internal consistency between multiple different measurements in each case. A primary uncertainty that is identified in the present analysis is the estimate of cloud-top height. The analysis would be significantly improved by the inclusion of coincident, independent

measurements of boundary layer height. Such measurements are now possible from the operational Cloud-Aerosol Lidar with Orthigonal Polarization (CALIOP) cloud height retrieval algorithm. However the satellite was not in orbit during the dates used in the present analysis.

The results presented above reveal the wealth of information that is available in the Lagrangian analysis developed here and in Chapter II. The present work represents a useful first step in the Lagragian characterization of low-level cloud sensitivities. There are many respects in which the current work can be extended to provide additional information on cloud sensitivities, such as the inclusion of additional satellite measurements, investigation of other subtropical regimes, or, as in ASTEX (Albrecht et al., 1995), to inform future field campaigns. The following chapter discusses another respect in which the present analysis can prove fruitful, in which model cloud sensitivities are compared to observations.

IV Model evaluation of aerosol-cloud interactions

IV.1 Abstract

Model output is evaluated in order to investigate the relationship between Aerosol optical depth (AOD) and cloud fraction (CF). Models provide the opportunity to perform controlled experiments, and thus separate the impacts of aerosols and meteorology on cloud cover. Comparison with the ECMWF model indicates that 43% of the observed AOD-CF sensitivity results from meteorological covariations. This is consistent with the results of Chapter II, although the correction is larger. However, there is contradicting evidence as to the adequacy of the ECMWF cloud parameterization. In contrast with the dynamical sensitivities of ECMWF clouds, which are found to compare well with those of MODIS, ECMWF cloud cover predictions correlate poorly with cloud cover observations made by MODIS. Since MODIS observations and ECMWF predictions of cloud cover differ significantly in a number of respects, a different model experiment is performed in which two configurations of the same model are run in parallel. Model output is obtained from the new GFDL atmospheric model, which includes an interactive aerosol-microphysics scheme. Simulations are compared with the scheme coupled to the ambient aerosol population and with the two decoupled, using a prescribed CCN spectrum. In the case of the GFDL model, the comparison

indicates that 100% of the aerosol-cloud correlation results from meteorological covariations. However, an investigation of model cloud sensitivities indicates that this result may not be applicable to the observations. Although meteorological covariations are evident in the AOD composites, cloud dynamical sensitivities differ substantially from those observed by MODIS. Specifically, the differences in meteorology between large and small cloud cases are much smaller than in the observations, indicating that the model clouds are either more sensitive to changes in the same variables, or dependent on other meteorological quantities that are not accounted for in the present analysis. We conclude that although the analysis cannot provided a quantitative correction to the estimated aerosol-cloud sensitivity, it qualitatively confirms the results of Chapter II. Further, the analysis demonstrates the potential for the Lagrangian analysis method to provide new diagnostic information on the performance of cloud parameterizations.

IV.2 Introduction

Ultimately, the goal of aerosol, cloud, and climate studies is to quantify the impacts of anthropogenic forcing on current and future climate scenarios. It is thus essential to develop reliable model treatments of aerosols, clouds, and the interactions between the two. The Intergovernmental Panel on Climate Change (IPCC) identifies aerosol-cloud impacts as the greatest uncertainty in the radiative forcing of climate (Forster et al., 2007). Likewise, low cloud parameterizations are cited as the primary source of uncertainty in General Circulation Model (GCM) projections of future climate (Meehl et al., 2007). The prior two chapters have described the application of a Lagrangian technique to observations of cloud and aerosol obtained from satellites. The present work applies the same technique to model output, providing comparisons with the observational sensitivities as well as a controlled test of the correlations observed in Chapter II.

Given the significant cooling effect of subtropical cloud regimes, small uncertainties in the interactions with aerosols can result in large differences in climate predictions. The challenges in developing accurate parameterizations of aerosol-cloud processes are widespread, ranging from assumptions about the activation of droplets and the evolution of the droplet spectrum (*e.g.*, Charlson et al., 2001) to a proper treatment of the mixing state of aerosols (Lohmann and Feichter, 2005). A major advantage of models is the ability to perform controlled experiments. As discussed in Chapter II, observational studies are limited by the ability to decouple variations in cloud properties due to aerosol from those due to other dynamic and thermodynamic changes in atmospheric state. In contrast, GCMs can be used to isolate the impacts of different forcings. For example, aerosol impacts on cloud microphysics can be evaluated by running two identical simulations that differ only in the coupling between cloud microphysics and aerosol properties. In this way all other forcings remain constant and the differences between the two simulations result from aerosol-induced changes in cloud microphysics. Although such simulations can be used to estimate the climate sensitivity to a specific perturbation, the present study is instead focused on evaluating the changes in the synoptic-scale sensitivities of cloud to aerosol. As in previous chapters, the synoptic-scale focus is chosen because it permits an investigation of the reasons behind the observed correlation between aerosols and cloud cover.

The Lagrangian synoptic-scale analysis is also useful in that it provides new focused diagnostic information on model performance. Recent model intercomparisons are consistent in identifying low-level cloud parameterizations as the largest source of uncertainty in projections of future climate (*e.g.:* Bony and Dufresne, 2005; Soden and Held, 2006; Meehl et al., 2007). In-depth diagnostic information is needed to motivate improvements in the current parameterizations. Typically, model intercomparisons and observational validations are concerned with the representation of large-scale, spatially or temporally averaged

fields. In contrast, the method applied in the present work is focused on evaluating the mean *sensitivities* at the synoptic scale. This permits an investigation of the mechanisms behind observed model behavior, and can thus provide new insight into the specific strengths and weaknesses of each parameterization.

Aerosol-cloud impacts have the potential to significantly alter the climate. In this study we use large-scale models to investigate the correlation between aerosol optical depth and cloud fraction observed in previous chapters. The first section compares cloud predictions from the European Centre for Medium Range Weather Forecasting (ECMWF) model to those observed by satellites, while later sections evaluate model output obtained from the Geophysical Fluid Dynamics Laboratory (GFDL) atmospheric model.

IV.3 Using MODIS and ECMWF to Assess aerosol-cloud sensitivities

We begin by revisiting the observational results of Chapter II, with the addition of a comparison between MODIS observations of aerosol optical depth (AOD) and ECMWF predictions of cloud cover. In previous chapters ECMWF operational analyses were used to supplement satellite observations with otherwise unavailable meterological fields. In those investigations, we sought to minimize model influence on meteorological fields by selecting those with the most direct ties to observations. In this section we compare cloud cover predictions from ECMWF, which are heavily influenced by the choice of model parameterization. The intent is to provide a first example of the use of models as a means of separating dynamical from aerosol influences on cloud cover.

The ECMWF model makes use of the aerosol climatology compiled by Tegen et al. (1997), which includes geographic and seasonal distributions of dust, sulfate, sea salt, and carbonaceous aerosols. This prescribed climatology is used

along with the assumption of a fixed relative humidity for radiative calculations in the model. A key point for the present comparison is that the model does not include a formulation by which aerosols can impact cloud microphysics. Cloud Condensation Nuclei (CCN) concentrations are assigned specified values over land and ocean, and cloud effective radius is parameterized following Martin et al. (1994). The parameterization of cloud microphysics only impacts the radiation scheme and is not included in the precipitation scheme. As discussed in Chapter II, back of the envelope calculations indicate that diabatic heating due to aerosols can be neglected for the range of optical depths considered. As a consequence, variations in model clouds that correlate with aerosol optical depth are strictly the result of meteorological influences.

The model parameterization of clouds follows the scheme of Tiedtke (1993), which is prognostic in both cloud water and cloud amount. An important detail of the parameterization is that the entrainment rate for stratocumulus clouds is parameterized as a fixed fraction of the surface flux. By construction, this results in an entrainment rate that compensates for changes in surface fluxes, and precludes the possibility of decoupling. Instead, the scheme differentiates between stratocumulus-capped boundary layers and shallow cumulus convection using an empirical threshold in lower tropospheric stability (ECMWF, 2006). As discussed in section IV.4.A below, empirical formulations such as this one can lead to large over-predictions of cloud cover in the stratocumulus to trade cumulus transition region.

The analysis follows the methodology of previous chapters, using the same spatial and temporal domains as in Chapter III (24N-40N, 35W-10W, JJA 2000-2006). The more rigid ice-cloud screening of Chapter II is employed to minimize contamination of AOD measurements by cirrus clouds, and aerosol optical depth is constrained to be less than 0.3 for the reasons outlined in Chapter II. It should be noted that, as discussed in Chapter III, filtering cloud observations for high clouds

Table IV.1: Correlations between selected aerosol, cloud, and meteorological variables. The meteorological variables are lagged based on the maximally-correlated lags identified in Chapter III. Lagged correlations are only shown for the 500m trajectories. 95% confidence limits are estimated using a Fisher transformation and accounting for the effective degrees of freedom.

var1	var2	R (95% conf.)
AOD	CF_{LIQ}	0.340 (0.325, 0.355)
AOD	R_E	-0.191 (-0.211, -0.171)
AOD	LWP_{MOD}	-0.098 (-0.118, -0.077)
AOD	LTS(36)	0.205 (0.188, 0.221)
AOD	SST(24)	-0.202 (-0.223, -0.182)
AOD	$q_{700}(0)$	0.043 (0.026, 0.059)
AOD	$WVP_{f15}(0)$	-0.099 (-0.122, -0.076)
AOD	$TA_{SFC}(6)$	-0.171 (-0.187, -0.154)
AOD	$F_{LH}(6)$	-0.283 (-0.327, -0.238)
AOD	$DIV_{SFC,E}(0)$	-0.0271 (-0.0441, -0.0101)
α_{exp}	AOD	-0.385 (-0.4, -0.371)
α_{exp}	CF_{LIQ}	0.017 (0.00037, 0.034)
α_{exp}	LTS(36)	0.099 (0.082, 0.116)

results in a sample bias towards a drier and more convergent free troposphere, both of which impact cloud sensitivities. With the more stringent sample selection used to minimize the impact of cirrus contamination on AOD measurements, the resultant sample bias is likely to be stronger.

Correlations between selected cloud, aerosol, and meteorological quantities are presented in Table IV.1, while composite back trajectories for large (LA), middle (MA), and small (SA) values of AOD are displayed in Figure IV.1. Table IV.1 shows correlations that complement the observational discussion of Chapter II along with additional variables that were found to associate strongly with low-level cloud cover in Chapter III. The meteorological variables are lagged based on the maximally-correlated lags identified in Chapter III, under the assumption that the observed differences in cloud properties will be most sensitive to meteorological differences at those times. The correlations show very similar relationships to those

found in Table II.2, including a strong but significant correlation with LTS. The differences in dynamical sensitivities are largely attributable to the larger study region used in the latter two chapters. There are several interesting points to make of these new observational correlations, in particular given the additional cloud sensitivities identified in Chapter III. In Chapter II we suggest that aerosols could be dispersed by increasing divergence, leading to a covariation between the two that is matched by the sensitivity of cloud cover to changes in low-level divergence. Although a small but significant difference is apparent in the back trajectories, the negligible correlation between the two suggests that this is not the case. The results of Chapter III showed that increases in cloud cover are associated with strengthened cold advection, cooler SSTs, and an increased latent heat flux in the later part of the trajectory. Both Figure IV.1 and Table IV.1 identify a strong association between AOD and these quantities. The substantial correlations between AOD and several cloud-relevant meteorological quantities serve to confirm the conclusion that meteorological covariations contribute to the observed correlation between AOD and CF_{LIQ}. Although perhaps somewhat obvious, it is important to note that such dynamical changes will impact both the modeled as well as the observed cloud cover, both of which are forced by the same meteorology.

Table IV.1 also displays the relationships between various quantities and the angström exponent (α_{exp}), defined by the exponential wavelength dependence of scattered radiation. Since the MODIS aerosol algorithm retrieves AOD at 7 separate wavelengths, ranging from 0.47 to 2.13 μm (King et al., 2003), the angström exponent can also be retrieved. Here we present results computed from the 0.56 and 0.86 μm retrievals. Since the weak wavelength dependence of scattering of visible light by large particles (e.g., cloud drops) contrasts with the scattering by smaller aerosol particles, an increase in cloud contamination or hygroscopic growth of aerosols will be accompanied by a decrease in the angström exponent. The strong correlation between AOD and angström exponent and substantial differences in the

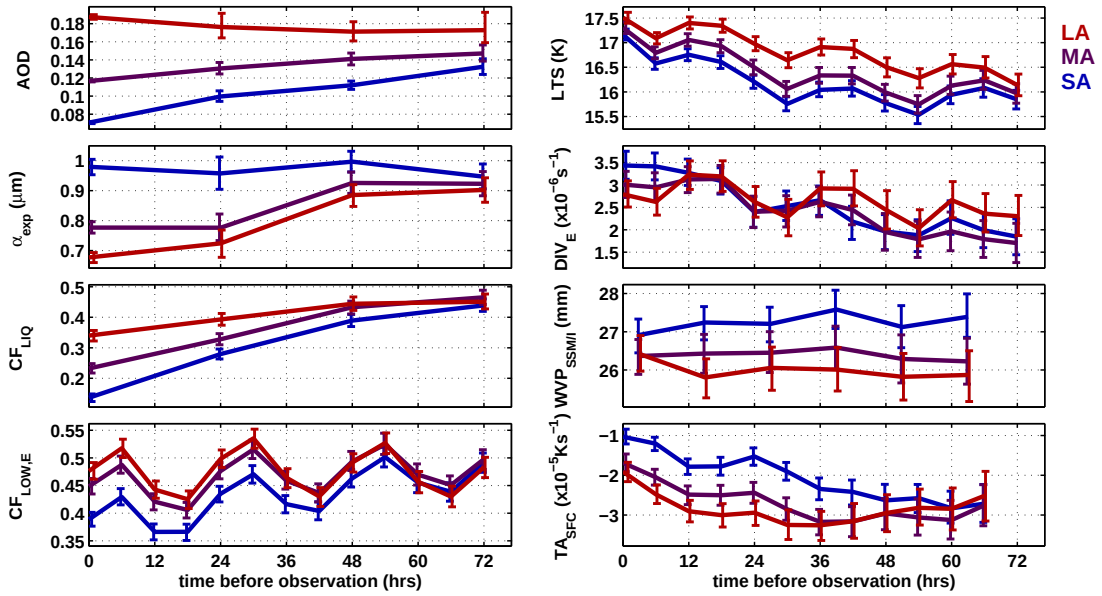

Figure IV.1: Composite back trajectories for cases with Large (LA), Middle (MA), and Small (SA) Aerosol Optical Depth (AOD). The left plots show AOD, angström exponent (α_{exp}), liquid water cloud fraction (CF_{LIQ}), and ECMWF low-level cloud cover, while the right plots show LTS, DIV_{SFC}, WVP_{f15} and along-trajectory SST advection (TA_{SFC}), all from ECMWF. Note that the relationships are slightly different to those seen in Chapter II due to the larger study region.

back trajectories indicate that, as suggested by Charlson et al. (2007), hygroscopic growth of aerosols in proximity to clouds could be contributing to the observed correlation between AOD and MODIS liquid water cloud fraction. One would expect this to be accompanied by a correlation with the humidity of the boundary layer, however none of the proxies for lower atmospheric humidity (LWP, q_{700}, or WVP) support this conclusion. To the contrary, the trajectory in column water vapor actually shows that the more polluted scenes are significantly drier than the clean cases. Although the latter two quantities do not account for changes in saturation in response to temperature variations, the small AOD (SA) cases are associated with colder SSTs, indicating that boundary layer humidity is actually inversely correlated with aerosol optical depth.

Table IV.2: As in Table IV.1 except comparing correlations of ECMWF and MODIS low cloud cover estimates.

	$R_{CF,ECMWF}$ (95% conf.)	$R_{CF,MODIS}$ (95% conf.)
AOD	0.133 (0.117, 0.15)	0.340 (0.325, 0.355)
α_{exp}	-0.044 (-0.061, -0.027)	0.017 (0.0004, 0.034)
CF_{LIQ}	0.379 (0.37, 0.389)	——

Alternatively, the association of dry upper air with low angström exponents could indicate that the increase in AOD is a result of dust plumes. Johnson et al. (2004) indicate that absorbing aerosols at moderate optical depths can impact low-level cloudiness. However, their estimates confine the column extinction to a thin layer that is either within or immediately above the boundary layer. Since it is unlikely that the dust aerosol is systematically confined to a thin layer immediately above the inversion, we do not believe that radiative heating due to dust can explain the observed differences in cloud cover. Instead, the correlation between α_{exp} and CF_{LIQ} may indicate that the association between AOD and α_{exp} results from cloud contamination in the MODIS clear-sky mask, which would artificially enhance the AOD-CF correlation.

Finally, we discuss the observed relationships with low-level cloud cover predicted by ECMWF. Table IV.2 and IV.1 indicate a smaller but significant association between AOD and ECMWF predictions of low-level cloud cover. Consistent with Chapter II, the non-zero correlation indicates that a portion of the observed aerosol-cloud sensitivity is due to meteorological covariations with AOD. If we assume that the ECMWF cloud parameterization accurately represents cloud meteorological sensitivities and composite the LA/SA cases to estimate sensitivities, this implies a correction of 43% to the observed sensitivity of cloud cover to changes in AOD. This is a significantly greater correction than that implied by the analysis of Chapter II. If accurate, this corrected sensitivity would suggest that on average, for every 0.1 increase in aerosol optical depth there is a microphysically-induced increase in low-level cloud cover of 10±2.4%. However, the comparison of model

cloud sensitivities to observed cloud sensitivities is contingent on the two sharing similar sensitivities. To the extent that the model representation of cloud cover shares similar sensitivities to the observed clouds, differences in the association of each with aerosol optical depth variations can be interpreted as resulting from aerosol impacts.

The correlation between ECMWF and MODIS low-level cloud cover indicates that the ECMWF model poorly represents the observed cloud field, explaining less than 15% of the variance in observed clouds. In Table IV.3, we compare the dynamical sensitivities of ECMWF and MODIS low-level cloud cover. Overall, despite showing sensitivities that are generally weaker and less significant, these show a favorable comparison with the observations. It is not clear why the correlation with MODIS cloud cover should be so weak while the sensitivities, though more uncertain, show a reasonable comparison with MODIS. The large uncertainties suggest that other factors are important in determining ECMWF cloud cover. Alternatively, these may be symptomatic of the interplay between the physically-based shallow convection and stratocumulus parameterizations, and the empirical relationship with LTS that distinguishes between the two, which may result in abrupt transitions in cloudiness. Inspection of the distribution in ECMWF cloud cover (not shown), reveals that the distribution is less U-shaped, showing a greater proportion of partially-cloudy scenes than MODIS. The ECMWF operational model is run at approximately thrice the resolution (T511 $\approx$ 40 km) than that at which it is archived (T106 $\approx$ 125 km), meaning that each lower-resolution prediction of cloud cover actually represents the average of several independent model predictions of low-level clouds. If disparate cloud scenes are included in the same average, this will have the effect of weakening the association between ECMWF cloud cover and the relevant dynamical forcings while increasing the proportion of partially-cloudy scenes. Although there is insufficient evidence to verify this hypothesis, it is consistent with the available observations. If true, it bodes

Table IV.3: Composite sensitivities of ECMWF and MODIS low-level cloud fraction (CF) with respect to selected meteorological quantities. The sensitivities are estimated by differencing the large (LC) and small (SC) cloud fraction composites. The 95% confidence limits are shown in parentheses.

variable	units	ΔCF/ΔX	
		ECMWF	MODIS
LTS(36)	K	0.323 (0.274, 0.372)	0.355 (0.328, 0.381)
SST(24)	K	-0.914 (-1.09, -0.724)	-1.23 (-1.37, -1.09)
$q_{700}(0)$	kg/kg	-7.65E3 (-22.7E3, 6.82E3)	1.82E3 (1.43E3, 2.19E3)
$WVP_{f15}(0)$	mm	-1.72 (-4.85, 1.21)	0.420 (0.331, 0.502)
$TA_{SFC}(6)$	K s^{-1}	-5.49E4 (-7.25E4, -3.70E4)	-6.81E4 (-8.05E4, -5.56E4)
$F_{LH}(6)$	W m^{-2}	-0.0645 (-0.137, 0.0109)	-0.099 (-0.022, -0.173)
$DIV_E(0)$	s^{-1}	-3.44E6 (-1.43E7, 7.36E6)	-3.30E5 (-3.77E5, -2.83E5)

well for the validity of ECMWF cloud predictions. However, we cannot definitively rule out the conclusion that the low correlation in Table IV.2 indicates that ECMWF clouds are ill-suited to provide a controlled test of the observed AOD-CF correlation.

The above evidence is consistent with the conclusions of Chapter II, showing that a significant portion of the observed aerosol-cloud sensitivity results from covariations between meteorological state and aerosol amount. We have quantified the correction based on the assumption that ECMWF clouds faithfully represent the sensitivities of observed clouds. However, the evidence is conflicting regarding the quality of ECMWF cloud predictions. As a result, we cannot state with high confidence that the quantitative correction computed above is representative of the true cloud sensitivity to changes in aerosol amount.

An important second conclusion can also be drawn from the above results. In a simulation characterized by realistic meteorology, model cloud predictions can in principle be used to perform controlled experiments that assess the impact of a specific forcing, such as the microphysical impact of aerosols on clouds. At issue in the above comparison is the potential lack of correspondence between the observations of cloud fraction and those produced by the model. A more apt

test would consist of an apples-to-apples comparison of the same phenomenon. Below we present one such experiment, in which the Geophysical Fluid Dynamics Laboratory (GFDL) Atmospheric Model is run with interactive microphysics and compared to a control run in which the CCN spectrum is held constant.

IV.4 Aerosol and Cloud sensitivities in the GFDL Atmospheric Model

IV.4.A Description of the Model

Simulations are performed using the next-generation atmospheric general circulation model (AGCM) developed at GFDL (hereafter AM3). The model builds upon the developments of AM2 (Anderson et al., 2004), with the following improvements. In contrast with the latitude-longitude grid of AM2, the new atmospheric model implements the "vertically Lagrangian" finite volume dynamical core (Lin, 2004) on a cubed-sphere grid. Radiative transfer calculations account for cloud overlap using the Monte Carlo Independent column approximation (McICA, Pincus et al., 2006). The atmospheric model is coupled to a land model which simulates vegetation, surface boundary conditions, and surface moisture, energy, and CO_2 fluxes. The deep convection scheme follows Donner (1993). The work presented in this chapter is motivated by new prognostic treatments of aerosols (Ginoux et al., 2001), shallow clouds (Bretherton et al., 2004) and aerosol activation (Ming et al., 2006), each of which is discussed below.

The new aerosol scheme predicts mass concentrations and distributions of sea salt, sulfate, organic carbon, black carbon, and dust aerosols. Emissions of primary aerosols and precursor gases are obtained from the Aerosol Intercomparison Project (AeroCom, http://nansen.ipsl.jussieu.fr/AEROCOM, Dentener et al., 2006). Given the rates and global distributions of emissions, the simulation solves

for the continuity equation for each species (*e.g.*, Ginoux et al., 2001; Li et al., 2008). Aerosol wet removal is proportional to the stratiform and convective precipitation rates and is dependent on aerosol chemistry. Aerosols are assumed to be externally mixed.

Consistent with the analysis of Chapter II, the present study analyzes the relationship between cloud properties and aerosol optical depth. Aerosol radiative properties are computed following Haywood et al. (1999) by using Mie theory along with an assumed lognormal size distribution and the appropriate refractive indeces. Specifically, since the model is prognostic in aerosol mass, aerosol number concentration is estimated by assuming that the aerosol size distribution can be described by a superposition of two to three lognormal distributions, depending on the species. These distributions are then scaled based on the model-predicted mass concentration and an assumed ratio of the number concentrations for fine, medium, and coarse mode aerosols. Hygroscopic growth is included for all hydrophyllic species. This includes organic carbon, which is assumed to be a mixture of approximately 80% soluble and 20% insoluble organic matter.

Low-level clouds are parameterized using the University of Washington (UW) scheme (Bretherton et al., 2004; Grenier and Bretherton, 2001). The parameterization couples a mass-flux scheme to a 1.5-order turbulence closer model with an entrainment closure at boundary-layer top. Incorporating both cloud water and amount as prognostic variables, the scheme is capable of simulating both stratocumulus-capped and cumuliform boundary layers and includes a formulation for simulating a seamless transition between the two. The parameterization also computes a subgrid scale inversion height, allowing the model to capture fine-scale variations in cloud water and boundary-layer thickness. These two details – the ability to simulate the transition between stratiform and cumuliform boundary layers and to circumvent the challenge of limited vertical resolution – represent important progress in the simulation of boundary layer clouds, permitting

the parameterization to faithfully represent the strong coupling between cloud-top properties, convection, and surface and radiative fluxes.

The importance of coupling an explicit entrainment scheme to a shallow cumulus scheme is demonstrated by McCaa and Bretherton (2004), who compare the Bretherton-Grenier (hereafter BG04) scheme to several existing mesoscale cloud parameterizations using the fifth-generation Pennsylvania State University–NCAR Mesoscale Model (MM5). Their results show that the increased entrainment in the BG04 scheme produces more realistic cloud forcing over the Northeast Pacific subtropical cloud regime. They also show that the seamless coupling to a shallow cumulus parameterization is needed to correctly simulate the decrease in cloud cover in the transition from stratocumulus to cumulus regimes. All schemes in the above comparison show a cool, dry bias in near-surface air, accompanied by slight overestimates of surface fluxes. Though the result may not be representative for a model such as AM3 that is designed to be run at low horizontal resolutions, McCaa and Bretherton (2004) also find a dramatic reduction in cloud cover over coastal regions as a result of a decrease in model resolution. The authors find evidence that this results from a change in horizontal diffusion and is thus not a consequence of the boundary-layer scheme. Nonetheless, it is possible that this indicates a sensitivity to model resolution in the BG04 cloud parameterization and should thus be noted.

Most important among the new parameterizations is the implementation of a new prognostic scheme for cloud droplet number concentration (Ming et al., 2007). The Ming et al. (2007) scheme adds the airmass-based cloud droplet concentration (n, number of droplets per unit airmass) as a third prognostic cloud variable. The continuity equation for n accounts for advection and turbulent transport as well as convective and stratiform sources and sinks of cloud droplets. In the specific case of boundary-layer clouds, sources and sinks of cloud droplets result from droplet activation, autoconversion, evaporation due to adiabatic warming,

and erosion of clouds through horizontal and vertical mixing. Autoconversion follows the scheme of Khairoutdinov and Kogan (2000), who use an empirical relationship between cloud water and droplet concentration based on results obtained from an explicit size-resolved microphysical scheme implemented in a large-eddy simulation. Droplet activation is computed using the method proposed by Ming et al. (2006), which uses an iterative scheme to solve for the cloud droplet concentration, accounting for aerosol chemistry as well as sub-grid scale variations in updraft velocity. Consistency with predicted cloud water is ensured by using the vertical velocity field to compute changes in both. Aerosol size distributions are calculated by assuming a fixed size distribution with two to three lognormal modes, as described above. The size distribution is then discretized into forty logarithmically spaced size bins in order to compute the size and number of activated aerosols. Since the scheme is based around the critical activation diameter and includes an empirically-determined effect of kinetic growth, it accounts for both surface tension and growth rate effects. In a test implementation of the scheme in AM2, Ming et al. (2006) show that the scheme leads to a representation of water path, cloud amount, and radiative forcing that agrees more closely with observations than when droplet concentrations are diagnosed from sulfate mass.

The model output obtained from GFDL also includes products derived from the MODIS simulator, developed by Dr. Yi Ming at GFDL. The method uses stochastically generated subcolumns to compute cloud properties, as described by Pincus et al. (2006). Cloud-top pressure and effective radius are obtained by scanning down from the top of each subcolumn until an optical depth of 2 is reached. At $\tau = 2$, the pressure and effective radius are recorded. The mean for all cloudy subcolumns within a grid box gives the retrieved cloud-top properties (Y. Ming, personal communication).

IV.4.B Model Setup

Model output is obtained from Dr. Yi Ming at GFDL. The model is forced using observationally-based sea surface temperature (SST) climatologies from the Second Atmospheric Model Intercomparison Project (AMIP II, Gates et al., 1999; Hurrell et al., 2008). Model output is archived for years 1983–1993 after allowing a model spin-up time of one year. As in previous chapters, the present study analyzes aerosol-cloud interactions during June through August, the season of maximum subtropical cloud coverage in the Northeast Atlantic. The study region is the same as that used in Chapter III. This region is much more broad than that of Chapter II, though a comparison with results for the latter region showed that the conclusions of the present study are not affected by the choice of study region.

Since a primary goal of the present study is to evaluate the magnitude of aerosol microphysical effects on cloud cover, a control simulation was designed for comparison with the simulation that includes the interactive aerosol-cloud scheme. Subtle considerations are important in the design of such a control scenario, since changes in the simulation can result in secondary effects which also impact cloud forcing. A "kitchen sink" approach to controlling for aerosol impacts could be to simply set ambient aerosol concentrations to a constant value. Interpretation of such a simulation would be complicated by the fact that all aerosol impacts, microphysical and otherwise, are different in the control run. Other studies (*e.g.,* Lohmann and Lesins, 2002) have compared simulated indirect effects to a control run in which cloud droplet concentrations are prescribed. One potential problem with this method is that the cloud droplet population no longer responds to the sub-grid distribution of updraft velocity. As a result, such a control scenario will no longer include dynamically-induced microphysical variations between clouds.

The present study avoids such complications by simply decoupling the nucleation parameterization from the aerosol scheme. Instead of responding to changes in ambient aerosol, the concentration of activated aerosols is computed

from a prescribed CCN spectrum that is constant everywhere. This means that variations in the direct and semi-direct impacts of aerosols as well as changes in the distribution of convective updrafts can still impact cloud properties in *both* the control and online simulations. Aerosol wet removal also remains as a sink mechanism in the control run. In the context of the model formulation, prescribing the CCN spectrum is equivalent to fixing the aerosol chemistry and mass. In all such scenarios, the prescribed values must be chosen so as to maintain the global energy balance. In the present simulation, a value of 5 mg m^{-3} sulfate aerosol is found to satisfy this requirement.

IV.4.C Aerosol and Cloud Climatologies

Figure IV.2 shows a comparison between the GFDL AGCM (AM3) and MODIS climatologies of aerosol optical depth and low-level cloud cover. For compatibility with the MODIS observations, only 12 UTC AM3 cloud cover predictions are included in the climatology. Both the GFDL model and in-situ observations agree that the diurnal minimum in low-level cloudiness occurs shortly thereafter (Bretherton et al., 1995b), meaning that this likely represents the average daily minimum value in cloud cover. Comparison with a climatology at 06Z, the approximate diurnal maximum in cloud cover, showed an overall increase in magnitude but very little change in the pattern of cloudiness. Qualitatively, the climatologies show that the overall structure and absolute magnitude of the observed fields is well reproduced by the model. A few notable differences warrant recognition. First, the model appears to underpredict aerosol amount in remote ocean areas as well as in proximity to the Northeast African and Iberian coasts, while overpredicting the magnitude of the plume advecting from North America. This may indicate that aerosol removal rates are too large in AM3, thus decreasing their atmospheric lifetime. In the cloud field, the model places the subtropical maximum in low-level cloudiness farther North than the maximum seen in the MODIS

climatology. In contrast with the model, the observations show a maximum in cloud cover ranging between 35W and 20W, and only extending up to approximately 22N. As discussed in previous chapters, our study region does not include this region because dust aerosol, which dominates in the region, is generally lofted too high to impact clouds through CCN activation but can significantly alter the radiative budget of the lower atmosphere, and would thus complicate the interpretation of aerosol-cloud correlations. The GFDL model also overpredicts cloud cover within the study region in all areas except near coasts, where it is significantly underpredicted. The underprediction near coasts could be a manifestation of the same phenomenon observed by BG04, possibly attributable to the low horizontal resolution of the model.

Since a comparison of the mean fields does not give information about the simulated variability in cloud cover, Figure IV.3 displays the histogram in AM3 low-level cloud cover for the study region. A histogram of MODIS low-level cloud fraction is also displayed for comparison. In order to ensure an appropriate comparison, the MODIS observations were degraded to the model resolution of 2°x2.5°. This resolution more closely approaches the spatial autocorrelation scale discussed in section III.4. Comparing the low-resolution MODIS histogram to its high-resolution counterpart in Figure III.5 reveals the expected increase in broken cloud scenes and decrease in overcast scenes when a longer averaging scale is used. The model shows a greater proportion of near overcast scenes but a less sharp distinction between near-overcast and 100% cloud cover. In contrast, the small cloud fraction cases show a more discrete transition from minimal cloud cover to clear-sky. Overall, the model cloud distribution is more U-shaped than in the observations. It is not clear whether these differences can be attributed to differences in the meteorology simulated by the model, or to differences in the cloud parameterization.

Aerosol optical depth from the GFDL model shows a comparable distri-

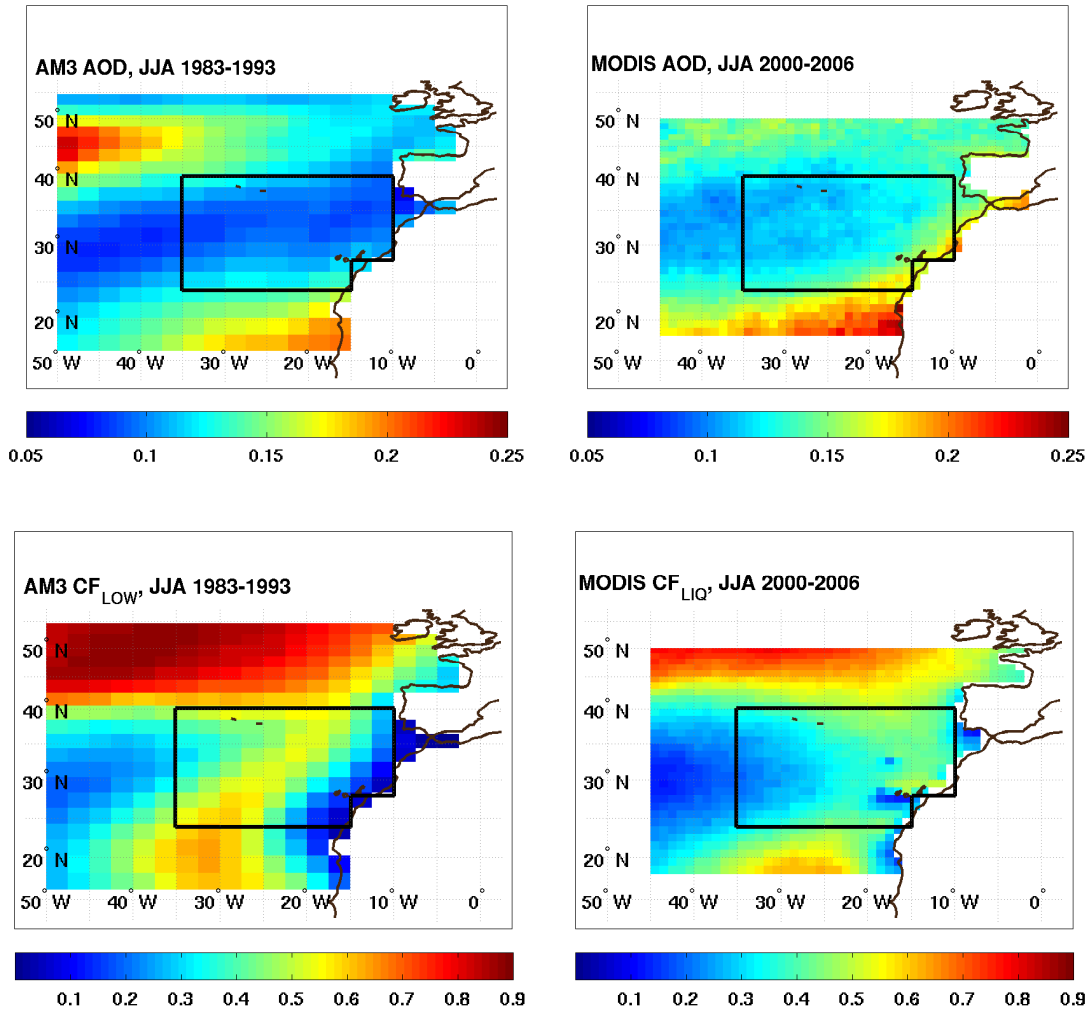

Figure IV.2: A comparison of GFDL and MODIS climatologies of aerosol optical depth (AOD) and low-level cloud fraction (CF). The model is seen to reproduce the overall structure of both fields well, though differences exist in coastal regions and in the stratocumulus to trade cumulus transition region.

bution to that retrieved by MODIS. Together with the strong correlation observed between AOD and α_{exp}, the slightly larger mode and the long tail of the distribution for the MODIS retrievals is consistent with the hypothesis that aerosol hygroscopic growth or cloud contamination contribute to artificially high optical depths in the presence of clouds. Since the GFDL model includes hygroscopic

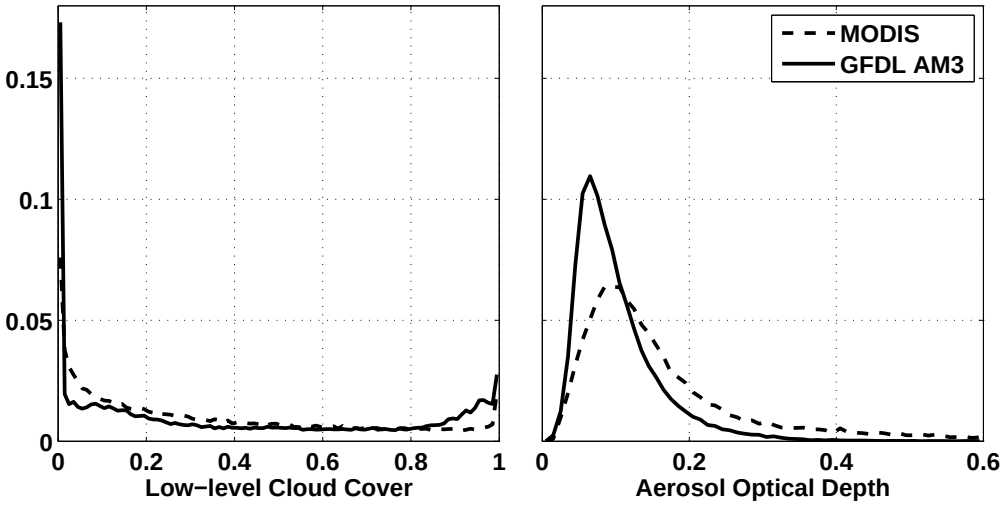

Figure IV.3: Comparison of AM3 and MODIS histograms of low-level cloud fraction and aerosol optical depth. The y-axis denotes the fraction of all points that fall into each bin, and the dashed lines delineate terciles (SC, MC, and LC) in cloud fraction.

growth in calculating the extinction optical depth, this is less likely to be the cause for the difference between the two distributions. However, it is still possible that cloud contamination of MODIS retrievals results in an artificial enhancement of AOD, in particular in the presence of greater cloud cover. This likelihood of this possibility is further reinforced by recent evidence that coincident retrievals from MODIS and the Multiangle Imaging Spectroradiometer (MISR) aboard Terra reveal vast differences in the pixels that each identifies as clear versus cloudy (Liu and Mishchenko, 2008). It is thus unclear whether to conclude that the GFDL model is underestimating aerosol optical depth, or whether the MODIS retrievals are biased high. In general, the distributions in cloud fraction and aerosol compare quite well. Taken with the comparison of climatological fields, these results indicate that the AM3 model faithfully represents the climatology and variance of cloud and aerosol properties over the Northeastern subtropical Atlantic.

Aerosol optical depth is used as the independent variable in this study

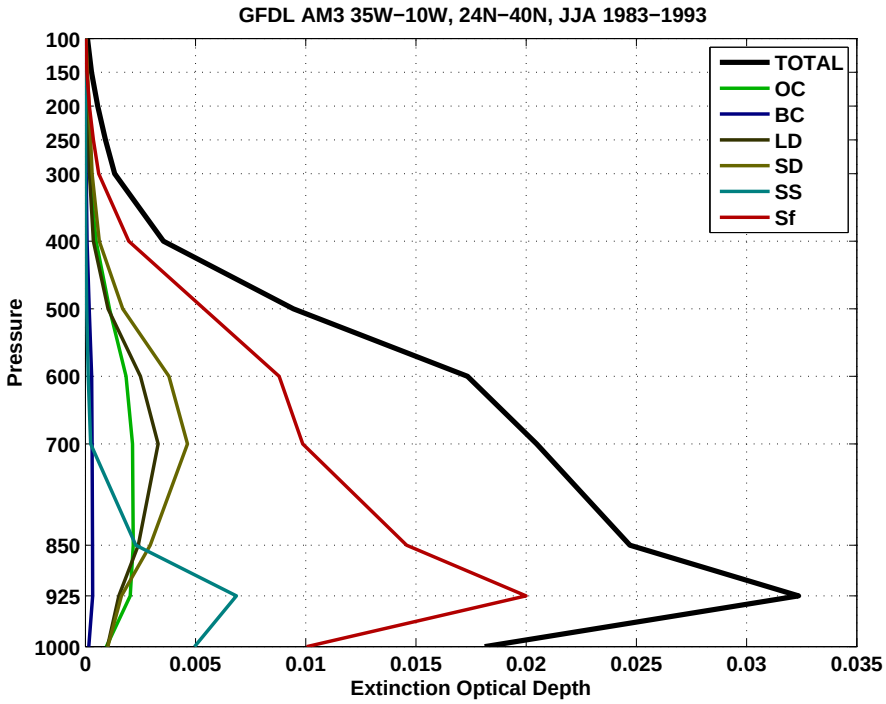

Figure IV.4: Climatological profiles of aerosol extinction from the GFDL atmospheric model. The profile of total extinction is shown alongside profiles of organic carbon (OC), black carbon (BC), large dust (LD), small dust (SD), sea salt (SS), and sulfate (Sf).

because of its relevance to the analysis of Chapter II and because it is routinely available from large scale observations. An assumption we discuss in Chapter II is whether AOD constitutes a valid proxy for boundary layer CCN concentration. An advantage of the present analysis is that the model data permits investigation of two important implications of this assumption: First, that the chemical composition of the aerosol is well-definied and varies consistently with respect to AOD, and second, that the boundary layer aerosol loading is well represented by the total column extinction.

Figure IV.4 shows the mean tropospheric profiles of aerosol extinction optical depth for the region and time period under consideration. Mean profiles are plotted for organic carbon (OC), black carbon (BC), large dust (LD), small

Table IV.4: Instantaneous correlations between column aerosol optical depth (AOD) and extinction in the lowest three model levels for total aerosol (AOD_{BL}), organic carbon ($AOD_{OC,BL}$), black carbon ($AOD_{BC,BL}$), large dust ($AOD_{LD,BL}$), small dust ($AOD_{SD,BL}$), sea salt ($AOD_{SS,BL}$), and sulfate ($AOD_{Sf,BL}$). The right-hand column shows the percent contribution of each species to the total extinction in the lowest three model layers.

variable	R_{AOD} (95% conf.)	Contribution to AOD_{BL}
AOD_{BL}	0.804 (0.802, 0.805)	100.00%
$AOD_{Sf,BL}$	0.713 (0.711, 0.716)	59.34%
$AOD_{SS,BL}$	0.151 (0.146, 0.156)	18.74%
$AOD_{OC,BL}$	0.520 (0.516, 0.524)	6.86%
$AOD_{BC,BL}$	0.587 (0.584, 0.591)	1.08%
$AOD_{SD,BL}$	0.287 (0.282, 0.292)	7.44%
$AOD_{LD,BL}$	0.287 (0.282, 0.291)	6.55%

dust (SD), sea salt (SS), sulfate (Sf), and total aerosol optical depth. Dust aerosols with radii smaller than 1 μm are labeled as small dust, while the remainder are categorized as large. The total extinction is peaked in the boundary layer, with sulfate and sea salt accounting for an average of 59% and 19%, respectively, of the total extinction in the lowest three model layers. The plot also shows that the dust and organic carbon components are less important at lower levels than in the middle troposphere. Since together these components account for approximately 22% of the variance in AOD but are lofted too high to impact cloud microphysics, variations in dust and carbonaceous aerosols will act to reduce the observed correlation between AOD and cloud cover.

In order to assess the relationship between column and boundary layer aerosol, Table IV.4 shows the correlation between extinction in the three lowest model levels and the column extinction. The percent contribution of each species to the total extinction in those same three layers is also shown. The first row shows that 65% (R^2) of the variance in boundary layer extinction (AOD_{BL}) can be described by variations in column AOD. Correlations of column AOD with

boundary-layer extinction for each of the six constituent species are consistent with the mean profiles, showing that sulfate is by far the most tightly tied to total extinction. Of some concern are the variations in sea salt aerosol, which contribute a substantial percentage to the boundary layer aerosol but are not well correlated with column AOD. Changes in AOD that are not matched by changes in boundary layer aerosol could include changes in the free tropospheric humidity, variations in aerosol chemistry, and changes in the vertical distribution of aerosols. Overall, the 35% of the variance in boundary layer aerosol that is not explained by variations in AOD will have the effect of decreasing the correlation observed between AOD and boundary layer cloud properties.

IV.4.D Evaluating the AOD-CF sensitivity in AM3

The analysis of AM3 output is pursued analagously to that of previous chapters. In order to assess the aerosol, cloud, and meteorological properties associated with polluted versus pristine marine conditions, we separate the data into terciles of AOD. As in the observational analysis above as well as in Chapter II the data are limited to AOD values less than 0.3 in order to minimize aerosol heating effects and exclude the occasional thick Saharan dust plumes that enter the study region. As indicated by Figure IV.3, this constraint only impacts a minuscule fraction of the data. Large (LA), middle (MA), and small (SA) cases of AOD are obtained by subsampling randomly from each tercile. To ensure a sample that is unbiased due to geographic, seasonal, or interannual variations, an equal number of samples is selected from each grid box and each month. Trajectories are computed from these initial positions using three-dimensional model winds to drive the HYSPLIT trajectory calculation. Model aerosol, cloud, and meteorological fields are interpolated onto trajectory positions. Composite trajectories are computed from the greater than 6000 trajectories in each tercile. Estimates of the degrees of freedom in a typical model sample are obtained as described in Chapter III using

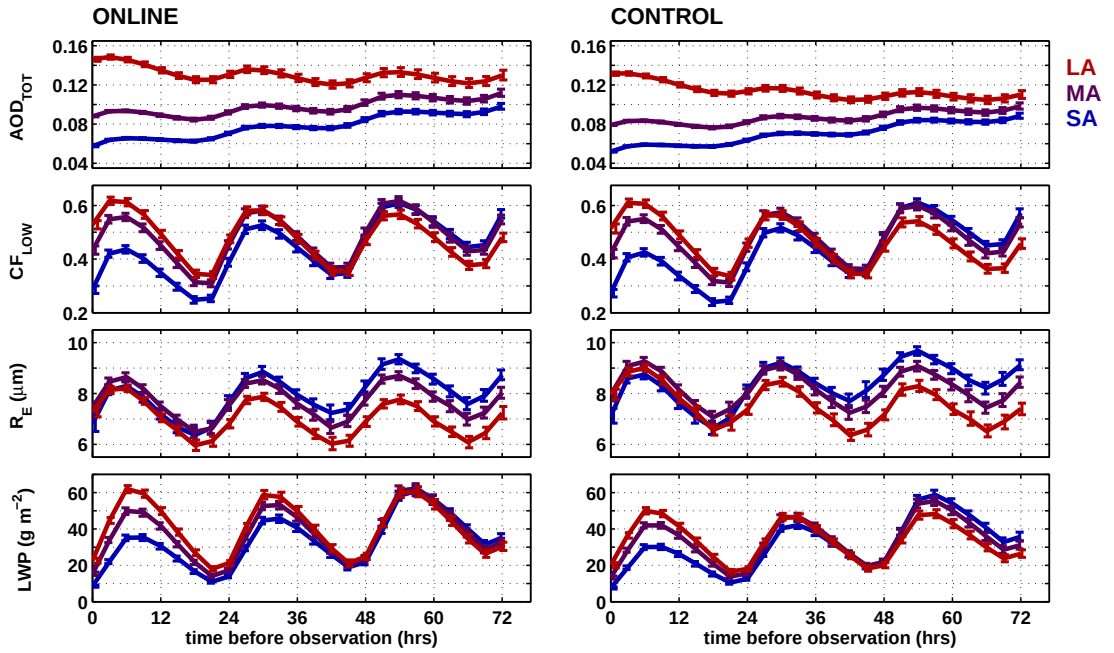

Figure IV.5: A comparison of composite trajectories of AOD, low-level cloud cover (CF_{LOW}), cloud-top effective radius (R_E), and in-cloud liquid water path (LWP) for the online and control runs. Error bars denote 95% confidence limits.

the autocorrelation scales identified in Table III.1. At the lower spatial resolution of the GFDL model, we obtain a consistent sample reduction by a factor of 2.5. This correction to the effective sample size is used in the bootstrap estimation of 95% confidence limits for each composite. The analysis is pursued identically for both the interactive aerosol (hereafter, "online") and the control (hereafter, "control") runs.

Figure IV.5 compares the composite trajectories of AOD, low-level cloud cover (CF_{LOW}), cloud-top effective radius (R_E), and in-cloud liquid water path (LWP) for the online and control runs. Some minor differences can be noted between the two runs. The spread in aerosol optical depth is slightly less for the control run, while there is actually a slightly greater spread in cloud cover. The diurnal cycle in liquid water path is also more pronounced for the online simulation. In general, however, the online and control composites are so similar as

Table IV.5: Composite sensitivities of low-level cloud fraction (CF) to aerosol optical depth (AOD) for the online and control simulations. Shown in the three right-hand columns are the sensitivities for middle to large cloud cover (LA-MA), small to medium cloud cover (MA-SA) and from small to large cloud cover (LA-SA). These highlight the non-linearity in observed cloud response.

Model Run	ΔCF/ΔAOD		
	LA-MA	MA-SA	LA-SA
Online	1.628 (1.254, 2.01)	4.829 (4.135, 5.528)	2.726 (2.480, 2.967)
Control	1.782 (1.328, 2.219)	5.436 (4.638, 6.215)	3.029 (2.734, 3.308)

to appear almost identical. Table IV.5 shows the AOD-CF sensitivities computed from composite differences between the three terciles. Since the present analysis includes the middle tercile in AOD we can note the nonlinearity in the observed sensitivity of CF_{LOW} to variations in AOD, with small cloud cover being much more sensitive to changes in AOD. None of the sensitivities computed for the online run are significantly different from those of the control run at the 95% confidence level. Since the control run only includes non-microphysical impacts on clouds, this means that for the present study region, the microphysical impact of aerosols on AM3 cloud cover is negligibly small. In fact, since the control sensitivities are larger, though not significantly different, we can have a high degree of confidence in this conclusion. Further, as discussed above, since the aerosol optical depths are fairly small, aerosol heating can be neglected as a cause for the changes in cloud cover. This implies that changes in the meteorology that covary with both AOD and cloud cover are responsible for 100% of the observed correlation between the two. Though not discussed in the present study, it should nonetheless be noted that in contrast with cloud cover, IV.5 indicates that there is a significant microphysical impact on cloud water path.

IV.4.E Discussion of AM3 results

Using a controlled modeling experiment we have shown evidence that *none* of the observed correlation between aerosol optical depth and cloud cover can be attributed to aerosol impacts on cloud microphysics. It is important to consider the context of the above result. To the extent that the model adequately represents the interactions between aerosols, clouds, and meteorology, the above experiment is applicable to the observational analysis in Chapter II and Section IV.3 above. Although the new GFDL model includes sophisticated formulations for aerosols, clouds, and dynamics, the model is of course an *approximation* to the current climate. One clear example is the use of a fixed aerosol size distribution. Since droplet activation depends nonlinearly on the amplitude and shape of the size distribution the exact consequence of this assumption is difficult to predict. However, it is likely that the constrained variability of the size distribution acts to reduce the simulated sensitivity of clouds to aerosols. Likewise, the assumption of an externally mixed aerosol neglects the changes in CCN activity associated with particle aging, source characteristics, and cloud processing. Specifically, by reducing the complexity of aerosol variations through the above simplifications, the variance in CCN activity will likely be reduced, thus decreasing the scale of aerosol-induced changes on cloud microphysics.

Regarding the potential for these approximations to impact AOD calculations, Kapustin et al. (2006) perform an in-depth comparison of satellite retrievals of AOD with in-situ measurements of aerosols. Although the analysis is intended to aid in the interpretation of remote sensing retrievals, several of their findings are applicable here. Their results suggest that the dominant source of uncertainty in using AOD as a proxy for boundary layer aerosol results from the growth of aerosols in the presence of elevated humidity. Size distribution parameters and chemistry of the aerosol are found to result in much smaller biases. Since the radiative calculation accounts for hygroscopic growth of the aerosol, the results of Kapustin et al.

Table IV.6: Correlations between selected aerosol and cloud variables. 95% confidence limits are estimated using a Fisher transformation and accounting for the effective degrees of freedom.

var1	var2	R (95% conf.)
AOD	CF_{LOW}	0.230 (0.219, 0.240)
AOD	R_E	-0.020 (-0.031, -0.009)
AOD	LWP	0.258 (0.247, 0.268)

(2006) suggest that the above approximations will not significantly bias the AOD estimates in AM3. Nevertheless, the assumptions of a fixed size distribution and externally mixed aerosols will still impact the variability and strength of aerosol-cloud interactions as simulated by the model, and thus constitute an important caveat to the above results.

Although the above reasoning indicates that the aerosol-cloud sensitivity could be underestimated by AM3, this does not explain the observed correlation between the two. The controlled experiment above indicates that to within the uncertainties in the present method, the entire correlation between aerosol optical depth and low-level cloud cover is incidental, resulting from covariation between aerosols, clouds and one or several other processes that influence both. The relevance of this result is contingent on the assumption that the mechanisms by which the AOD-CF correlation come about in the model are representative of those observed by satellite. We begin by evaluating the instantaneous correlations between aerosol and cloud properties, shown in Table IV.6. This mirrors the observational correlations taken over the same region and shown in Table IV.1. As in the observations, there is a significant correlation between AOD and low-level cloud cover, though the AM3 model shows a smaller association between the two. In contrast with the observations, the correlation with effective radius is negligible, while the correlation with liquid water path is significantly greater than that with CF_{LOW}.

Table IV.7 shows a comparison of AOD and CF correlations for a number of aerosol and meteorological variables. Variations in sulfate aerosol are seen to

Table IV.7: As in Table IV.6 except comparing correlations with AOD to those with low-level cloud fraction.

var1	R_{AOD} (95% conf.)	R_{CF} (95% conf.)
AOD_{Sf}	0.864 (0.861, 0.867)	0.325 (0.315, 0.335)
AOD_{SS}	0.215 (0.204, 0.226)	0.566 (0.558, 0.574)
AOD_{OC}	0.673 (0.667, 0.679)	0.056 (0.045, 0.067)
AOD_{BC}	0.791 (0.787, 0.795)	0.103 (0.092, 0.115)
AOD_{SD}	0.591 (0.584, 0.599)	-0.158 (-0.169, -0.147)
AOD_{LD}	0.583 (0.575, 0.59)	-0.170 (-0.181, -0.159)
LTS(36)	0.229 (0.218, 0.240)	0.055 (0.044, 0.067)
SST(24)	0.202 (0.191, 0.214)	-0.067 (-0.079, -0.055)
$q_{700}(0)$	0.518 (0.509, 0.526)	-0.006 (-0.017, 0.006)
WVP(0)	0.436 (0.426, 0.445)	0.122 (0.111, 0.133)
$TA_{SFC}(6)$	0.121 (0.109, 0.133)	0.010 (-0.002, 0.022)
$F_{LH}(6)$	-0.161 (-0.172, -0.150)	0.173 (0.162, 0.184)
$DIV_{SFC}(0)$	-0.310 (-0.321, -0.300)	-0.032 (-0.0433, -0.0207)

be most strongly linked to changes in total aerosol extinction, but are second to sea salt in their association with low-level cloud cover. The strong relationship to sea salt aerosol may be a clue as to the source of the correlation with cloud cover, and is discussed below. There is also clear evidence for meteorological covariation with AOD. As in Section IV.3, correlations with meteorological quantities are computed for the maximally-correlated lags identified in Chapter III. Consistent with the observational correlations seen in Table IV.1, lower tropospheric stability (LTS) and surface latent heat flux (F_{LH}) are both strongly correlated with AOD. The model data also shows a strong negative correlation between AOD and surface divergence, a relationship that is not present in the observations. Based on the observational analysis of Chapter III, all of the above covariations should be expected to associate strongly with cloud cover. In contrast, AM3 clouds are not strongly related to any of these, the latent heat flux actually showing a strong relationship that is opposite in sign to the AOD correlation.

It is possible that the maximally-correlated lags for AM3 are not the same as those identified in the observations. Figure IV.6 shows a comparison of

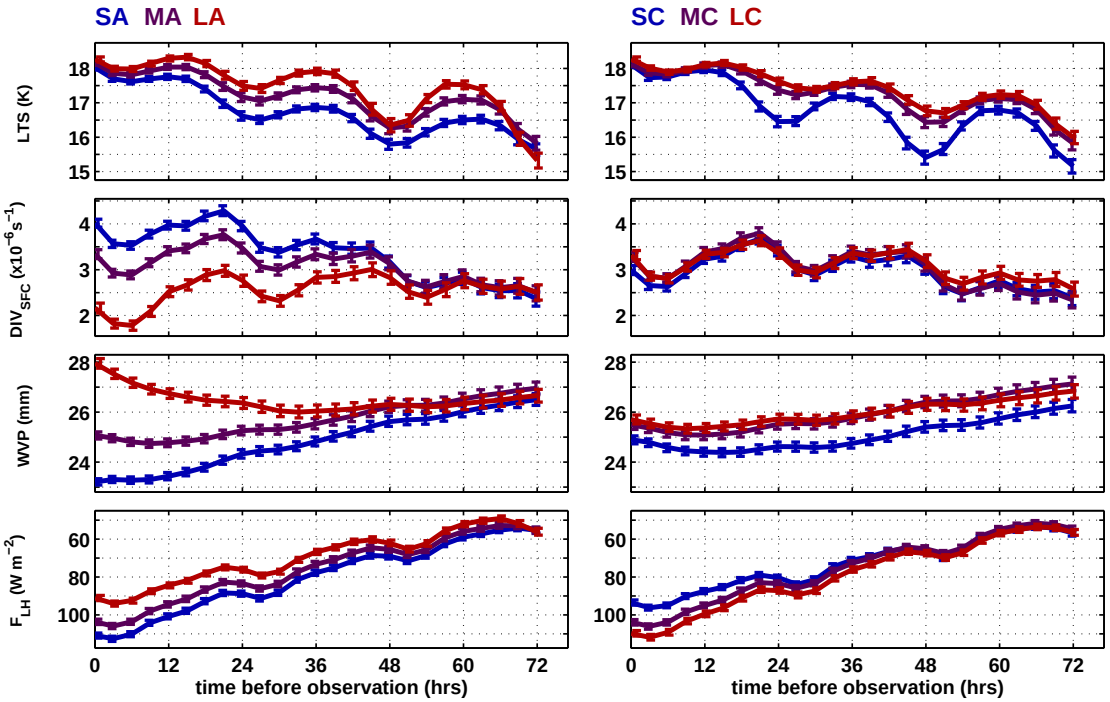

Figure IV.6: The left hand plot shows composite trajectories for terciles in AOD (LA/MA/SA), while the right hand plot shows composite trajectories for terciles in low-level cloud cover (LC/MC/SC). Both plots show composite back trajectories for stability, divergence, column water vapor, and latent heat flux.

the composite back trajectories for LA/MA/SA cases with those for LC/MC/SC. Consistent with the correlations, despite showing a strong relationship between AOD and all four meteorological quantities, the differences are drastically smaller, if not of opposite sign, with respect to cloud cover. Again, in the specific case of the latent heat flux the sign is reversed, suggesting that the covariation between AOD and F_{LH} actually *reduces* the observed correlation between AOD and CF. There is also no significant association with surface divergence, although differences in cloud height do modulate the cloud-top subsidence rate. However, the association with cloud cover is of the same sign and significant for both stability and column water vapor. LTS also shows a substantial nocturnal dip in stability for all cases, though it is especially strong for the SC case. This may reflect the nocturnal enhancement

in entrainment, and could indicate a more cumuliform boundary layer for the SC cases. Relative to the observational analysis of Chapter III, the differences in LTS and WVP are smaller, possibly implying that AM3 clouds are more sensitive to changes in water path and stability.

Figure IV.7 shows a comparison between the composites in AM3 low-level cloud fraction and those observed in Chapter III. As in Figure III.12, meteorological quantities are chosen for their strong association with changes in cloud cover. Composites are plotted for the lags identified in Tables III.3 and III.4. It should be noted that although the water path is dramatically underestimated at 0 hours, as seen in Figure IV.5 this is primarily a reflection of a strong diurnal cycle in water path, since the model estimate more closely matches the observations at a lag of 6 hours. With the exception of the surface latent heat flux, to which AM3 clouds show a stronger sensitivity, overall AM3 clouds show significantly reduced sensitivities to those observed by MODIS. In the case of surface divergence, AM3 clouds even show a weak sensitivity that is opposite in sign to that seen in the observations. The same is true for temperature advection, though the differences are less significant. Neither of these relationships is consistent with the predictions of simple bulk boundary layer models or the observations of Chapter III, which associate increased cold advection and decreased divergence with cloud growth. The fact that these associations are opposite in sign suggests that the model clouds are dependent on other factors not included in Figure IV.7 or Table IV.7. One possibility is that the metrics identified in the previous chapter lack some critical meteorological diagnostic. However, an examination of a more complete set of meteorological fields did not reveal any that are more noteworthy than those presented. Alternatively, the parameterization could depend nonlinearly on a combination of the observed fields or be influenced by a coupling between different model parameterizations.

Apart from LTS, the only meteorological relationship that shows some

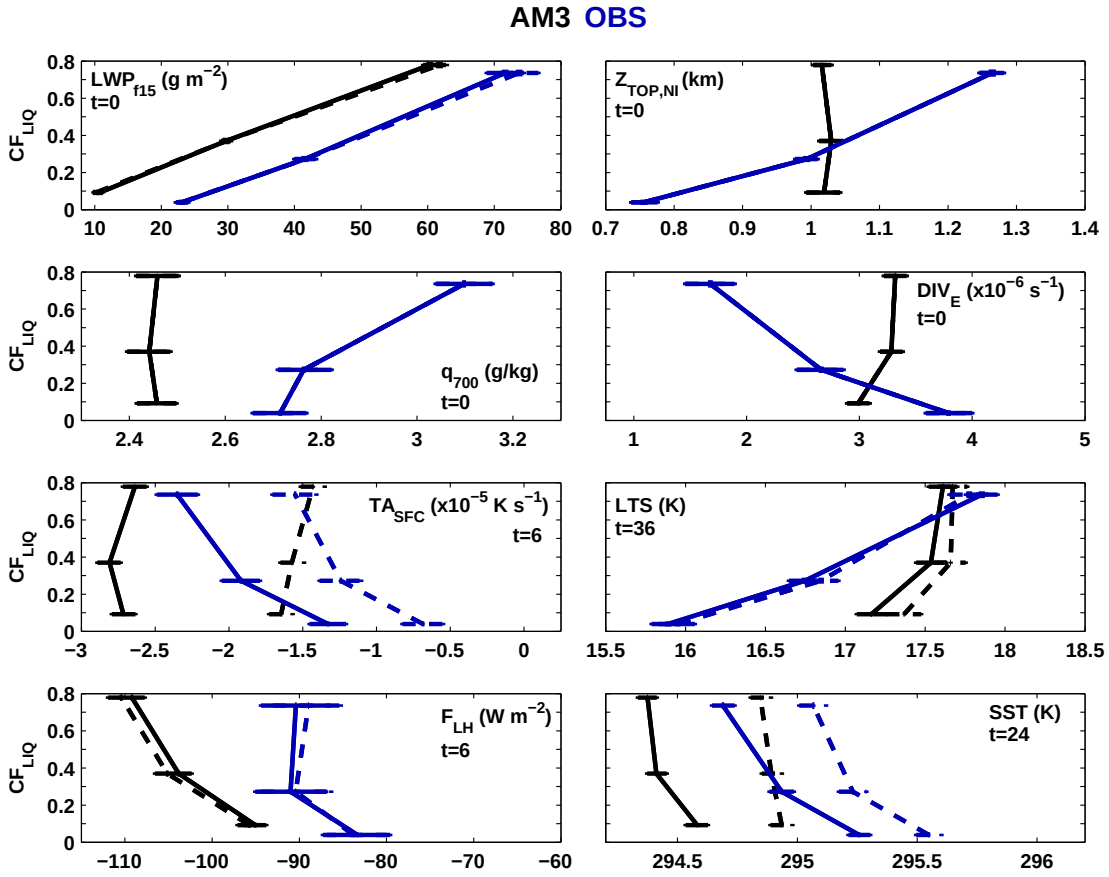

Figure IV.7: As in Figure III.12, with the addition of composites of low-level cloud cover obtained from the GFDL AM3 model (black lines) for comparison with the observational sensitivities (blue lines) discussed in Chapter III. Error bars denote 95% confidence limits and solid lines denote the composites for the 500m trajectories while dashed lines are for the 2000m trajectories.

continuity between AOD and AM3 cloud cover is that of column water vapor. This is consistent with the strong correlation between AOD and water path seen in Table IV.6. The above relationships are matched by strong correlations between AOD and specific humidity at 700 hPa (q_{700}) as well as mid-level and high cloud cover. The correlation with free tropospheric humidity implies that greater than 25% of the variance in aerosol extinction can be explained by variations in q_{700}. As proxies for elevated relative humidity in the atmospheric column, these all point to

the important role of hygroscopic growth in modifying column extinction. However, among these only column vapor and cloud water vary significantly with respect to changes in cloud cover. This is not inconsistent, since these imply that the changes in aerosol extinction are primarily associated with humidification of the boundary layer. The result is also consistent with the strong correlation between low-level cloud cover and sea salt aerosol, which is largely confined to the lowest model levels and therefore most affected by changes in boundary layer humidity. Unfortunately, model parameters that could confirm this hypothesis, such as aerosol mass profiles and the angström exponent, were not archived due to space limitations. As a result, although the evidence consistently points to aerosol hygroscopic growth as the cause for the correlation between AOD and CF, we cannot definitively conclude that this is the case.

The results of Section IV.4.D show that within the AM3 model the microphysical impact of aerosols on low-level cloud cover is negligible. Here we have discussed the context of this result as well as some potential explanations for the strong correlation observed between aerosol optical depth and low-level cloud cover. Apart from LTS and column water vapor, none of the meteorological quantities examined revealed systematic covariations with both AOD and cloud cover, indicating that meteorological impacts on cloud cover are unlikely to be the cause for the association between AM3 clouds and aerosol extinction. Instead, the above evidence suggests that the majority of the aerosol-cloud correlation results from the hygroscopic growth of aerosols associated with elevated boundary layer humidity in the presence of clouds. As discussed above, this conclusion is only relevant to the observational results of Chapter II if the model clouds faithfully represent observed cloud sensitivities. If not, it is impossible to know if the observed clouds are subject to covariations that the modeled clouds do not sense, nor is it possible to know if the converse is true. A comparison of AM3 and MODIS cloud sensitivities showed that apart from column water vapor and LTS, AM3 clouds are

generally insensitive to the meteorological quantities identified in Chapter III and in some cases even show a relationship that is opposite in sign. Since the AM3 clouds do not share the same sensitivities as those observed by MODIS, we cannot conclude that the controlled experiment of Section IV.4.D is representative of the true sensitivity of cloud cover to aerosol.

IV.5 Conclusions

A primary uncertainty in climate projections is the radiative forcing resulting from aerosol impacts on clouds. As discussed in previous chapters, it is important to separate aerosol from meteorological impacts on cloud forcing. Climate simulations provide the opportunity to separately quantify the impact of different forcing agents by permitting controlled experiments. In this chapter, we have presented evidence from both the ECMWF and GFDL models that qualitatively corroborates the results of Chapter II, indicating that the correlation between AOD and CF is significantly influenced by covariations between AOD and cloud-relevant meteorological quantities.

Another major uncertainty in climate projections results from the parameterizations of low-level clouds. The work presented above applies the Lagrangian trajectory analysis method to the evaluation of model predictions of cloud cover. By investigating synoptic-scale sensitivities, the method provides new diagnostic information on the performance of cloud parameterizations. In particular, it is possible to examine the reasons behind the observed correlation between AOD and CF. Unfortunately, neither model shows a consistently strong correspondence with observed cloud cover. Although the ECMWF model appears to exhibit the correct dynamical sensitivities, it is poorly correlated with MODIS cloud cover. The GFDL model proves particularly difficult to interpret. Although composite trajectories for AOD reveal a number of strong meteorological covariations, cloud

cover is only weakly associated with LTS and WVP. Other meteorological quantities that were examined vary negligibly with respect to cloud cover, and some even show changes that are opposite in sign to the sensitivities identified in Chapter III. This may suggest that other factors, such as details internal to the cloud parameterization, the persistence of boundary-layer structure within the model, and interactions between different model parameterizations, could play a significant role in determining AM3-predicted cloud cover. Alternatively, it is simply possible that the GFDL model is much more sensitive to changes in stability, column water vapor, and surface flux but is generally insensitive to changes in divergence. Without performing a more controlled test of the model parameterization, it is not possible to isolate the dominant controls on AM3 cloud fraction.

The work demonstrates the synergistic use of models and observations in the assessment of both aerosol and cloud sensitivities. The Lagrangian analysis method provides detailed diagnostic information in each case, while simulations provide the opportunity to alternately remove and reinstate the microphysical coupling between aerosols and clouds. Results from both the ECMWF and GFDL models qualitatively confirm the results of Chapter II, indicating that a substantial fraction of the AOD-CF correlation results from meteorological covariations. In the case of ECMWF, it is suggested that cloud contamination of MODIS retrievals is the most likely cause for the correlation. For AM3, the balance of evidence suggests that aerosol hygroscopic growth, dominated by remotely-generated sea-salt aerosols, is responsible for the observed aerosol-cloud correlation. As discussed above, comparison of model and observational cloud sensitivities reveals significant differences in the response to large-scale meteorology. This suggests that the model-estimated corrections to the AOD-CF sensitivity are not generally applicable to the observations. Further work is needed to fully characterize the sensitivities of model clouds and separate the performance of cloud parameterizations from the impacts of other aspects of each model.

V Conclusion

The work presented in this dissertation is focused on separately quantifying the aerosol and meteorological impacts on low-level cloudiness in the subtropical Northeast Atlantic. In pursuit of this goal, a new technique is developed which evaluates the Lagrangian impacts on cloud evolution through the use of three-dimensional parcel trajectories and the combination of satellite observations with meteorological analyses. Chapter II applies this technique to the evaluation of the observed association between aerosol optical depth and low-level cloud cover. It is shown that a significant portion of the relationship results from a meteorological covariation between lower tropospheric stability and AOD, a quantity that also impacts cloudiness. With the goal of identifying other meteorological quantities that may impact the AOD-CF correlation, Chapter III untertakes an investigation of the meteorological sensitivities of these clouds using the Lagrangian method developed in the previous chapter. It is found that lower tropospheric stability, surface divergence, free tropospheric humidity, sea surface temperature, and cold advection all contribute significantly to changes in cloud cover. An additional finding is that these quantities are best correlated with cloud properties at varying lags, with longer lags generally corresponding to thermodynamic influences on boundary layer properties, while synoptic-scale changes in subsidence rate and divergence correspond best at short lags. In Chapter IV, model simulations are used to perform controlled experiments in which the impact of aerosols is separated from that of meteorology on cloud fraction. Both the ECMWF and GFDL atmo-

spheric models are shown to agree qualitatively with Chapter II in finding that a substantial portion of the AOD-CF relationship results from meteorological covariations. The dynamical sensitivities of Chapter III provide a useful validative test of the representation of boundary layer clouds in each model. Unfortunately, neither model appears to adequately simulate cloud cover relative to the sensitivities assessed in Chapter III.

These results highlight a number of possible venues for continued investigation. The work of Chapters III and IV reveal the wealth of information that can be gained through the application of the Lagrangian analysis. Detailed diagnostic information is shown to be both useful both for assessing observed relationships between aerosol, meteorological, and cloud properties, but also to isolate specific sources of model bias. Application of the technique to other, perhaps more predictable, stratocumulus regions could prove enlightening. In particular, the Californian, Peruvian, and Namibian stratocumulus regions are all subject to subtle differences in geography, climatology, and cloud properties. Significantly, these also differ in terms of the ambient aerosol characteristics, both in quantity and in composition. These too may prove to function as informative controlled experiments, in which cloud response to changes in aerosol characteristics can be assessed.

The work has also identified several areas that remain a challenge, both in terms of observational and model assessments. In Chapter III, cloud top height estimates are identified as a dominant uncertainty in the analysis, and a re-implementation of the experiment to correspond with CALIPSO could significantly improve entrainment estimates. Likewise, remotely sensed profiles of temperature and water vapor from the Atmospheric InfraRed Sounder (AIRS) could provide observational validation of the association between CF, AOD, and humidity both above and below the inversion. Inclusion of AIRS retrievals would be contingent on resolving the constraint imposed by the need for clear sky pix-

els in the profile retrievals. Finally, the observational analysis has the potential to be coupled with the analysis of measurements from field campaigns. This approach has a precendent in the ASTEX experiment (Albrecht et al., 1995), and could prove useful in the analysis of observations from the VAMOS (Variability of the American Monsoon Systems) Ocean-Cloud-Atmosphere-Land Study (VOCALS, Wood, 2006). Focusing on the Southeast Pacific stratocumulus regime, the VOCALS campaign will incorporate large-scale measurements of dynamic and thermodynamic conditions with multi-scale investigations of cloud and atmospheric properties. Combined with the focused observations of VOCALS, the Lagrangian analysis could be applied to identify the origin of different airmasses and quantify the history of meteorological influences that lead to each observation.

Results from the model analysis of Chapter IV also identify several directions for future work. In particular, one challenge in the evaluation of cloud parameterizations is the separation of errors that result from inadequacies of the cloud parameterization from those that result from other aspects of the model configuration. Since the goal is to motivate improvements in cloud parameterizations, a natural next step is to perform side-by-side comparisons of parameterization performance under a common set of forcings. Cloud and microphysical parameterizations can be run in single column mode along the Lagrangian trajectories. Forced by identical meteorology, this would permit evaluation of parameterizations independent of other differences in model configuration. This approach provides a great deal of flexibility in exploring the potential sources of model bias, including vertical resolution, empirically versus physically-based schemes, etc. By comparing the simulated response to identical forcings, results would shed light on the specific strengths and weaknesses of each parameterization.

As stated in the introduction, this dissertation seeks to investigate the role of aerosols and clouds in perturbing the Earth's energy balance. Specifically, the work described herein is designed to assess the microphysical impacts of aerosols

on subtropical low-level cloud cover. Essential to the pursuit of this goal is the independent quantification of aerosol impacts, meaning the separation of aerosol and meteorological impacts on cloud forcing. The work describes the development of a Lagrangian technique designed to investigate the observed relationships between aerosols, clouds, and meteorology. Application of the method identifies meteorological covariations that impact the observed relationship between aerosols and clouds as well as new information regarding the meteorological sensitivities of subtropical clouds. Ultimately, the goal of such work is to provide improved projections of future climate. We have presented results that discuss model simulations of aerosol-cloud interactions and used the Lagrangian analysis to conduct an informative assessment of model cloud predictions. Although the results identify ample opportunities for continued investigation, we consider the present work to be an important contribution to the body of knowledge concerning aerosol-cloud-climate sensitivities.

References

Ackerman, A., Kirkpatrick, M., Stevens, D., and Toon, O., 2004: The impact of humidity above stratiform clouds on indirect aerosol climate forcing. *Nature*, **432**(7020), 1014–1017. ISSN 0028-0836. doi:10.1038/nature03174.

Ackerman, A., Toon, O., Stevens, D., Heymsfield, A., Ramanathan, V., and Welton, E., 2000: Reduction of Tropical Cloudiness by Soot. *Science*, **288**(5468), 1042.

Albrecht, B., 1989: Aerosols, Cloud Microphysics, and Fractional Cloudiness. *Science*, **245**(4923), 1227–1230. ISSN 0036-8075.

Albrecht, B., Bretherton, C., Johnson, D., Scubert, W., and Frisch, A., 1995: The Atlantic Stratocumulus Transition Experiment: ASTEX. *Bulletin of the American Meteorological Society*, **76**(6), 889–904.

Anderson, J., Balaji, V., Broccoli, A., Cooke, W., Delworth, T., Dixon, K., Donner, L., Dunne, K., Freidenreich, S., Garner, S., Gudgel, R., Gordon, C., Held, I., Hemler, R., Horowitz, L., Klein, S., Knutson, T., Kushner, P., Langenhost, A., Lau, N., Liang, Z., Malyshev, S., Milly, P., Nath, M., Ploshay, J., Ramaswamy, V., Schwarzkopf, M., Shevliakova, E., Sirutis, J., Soden, B., Stern, W., Thompson, L., Wilson, R., Wittenberg, A., Wyman, B., and GFDL Global Atmospheric Model Dev, 2004: The new GFDL global atmosphere and land model AM2-LM2: Evaluation with prescribed SST simulations. *Journal of Climate*, **17**(24), 4641–4673. ISSN 0894-8755.

Anderson, T., Charlson, R., Winker, D., Ogren, J., and Holmen, K., 2003: Mesoscale variations of tropospheric aerosols. *Journal of the Atmospheric Sciences*, **60**(1), 119–136. ISSN 0022-4928.

Bony, S., and Dufresne, J., 2005: Marine boundary layer clouds at the heart of tropical cloud feedback uncertainties in climate models. *Geophysical Research Letters*, **32**, 20.

Bretherton, C., Austin, P., and Siems, S., 1995a: Cloudiness and Marine Boundary Layer Dynamics in the ASTEX Lagrangian Experiments. Part II: Cloudiness,

Drizzle, Surface Fluxes, and Entrainment. *Journal of the Atmospheric Sciences*, **52**(16), 2724–2735.

Bretherton, C., Klinker, E., Betts, A., and Coakley Jr, J., 1995b: Comparison of Ceilometer, Satellite, and Synoptic Measurements of Boundary-Layer Cloudiness and the ECMWF Diagnostic Cloud Parameterization Scheme during ASTEX. *Journal of the Atmospheric Sciences*, **52**(16), 2736–2751.

Bretherton, C., McCaa, J., and Grenier, H., 2004: A New Parameterization for Shallow Cumulus Convection and Its Application to Marine Subtropical Cloud-Topped Boundary Layers. Part I: Description and 1D Results. *Monthly Weather Review*, **132**(4), 864–882.

Bretherton, C., and Wyant, M., 1997: Moisture Transport, Lower-Tropospheric Stability, and Decoupling of Cloud-Topped Boundary Layers. *Journal of the Atmospheric Sciences*, **54**(1), 148–167.

Charlson, R. J., Ackerman, A. S., Bender, F. A.-M., Anderson, T. L., and Liu, Z., 2007: On the climate forcing consequences of the albedo continuum between cloudy and clear air. *Tellus Series B - Chemical and Physical Meteorology*, **59**(4), 715–727. ISSN 0280-6509. doi:10.1111/j.1600-0889.2007.00297.x.

Charlson, R. J., Seinfeld, J. H., Nenes, A., Ku lmala, M., Laaksonen, A., and Facchini, M. C., 2001: Reshaping the Theory of Cloud Formation. *Science*, **292**(5524), 2025–2026. doi:10.1126/science.1060096.

Chelton, D., and Freilich, M., 2005: Scatterometer-Based Assessment of 10-m Wind Analyses from the Operational ECMWF and NCEP Numerical Weather Prediction Models. *Monthly Weather Review*, **133**(2), 409–429.

Conover, J., 1966: Anomalous Cloud Lines. *Journal of the Atmospheric Sciences*, **23**(6), 778–785.

Dentener, F., Kinne, S., Bond, T., Boucher, O., Cofala, J., Generoso, S., Ginoux, P., Gong, S., Hoelzemann, J., Ito, A., et al., 2006: Emissions of primary aerosol and precursor gases in the years 2000 and 1750 prescribed data-sets for AeroCom. *Atmospheric Chemsitry and Physics*, **6**, 4321–4344.

Donner, L., 1993: A Cumulus Parameterization Including Mass Fluxes, Vertical Momentum Dynamics, and Mesoscale Effects. *Journal of the Atmospheric Sciences*, **50**(6), 889–906.

Draper, D., and Long, D., 2002: An assessment of SeaWinds on QuikSCAT wind retrieval. *Journal of Geophysical Research - Atmospheres*, **107**, 3212.

Ebuchi, N., Graber, H., and Caruso, M., 2002: Evaluation of Wind Vectors Observed by QuikSCAT/SeaWinds Using Ocean Buoy Data. *Journal of Atmospheric and Oceanic Technology*, **19**(12), 2049–2062.

ECMWF, 2006: IFS Documentation – Cy31r1, Operational implementation. PART IV: Physical Processes. World Wide Web electronic publication.

ECMWF, 2007: The ecmwf operational analysis and forecasting system. World Wide Web electronic publication.

Forster, P., Ramaswamy, V., Artaxo, P., Berntsen, T., Betts, R., Fahey, D., Haywood, J., Lean, J., Lowe, D., Myhre, G., Nganga, J., Prinn, R., Raga, G., Schulz, M., and Dorland, R. V., 2007: *Changes in Atmospheric Constituents and in Radiative Forcing. In: Climate Change 2007: The Physical Science Basis. Contribution of Working Group I to the Fourth Assessment Report of the Intergovernmental Panel on Climate Change*. Cambridge University Press, Cambridge, United Kingdom and New York, NY, USA.

Gao, B., Kaufman, Y., Tanre, D., and Li, R., 2002: Distinguishing tropospheric aerosols from thin cirrus clouds for improved aerosol retrievals using the ratio of 1.38-mu m and 1.24-mu m channels. *Geophysical Research Letters*, **29**(18). ISSN 0094-8276. doi:10.1029/2002GL015475.

Gates, W., Boyle, J., Covey, C., Dease, C., Doutriaux, C., Drach, R., Fiorino, M., Gleckler, P., Hnilo, J., Marlais, S., et al., 1999: An Overview of the Results of the Atmospheric Model Intercomparison Project (AMIP I). *Bulletin of the American Meteorological Society*, **80**(1), 29–56.

Geier, E., Green, R., Kratz, D., Minnis, P., Miller, W., Nolan, S., and Franklin, C., 2003: CERES data management system: Single Satellite Footprint TOA/Surface fluxes and clouds (SSF) collection document. Release 2, version 1, 212 pp and appendixes. *Radiat. and Aerosol Branch, Atmos. Sci. Res., NASA Langley Res. Cent., Hampton, Va.(Available online at http://asd-www.larc.nasa.gov/ceres/collect_guide/SSF_CG. pdf)*.

Ginoux, P., Chin, M., Holben, B., Lin, S., Tegen, I., Prospero, J., and Dubovik, O., 2001: Sources and distributions of dust aerosols simulated with the GOCART model. *Journal of Geophysical Research*, **106**(D17), 20.

Grenier, H., and Bretherton, C., 2001: A Moist PBL Parameterization for Large-Scale Models and Its Application to Subtropical Cloud-Topped Marine Boundary Layers. *Monthly Weather Review*, **129**(3), 357–377.

Harris, J., Draxler, R., and Oltmans, S., 2005: Trajectory model sensitivity to differences in input data and vertical transport method. *Journal of Geophysical Research - Atmospheres*, **110**.

Haywood, J. M., Ramaswamy, V., and Soden, B. J., 1999: Tropospheric Aerosol Climate Forcing in Clear-Sky Satellite Observations over the Oceans. *Science*, **283**(5406), 1299–1303. doi:10.1126/science.283.5406.1299.

Hoppel, W., Fitzgerald, J., Frick, G., Larson, R., and Mack, E., 1990: Aerosol size distributions and optical properties found in the marine boundary layer over the Atlantic Ocean. *Journal of Geophysical Research - Atmospheres*, **95**(D4), 3659–3686.

Hurrell, J., Hack, J., Shea, D., Caron, J., and Rosinski, J., 2008: A new sea surface temperature and sea ice boundary data set for the community atmosphere model. *Journal of Climate.* in press.

Johnson, B., Shine, K., and Forster, P., 2004: The semi-direct aerosol effect: Impact of absorbing aerosols on marine stratocumulus. *Quarterly Journal-Royal Meteorological Society*, **130**, 1407–1422.

Kapustin, V., Clarke, A., Shinozuka, Y., Howell, S., Brekhovskikh, V., Nakajima, T., and Higurashi, A., 2006: On the determination of a cloud condensation nuclei from satellite: Challenges and possibilities. *Journal of Geophysical Research*, **111**(D4).

Kaufman, Y., Koren, I., Remer, L., Rosenfeld, D., and Rudich, Y., 2005a: The effect of smoke, dust, and pollution aerosol on shallow cloud development over the Atlantic Ocean. *Proceedings of the National Academy of Sciences of the United States of America*, **102**(32), 11207–11212. ISSN 0027-8424. doi: 10.1073/pnas.0505191102.

Kaufman, Y., Remer, L., Tanre, D., Li, R., Kleidman, R., Mattoo, S., Levy, R., Eck, T., Holben, B., Ichoku, C., Martins, J., and Koren, I., 2005b: A critical examination of the residual cloud contamination and diurnal sampling effects on MODIS estimates of aerosol over ocean. *IEEE Transactions on Geoscience and Remote Sensing*, **43**(12), 2886–2897. ISSN 0196-2892. doi: 10.1109/TGRS.2005.858430.

Khairoutdinov, M., and Kogan, Y., 2000: A New Cloud Physics Parameterization in a Large-Eddy Simulation Model of Marine Stratocumulus. *Monthly Weather Review*, **128**(1), 229–243.

King, M., Menzel, W., Kaufman, Y., Tanre, D., Gao, B., Platnick, S., Ackerman, S., Remer, L., Pincus, R., and Hubanks, P., 2003: Cloud and aerosol properties, precipitable water, and profiles of temperature and water vapor from MODIS. *IEEE Trasactions on Geoscience and Remote Sensing*, **41**(2), 442–458. ISSN 0196-2892. doi:10.1109/TGRS.2002.808226.

Klein, S., and Hartmann, D., 1993: The seasonal cycle of low stratiform clouds. *Journal of Climate*, **6**(8), 1587–1606. ISSN 0894-8755.

Klein, S., Hartmann, D., and Norris, J., 1995: On the relationships among low-cloud structure, sea-surface temperature, and atmospheric circulation in the summertime Northeast Pacific. *Journal of Climate*, **8**(5, Part 1), 1140–1155. ISSN 0894-8755.

Lewis, G., Austin, P., and Szczodrak, M., 2004: Spatial statistics of marine boundary layer clouds. *Journal of Geophysical Research - Atmospheres*, **109**.

Li, F., Ginoux, P., and Ramaswamy, V., 2008: Distribution, transport, and deposition of mineral dust in the Southern Ocean and Antarctica: Contribution of major sources. *Journal of Geophysical Research-Atmospheres*, **113**(D10). ISSN 0148-0227. doi:10.1029/2007JD009190.

Liepert, B., Feichter, J., Lohmann, U., and Roeckner, E., 2004: Can aerosols spin down the water cycle in a warmer and moister world? *Geophysical Research Letters*, **31**(6). ISSN 0094-8276. doi:10.1029/2003GL019060.

Lilly, D., 1968: Models of cloud-topped mixed layers under a strong inversion. *Quart. J. Roy. Meteor. Soc*, **94**, 292–309.

Lin, S., 2004: A Vertically Lagrangian Finite-Volume Dynamical Core for Global Models. *Monthly Weather Review*, **132**(10), 2293–2307.

Liu, L., and Mishchenko, M., 2008: Toward unified satellite climatology of aerosol properties: Direct comparisons of advanced level 2 aerosol products. *Journal of Quantitative Spectroscopy and Radiative Transfer*, **109**(14), 2376–2385.

Lohmann, U., and Feichter, J., 2005: Global indirect aerosol effects: a review. *Atmospheric Chemistry and Physics*, **5**, 715–737. ISSN 1680-7324.

Lohmann, U., Koren, I., and Kaufman, Y., 2006: Disentangling the role of microphysical and dynamical effects in determining cloud properties over the Atlantic. *Geophysical Research Letters*, **33**(9). ISSN 0094-8276. doi: 10.1029/2005GL024625.

Lohmann, U., and Lesins, G., 2002: Stronger constraints on the anthropogenic indirect aerosol effect. *Science*, **298**(5595), 1012–1015. ISSN 0036-8075.

Loukachine, K., and Loeb, N., 2003: Application of an Artificial Neural Network Simulation for Top-of-Atmosphere Radiative Flux Estimation from CERES. *Journal of Atmospheric and Oceanic Technology*, **20**(12), 1749–1757.

Martin, G., Johnson, D., and Spice, A., 1994: The Measurement and Parameterization of Effective Radius of Droplets in Warm Stratocumulus Clouds. *Journal of the Atmospheric Sciences*, **51**(13), 1823–1842. ISSN 0022-4928.

Matheson, M., Coakley, J., and Tahnk, W., 2005: Aerosol and cloud property relationships for summertime stratiform clouds in the northeastern Atlantic from Advanced Very High Resolution Radiometer observations. *Journal of Geophysical Research - Atmospheres*, **110**(D24). ISSN 0148-0227. doi: 10.1029/2005JD006165.

Matheson, M., Coakley Jr, J., and Tahnk, W., 2006: Effects of threshold retrievals on estimates of the aerosol indirect radiative forcing. *Geophysical Research Letters*, **33**(7).

Mauger, G. S., and Norris, J. R., 2007: Meteorological bias in satellite estimates of aerosol-cloud relationships. *Geophysical Research Letters*, **34**(16), L16824, doi:10.1029/2007GL029952.

McCaa, J., and Bretherton, C., 2004: A new parameterization for shallow cumulus convection and its application to marine subtropical cloud-topped boundary layers. Part II: Regional simulations of marine boundary layer clouds. *Monthly Weather Review*, **132**(4), 883–896. ISSN 0027-0644.

McNoldy, B., Ciesielski, P., Schubert, W., and Johnson, R., 2004: Surface winds, divergence, and vorticity in stratocumulus regions using QuikSCAT and reanalysis winds. *Geophysical Research Letters*, **31**.

Meehl, G., Stocker, T., Collins, W., Friedlingstein, P., Gaye, A., Gregory, J., Kitoh, A., Knutti, R., Murphy, J., Noda, A., Raper, S., Watterson, I., Weaver, A., and Zhao, Z.-C., 2007: *Global Climate Projections. In: Climate Change 2007: The Physical Science Basis. Contribution of Working Group I to the Fourth Assessment Report of the Intergovernmental Panel on Climate Change*. Cambridge University Press, Cambridge, United Kingdom and New York, NY, USA.

Milliff, R., Morzel, J., Chelton, D., and Freilich, M., 2004: Wind Stress Curl and Wind Stress Divergence Biases from Rain Effects on QSCAT Surface Wind Retrievals. *Journal of Atmospheric and Oceanic Technology*, **21**(8), 1216–1231.

Ming, Y., Ramaswamy, V., Donner, L., and Phillips, V., 2006: A New Parameterization of Cloud Droplet Activation Applicable to General Circulation Models. *Journal of the Atmospheric Sciences*, **63**(4), 1348–1356.

Ming, Y., Ramaswamy, V., Donner, L., Phillips, V., Klein, S., Ginoux, P., and Horowitz, L., 2007: Modeling aerosol-cloud interactions with a self-consistent cloud scheme in a general circulation model. *Journal of Atmospheric Sciences*, **64**(4).

Myhre, G., Stordal, F., Johnsrud, M., Kaufman, Y., Rosenfeld, D., Storelvmo, T., Kristjansson, J., Berntsen, T., Myhre, A., and Isaksen, I., 2007: Aerosol-cloud interaction inferred from MODIS satellite data and global aerosol models. *Atmos. Chem. Phys*, **7**, 3081–3101.

Norris, J., and Iacobellis, S., 2005: North Pacific Cloud Feedbacks Inferred from Synoptic-Scale Dynamic and Thermodynamic Relationships. *Journal of Climate*, **18**(22), 4862–4878.

Oreopoulos, L., Cahalan, R., Marshak, A., and Wen, G., 2000: A New Normalized Difference Cloud Retrieval Technique Applied to Landsat Radiances over the Oklahoma ARM Site. *Journal of Applied Meteorology*, **39**(12), 2305–2321.

Pincus, R., Hemler, R., and Klein, S., 2006: Using Stochastically Generated Subcolumns to Represent Cloud Structure in a Large-Scale Model. *Monthly Weather Review*, **134**(12), 3644–3656.

Platnick, S., King, M., Ackerman, S., Menzel, W., Baum, B., Riedi, J., and Frey, R., 2003: The MODIS cloud products: Algorithms and examples from Terra. *IEEE Transactions on Geoscience and Remote Sensing*, **41**(2), 459–473. ISSN 0196-2892. doi:10.1109/TGRS.2002.808301.

Ramanathan, V., Cess, R., Harrison, E., Minnis, P., Barkstrom, B., Ahmad, E., and Hartmann, D., 1989: Cloud-Radiative Forcing and Climate: Results from the Earth Radiation Budget Experiment. *Science*, **243**(4887), 57–63.

Rosenfeld, D., 2000: Suppression of rain and snow by urban and industrial air pollution. *SCIENCE*, **287**(5459), 1793–1796. ISSN 0036-8075.

Rotstayn, L., and Lohmann, U., 2002: Tropical rainfall trends and the indirect aerosol effect. *JOURNAL OF CLIMATE*, **15**(15), 2103–2116. ISSN 0894-8755.

Rozendaal, M., and Rossow, W., 2003: Characterizing Some of the Influences of the General Circulation on Subtropical Marine Boundary Layer Clouds. *Journal of the Atmospheric Sciences*, **60**(5), 711–728.

Schubert, W., Wakefield, J., Steiner, E., and Cox, S., 1979: Marine Stratocumulus Convection. Part I: Governing Equations and Horizontally Homogeneous Solutions. *Journal of the Atmospheric Sciences*, **36**(7), 1286–1307.

Schwartz, S., Harshvardhan, and Benkovitz, C., 2002: Influence of anthropogenic aerosol on cloud optical depth and albedo shown by satellite measurements and chemical transport modeling. *Proceedings of the National Academy of Sciences of the United States of America*, **99**(4), 1784–1789. ISSN 0027-8424. doi: 10.1073/pnas.261712099.

Slingo, A., 1990: Sensitivity of the Earth's radiation budget to changes in low clouds. *Nature*, **343**(6253), 49–51.

Soden, B., and Held, I., 2006: An Assessment of Climate Feedbacks in Coupled Ocean–Atmosphere Models. *Journal of Climate*, **19**(14), 3354–3360.

Stevens, B., Beljaars, A., Bordoni, S., Holloway, C., Koehler, M., Krueger, S., Savic-Jovcic, V., and Zhang, Y., 2007: On the structure of the lower troposphere in the summertime stratocumulus regime of the northeast Pacific. *Monthly Weather Review*, **135**(3), 985–1005. ISSN 0027-0644. doi:10.1175/MWR3427.1.

Stiles, B., 1999: Special wind vector data product: Direction interval retrieval with threshold nudging (DIRTH), product description version 1.1. *Jet Propulsion Laboratory, Pasadena, CA*.

Stohl, A., Hittenberger, M., and Wotawa, G., 1998: Validation of the lagrangian particle dispersion model FLEXPART against large-scale tracer experiment data. *Atmospheric Environment*, **32**(24), 4245–4264.

Stohl, A., and Seibert, P., 1998: Accuracy of trajectories as determined from the conservation of meteorological tracers. *Quarterly Journal of the Royal Meteorological Society*, **124**(549), 1465–1484.

Tegen, I., Hollrig, P., Chin, M., Fung, I., Jacob, D., and Penner, J., 1997: Contribution of different aerosol species to the global aerosol extinction optical thickness: Estimates from model results. *Journal of Geophysical Research*, **102**(D20).

Tiedtke, M., 1993: Representation of Clouds in Large-Scale Models. *Monthly Weather Review*, **121**(11), 3040–3061.

Twohy, C., Petters, M., Snider, J., Stevens, B., Tahnk, W., Wetzel, M., Russell, L., and Burnet, F., 2005: Evaluation of the aerosol indirect effect in marine stratocumulus clouds: Droplet number, size, liquid water path, and radiative impact. *Journal of Geophysical Research - Atmospheres*, **110**(D8).

Twomey, S., 1977: Influence of Pollution on the Shortwave Albedo of Clouds. *Journal of the Atmospheric Sciences*, **34**(7), 1149–1152. ISSN 0022-4928.

Wentz, F., 1997: A well-calibrated ocean algorithm for SSM/I. *Journal of Geophysical Research - Atmospheres*, **102**(C4), 8703–8718.

Wentz, F., and Spencer, R., 1998: SSM/I Rain Retrievals within a Unified All-Weather Ocean Algorithm. *Journal of the Atmospheric Sciences*, **55**(9), 1613–1627.

Wielicki, B., and Parker, L., 1992: On the determination of cloud cover from satellite sensors: the effect of sensor spatial resolution. *Journal of Geophysical Research, Atmospheres*, **97**(12), 12799–12823.

Wood, R., 2006: VOCALS-SouthEast Pacific Regional Experiment (REx). World Wide Web electronic publication.

Wood, R., and Bretherton, C. S., 2006: On the relationship between stratiform low cloud cover and lower-tropospheric stability. *Journal of Climate*, **19**(24), 6425–6432. ISSN 0894-8755.

Wyant, M., Bretherton, C., Rand, H., and Stevens, D., 1997: Numerical Simulations and a Conceptual Model of the Stratocumulus to Trade Cumulus Transition. *Journal of the Atmospheric Sciences*, **54**(1), 168–192.

Xu, K., Wong, T., Wielicki, B., Parker, L., Lin, B., Eitzen, Z., and Branson, M., 2007: Statistical Analyses of Satellite Cloud Object Data from CERES. Part II: Tropical Convective Cloud Objects during 1998 El Niño and Evidence for Supporting the Fixed Anvil Temperature Hypothesis. *Journal of Climate*, **20**(5), 819–842.